論文 / 著書情報
Article / Book Information

題目(和文)	骨軟骨治療のための水酸アパタイトとコラーゲンを基材とした二層足場材料の研究
Title(English)	Study on hydroxyapatite and collagen based bilayer scaffolds for osteochondral treatment
著者(和文)	IrawanVincent
Author(English)	Vincent Irawan
出典(和文)	学位:博士(工学), 学位授与機関:東京工業大学, 報告番号:甲第11282号, 授与年月日:2019年9月20日, 学位の種別:課程博士, 審査員:生駒 俊之,鶴見 敬章,中島 章,宮内 雅浩,松下 伸広
Citation(English)	Degree:Doctor (Engineering), Conferring organization: Tokyo Institute of Technology, Report number:甲第11282号, Conferred date:2019/9/20, Degree Type:Course doctor, Examiner:,,,,
学位種別(和文)	博士論文
Type(English)	Doctoral Thesis

Doctoral Thesis

Vincent Irawan

16D28059

Supervised by

Professor Toshiyuki IKOMA

School of Materials and Chemical Technology

Tokyo Institute of Technology

2019

Abstract

Osteochondral injury, a simultaneous damage of articular cartilage and bone tissues, requires implantation of a bilayer scaffold (porous bodies / sponges) in which the first and second layer is optimized for cartilage and bone tissues regeneration, respectively. To promote the cartilage regeneration, the first layer is combined with cartilage tissue-engineering strategy that is a deliberate attempt to obtain *in vitro* cartilage by culturing and maturing stem cells. Collagen-based material is a gold standard for tissue-engineering scaffold, and commonly fabricated from the monomeric form of collagen (liquid state), owing to easiness of fabrication. Nonetheless, collagen in the native tissues exist in the fibrillar form (gel-like state), thereby the fibrillar collagen scaffold is expected to elicit more superior biological properties to the monomeric counterpart. Composite material of collagen and hydroxyapatite (HAp) is generally used as a scaffold for bone tissue. The current methods to fabricate bilayer scaffold is by knitting or gluing collagen sponge and collagen-HAp composite, which pose risk of delamination. Therefore, a continuous bilayer scaffold: collagen sponge with gradient content of HAp is desired. Electrolysis was previously used to simultaneously deposit fibrillar collagen and HAp; justifying the attempt to investigate electrolysis to fabricate continuous bilayer scaffold. Iron-oxide nanoparticle (IONP) with magnetic property has been reported to support bone cells proliferation. This thesis initially aims to elucidate the advantage of fibrillar to monomeric collagen sponges as a cartilage tissue-engineering scaffold; thereafter, the thesis focuses to construct a continuous bilayer scaffold optimized for regenerating osteochondral injury. It was discovered that collagen structure influenced the morphology of attached fibroblast, with the fibrillar collagen sponge supported higher proliferation rate to monomeric sponges. Next, electrolysis was used to prepare fibrillar collagen/HAp scaffold; chitosan was added to improve the fibril formation of collagen. Fibrillar collagen/HAp/chitosan sponges supported the faster proliferation of mesenchymal stem cells and the larger production of cartilage tissue-related extracellular matrices compared to the monomeric collagen/HAp/chitosan sponges. Next, electrolysis was used to produce fibrillar collagen-chitosan scaffolds with gradient HAp content; further addition of IONP successfully improved the proliferation rate of osteoblast (bone cells) cultured in the HAp-rich region of scaffolds. In parallel, other configuration of a continuous bilayer scaffold consisting of collagen/HAp sponge and IONP-impregnated HAp-sintered body was fabricated by simultaneously electrolyzing the latter structure in the presence of collagen/HAp solution. In conclusion, a fibrillar collagen scaffold containing IONP and gradient content of HAP is considered as an ideal scaffold to simultaneously regenerate cartilage and bone tissues in the osteochondral injury.

Table of Contents

LIST OF FIGURES

Chapter 1-Introduction

1.1 What is osteochondral injury?

The life expectancy of people around the world are steadily pushed into large value, owing mainly to the advance of medical technology (Fig. 1.1)[1]. Nonetheless, the increasing of life-expectancy translates to the higher sufferer of age-related diseases, such as knee join defect (Fig. 1.2)[2].

Knee joint or synovial joint is a structure that exists between bones that allows frictionless movement and transfer of load between bones (Fig. 1.3) [3–6]. Synovial joint consist mainly of a specialized tissue called articular cartilage (AC) and the underlying subchondral bone (Fig. 1.3). AC mainly function to provide frictionless movement between the bones [7,8], whereas subchondral bone has been known to take burden load [9]. Due to the dynamic loading applied to this structure, bone joints are naturally exhausted with the age of human [10–12]. Other factors such as accident, or excessive training might contribute to the occurrence of joint injury at the early age [13,14]. The injury of synovial joint is notoriously known for its sluggish regeneration capacity [13–15]., thereby, the untreated injury continues to degenerate overtime and subsequently propagates to the underlying bone tissue (osteochondral injury), causing joint stiffness and painfulness, which in turn impair physical and emotional state of the sufferer [16,17].

1.2 The currently available medical treatments of osteochondral injury

There are two kinds of medical intervention mainly used in the treatment of osteochondral injury, that is microfracture and mosaicplasty (Fig. 1.4) [2].

Microfractures involves deliberate physical penetration down into deeper region of subchondral bone, as to allow mesenchymal stem cells, platelets, and other factors to fill the defect [18]. The platelet form temporary scaffold which promote recruitment of

surrounding cells, necessary for inducing tissue regeneration. Microfracture does not requires invasive surgery, easy to perform and well tolerated by patients [19]. Microfracture is beneficial in reducing symptom of joint injury (pain, stiffness) in the initial 11 months after treatment [20]; however, the regenerated tissue is not compositionally similar to AC tissue, suggesting the possibility of recurrence of joint injury[19].

Mosaicplasty involves extraction of osteochondral plugs from non-weight bearing area and the subsequent implantation into the injured area [20–22]. Mosaicplasty was deemed as technically demanding for the surgeon, as it requires two-times surgery (donor extraction and transplantation) [20]. The applicability of mosaicplasty also limited by the location of osteochondral defect and other investigators also reported the complication at donor site of osteochondral plug [15,22]. Several clinical studies revealed that mosaicplasty greatly support the osteochondral regeneration at injured area [23,24]. Nonetheless, several clinical studies revealed that mosaicplasty greatly support the osteochondral regeneration at injured area, implying the importance to simultaneously regenerate cartilage and bone tissue [25].

1.3 **Tissue-engineering: a promising approach to regenerate osteochondral injury**

What is tissue engineering?

Instead of relying on the availability of donor tissue, several investigators have proposed a concept to fabricate tissue in the lab (tissue-engineering) [26–28]. Initially, particular cells are isolated from the patient, expanded in the tissue culture plate, and seeded in the housing structure (scaffold) (Fig. 1.5). Next, the cell-seeded scaffold is matured *in vitro* to induce the tissue formation. Several important events occurred during *in vitro* maturation that is increasing of cell number and secretion of matrix molecules. After

maturation for several weeks, tissue-engineered construct is obtained and implanted back into the patient. The implanted tissue-engineered construct is expected to: (1) deliver cells as the replacement of dying cells at the injury site, (2) provide newly secreted matrix molecules as to promote integration with surrounding tissue, (3) fill defect space and temporarily bear the mechanical load

Source of cells for tissue engineering

There are two main types of cells that commonly used in tissue engineering, that is native cells and adult stem cells [25,29,30]. Native cells are the differentiated cells that reside in the specific tissue, such as chondrocyte in articular cartilage tissue or osteoblast in bone-tissue [31,32]. On the other hand, adult stem cells are the undifferentiated cells that are distributed in various tissues, such as, mesenchymal stem cells that reside in fat tissue or bone marrow area [33]. The native cells readily secrete relevant matrix molecules; however, native cells generally suffered from the low cells numbers [8,15], as it generally showed the limited cell proliferation capacity. Moreover, the extraction source for native cells are limited to the particular tissue of interest. In contrast to the native cells, the main advantages of mesenchymal stem cell (MSC) is abundant cell number. MSC show high proliferation capacity and MSC can be extracted from various sources [34]. However, MSC should be differentiated in the particular lineage before secreting specific matrix molecules [35–37]. Based on these criteria, MSC is generally considered as a feasible option for tissue-engineering.

Expansion and differentiation of mesenchymal stem cells (MSC)

Expansion and differentiation of MSC are generally conducted by exposing the cells to different type of mediums (Fig. 1.6) [33]. To expand the cells, a mixture of basal medium

and fetal bovine serum is compulsory. Basal medium contains vitamins and amino acids necessary to sustain the minimum growth of cells; whereas fetal bovine serum is a chemically undefined media that generally contain soluble factors necessary to support the attachment and proliferation of cells [38,39]. On the other hand, to differentiate the MSC into the adults, a mixture of basal medium and a set of differentiating factors is required (differentiating medium [40,41]). MSC is cultured in the differentiating medium for several weeks to induce the maturation into the particular type of cells.

In addition to the biological factors, physical parameters of substrate, onto which the cells are attached, also determine the proliferation and differentiation tendency of cells [42–45]. The attachment of cells onto substrate is generally mediated by ligand, that is a particular amino acid sequences, carbohydrate, which are capable to be directly recognized by cells receptor. The low / high density of ligand distribution has been shown to inhibit / promote the proliferation of cells [46]. In the context of MSC differentiation, the low / high density of ligand distribution was associated with the tendency of MSC to differentiate into cartilage / bone-cells, respectively [47]. In the other study, it was also shown that MSC cultured on the substrate with low elastic modulus (1-4 kPa) are induced to differentiate into cartilage cells [48,49] as opposed to differentiation into bone cells for MSC cultured on high elastic modulus (100 kPa)[42,50,51].

1.4 Criteria of scaffolds for tissue engineering

The first step for tissue-engineering is the seeding and infiltration of cells throughout the inside of the scaffolds [52]. To allow cells infiltration, scaffold should be highly porous (99% porosity). High porosity not only allow cell distribution inside scaffold, but also allow circulation of cell culture medium to take place [53], which are beneficial for the growth of cells.

In addition to porosity, scaffold material should facilitate cell attachment [27,54–56]. Cell attachment is mediated through the binding of cell receptor and the particular ligands. Cell attachment is the foremost event that should be done by cells before it commences the activities (migration, proliferation, differentiation) [57–59]. If the cells fail to form attachment, it will undergo self-induced death (anoikis) [60]. In the context of tissue-engineering, attachment of cells and scaffold material is of high importance, as scaffold mainly function to carry the cells into injured tissue.

After forming attachment, cell generally exert traction on the surrounding scaffold [61–63], thereby causing the shrinkage of scaffold in the process [64]. The excessive shrinkage is not desirable for tissue engineering, as it might collapse porous structure necessary for circulation of oxygen or growth media [65]. To prevent cell-mediated shrinkage, scaffold material is designed to exhibit sufficient compressive modulus as to resist cell-mediated traction [66]. Moreover, scaffold should show sufficient compressive strength as to withstand the handling stress by operator or surgeon during tissue-engineering or before implantation in the injured site [67].

1.5 Type I collagen as the scaffold of tissue engineering

Type I collagen is a major component of mammalian flesh (Fig. 1.7). It exists as fibrillar state, which consist of smaller monomer of sequences of amino acids [15,68,69]. Adhesion of type I collagen and cells is mediated by cell receptor-integrin . Alpha-domain of integrin is capable of recognizing multiple binding sites in integrin, such as GFOGER and GROGER (amino acid sequences with single letter amino acid nomenclature) [70,71]. Binding of GFOGER and cells might activate the signaling pathway necessary for cell survival, cell proliferation, modulation of cell proliferation [72–74].

Other materials such as metal or ceramic lack the cell-binding ligand that is capable to

recognized by cells, thereby collagen is widely used as a scaffold material.

1.6 State-of-the art of osteochondral tissue-engineering employing collagen as the porous scaffold

To accommodate simultaneous regeneration of cartilage and bone tissue in osteochondral interface, scaffold consisting of two different materials are commonly joined in a single structure (bilayer structure) [75–78]. The first layer is generally made from collagen and intended to optimize the cartilage tissue formation (Fig. 1.8). The second layer is made from calcium phosphate or synthetic polymer which is optimize for regenerating the bone tissue. The two layers were subsequently joined in a single structure by knitting or gluing.

In the next step, investigators mainly focused on conducting the cartilage tissue-engineering for the first layer, while leaving the second layer without bone tissue-engineering treatment [75,76]. One of the argument was to avoid practical difficulty. In a single cell culture reactor, it is not possible to efficiently differentiate MSC in the different pathway, whereas side-by-side differentiation is an exhaustive and time consuming process (MSC need at least 3 weeks to fully mature into the differentiated cells). Second reason is osteoblast, a bone-forming cell, exhibit relatively strong capacity to proliferate and secrete matrix molecule [32,79]. Thereby, as long as the second layer support osteoblast attachment and proliferation, bone tissue formation naturally follow.

Lastly, the tissue-engineered scaffolds are implanted into the animal models for 2-4 months before final scaffold evaluation. Good results were generally obtained as evidenced from the formation of cartilage-like and bone-like tissues in the cell/scaffold construct after months of implantation in the osteochondral defect [76]. The implanted scaffold was also reported to be well integrated with the surrounding tissue. Other

investigator reported the increasing of mechanical properties (Young's modulus and compressive strength) of tissue-engineering construct after months of implantation in the osteochondral tissue [75]. The improvement of mechanical properties was associated with the formation of articular cartilage and bone tissue in the implanted construct [28,80]. Taken together, the implantation of tissue-engineered bilayer construct generally showed acceptable regeneration results.

These bilayer scaffolds were joined by physical means which introduce distinct interface. Several authors have raised questions regarding the interface stability of bilayer scaffolds years after implantation [3,81]. Thereby, other type of bilayer scaffold configuration is needed.

1.7 **Continuous bilayer scaffolds: collagen scaffold with gradient content of HAp**

To eliminate the introduction of distinct interface in the bilayer scaffold, the concept of continuous bilayer scaffold was proposed (Fig. 1.9) [82,83]. The structure depends on collagen region with less amount of HAp to support cartilage-tissue engineering, whereas collagen region with higher amount of HAp is expected to stimulate bone tissue formation [84]. HAp is selected due to its capacity to support bone tissue formation [84,85].

To fabricate the continuous bilayer scaffolds of collagen/HAp, electrolysis method was used. Electrolysis had long been used to fabricate collagen coating with varying HAp content throughout the coating [86,87]. HAp was initially dissolved in the low pH collagen solution as to release the calcium and phosphate ions. Application of current in constant potential mode revealed that collagen fibrils together with calcium phosphate particles were thinly deposited (~100 μm) on the negatively charged electrode (cathode) [86]. At cathode, the water molecules was reduced to hydroxyide ions, resulting in the increasing of local pH, causing the concurrent precipitation of collagen and HAp. Other investigators

conducted electrolysis of the similar electrolyte system, by applying alternating potential mode; collagen layers with alternating HAp-rich and HAp-poor regions were obtained[87]. Negatively charged electrode attracted positive calcium ions and subsequent OH^- production caused formation of HAp-rich layer; whereas collagen molecules were attracted when the same electrode was positively charged, thus forming HAp-poor layer. Based on these results, it was hypothesized that by dissolving proper amount of HAp (controlling concentration of calcium and phosphate salts), collagen fibril with gradient HAp content could be obtained. .

1.8 **Identification of research problems**

By electrolysis method, monomeric collagen is transformed into the fibrillar state. On the other hand, the conventional porous scaffolds of osteochondral tissue engineering are generally fabricated from the monomeric sponge [75–77]. The influence of fibrillar state of collagen to the physical properties (mechanical properties or water-absorption capacity), cell proliferation/differentiation supporting capacity of collagen/HAp sponges was unknown.

The next research problem is the fibrilogenesis by electrolysis. It was mentioned that electrolysis relies on high pH to rapidly induce collagen fibrilogenesis [86]. On the other hand, it was previously shown that collagen monomers rapidly aggregate into the numerous nuclei at high pH, resulting in the formation of immature collagen fibrils [88].

Several investigators proposed the usage of chitosan to improve the fibrilogenesis of collagen. Chitosan is a linear polysaccharide of glucosamine and N-acetyl glucosamine mainly derived from deacetylation of chitin which commonly finds in crustacean (crabs, shrimp, and lobster) shells or cell wall of fungi [89] At the low pH, chitosan are positively charged due to presence of numerous amine groups [90]. Chitosan formed polyionic

complex with negatively charged monomeric collagen [91–93], which in turn inhibit rapid formation of collagen nucleus, resulting in the proper growth of collagen nucleus into fibril (Fig. 1.11). It was hypothesized that addition of chitosan into electrolysis system of collagen could improve the fibrilogenesis of collagen.

HAp to promote bone regeneration. Is it enough?

MaioRegen® is the clinically available bilayer scaffold that relies on collagen-ricHApatite-rich layers to promote regeneration of cartilage and bone tissues, respectively [83,94]. A subsequent clinical study conducted in Denmark, revealed that MaioRegen® failed to induce the osteochondral regeneration at 1 and 2.5 years after implantation (Fig. 1.12) [94]. It was proposed that HAp-rich layer of MaioRegen® failed to initiate the formation of bone tissue.

HAp is commonly used to support the bone tissue regeneration, due to its capacity to induce the bone matrix formation by osteoblast [95–97]. Nonetheless, HAp does not strongly promote proliferation of osteoblast [98]. Osteochondral injury was considered to cause numerous death of osteoblast, as a result not enough osteoblast was available to deposit new bone matrix.

In the past, researchers have investigated influences of exposing various types of nanoparticles to the mammalian cells. TiO_2 with the size of 15 nm / 200 nm [98] was showed to decrease cell proliferation, mobility, and traction. Alumina (10 nm / 20 nm) [99] was showed to increase expression of cytoskeletal protein and enhance adhesion capacity of cells. Iron-oxide nanoparticles (5 nm / 10 nm) was showed to increase cell polarization, increase cell proliferation [99–101].

The findings that iron-oxide nanoparticles (IONP) were beneficial in promoting cell proliferation prompted several investigators to incorporate IONP into the porous scaffolds

as to promote bone cells proliferation (Fig. 1.13) [102–104] .

1.9 Thesis objective and overview

1. Investigate the feasibility of fibrillar collagen sponges as a porous scaffold for tissue-engineering application as compared to the monomeric sponges

2. Utilize electrolysis to fabricate a continuous bilayer scaffold optimized for osteochondral tissue engineering

This thesis composed of 6 Chapters,

Chapter-1 describe the background and objective of the thesis.

Chapter 2 describe the investigation of influence collagen fibrilar state (monomeric / fibrillar) in collagen/HAp sponge might influence the mechanical and biological properties of collagen/HAp sponges was investigated.

Chapter 3 describe the fabrication of fibrillar and monomeric sponge consisting of collagen, chitosan, and HAp and the evaluation of influence of collagen fibrillar state in the sponges to the proliferation, chondrogenic differentiation, and matrix secretion capacity of human mesenchymal stem cells (MSC).

Chapter 4 describes the utilization of electrolysis as a method to fabricate a continuous bilayer structure consisting of fibrillar collagen/chitosan sponge with the gradient HAp content and the subsequent evaluation of the influence of IONP addition to the mechanical properties and osteoblast-proliferation supporting capacity of fibrillar bilayer structure.

Chapter 5 describes fabrication of a continuous bilayer structure consisting of fibrillar collagen/HAp sponge and HAp-sintered body and subsequent evaluation of magnetic properties and biocompatibility of bilayer structure after addition of iron-oxide nanoparticles.

Chapter 6, the thesis was summarized and the conclusion for future work was given.

Structure of the thesis

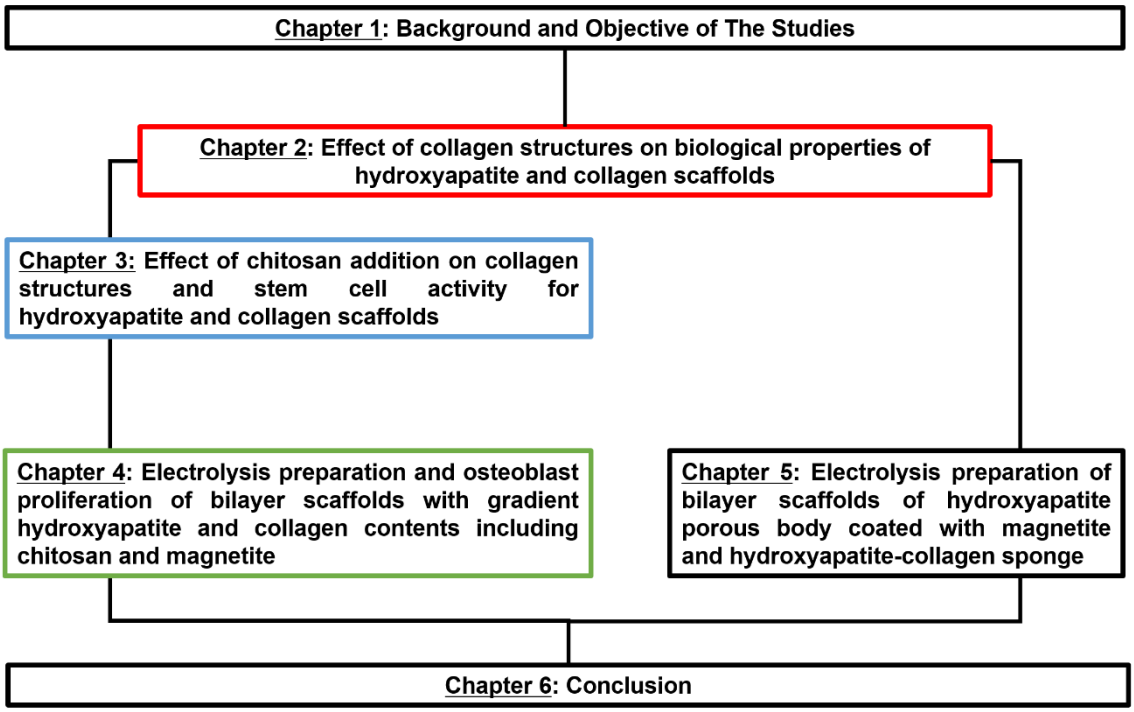

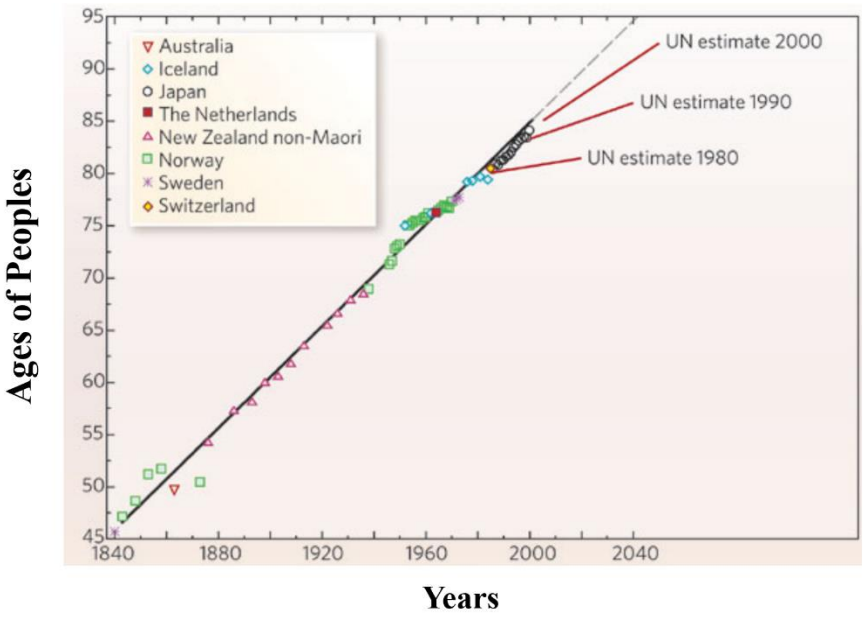

Fig.1.1 Progression of life expectancy of people in world [1]

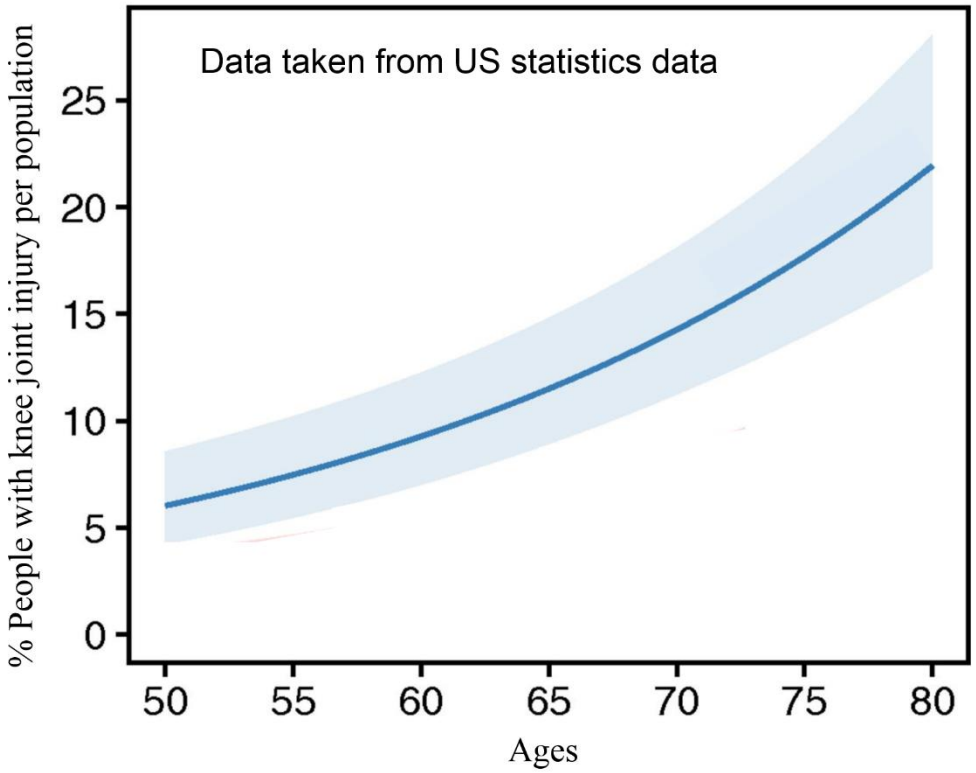

Fig.1.2 Association of knee injury with ages [2].

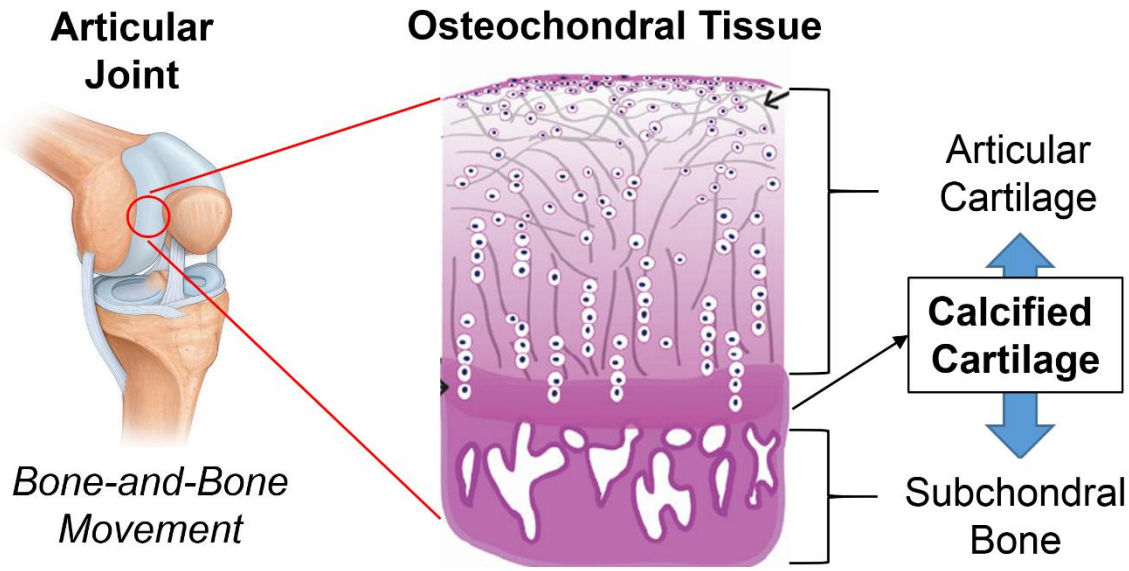

Fig.1.3 Anatomy of osteochondral tissue [6]. Image taken with permission from [6].

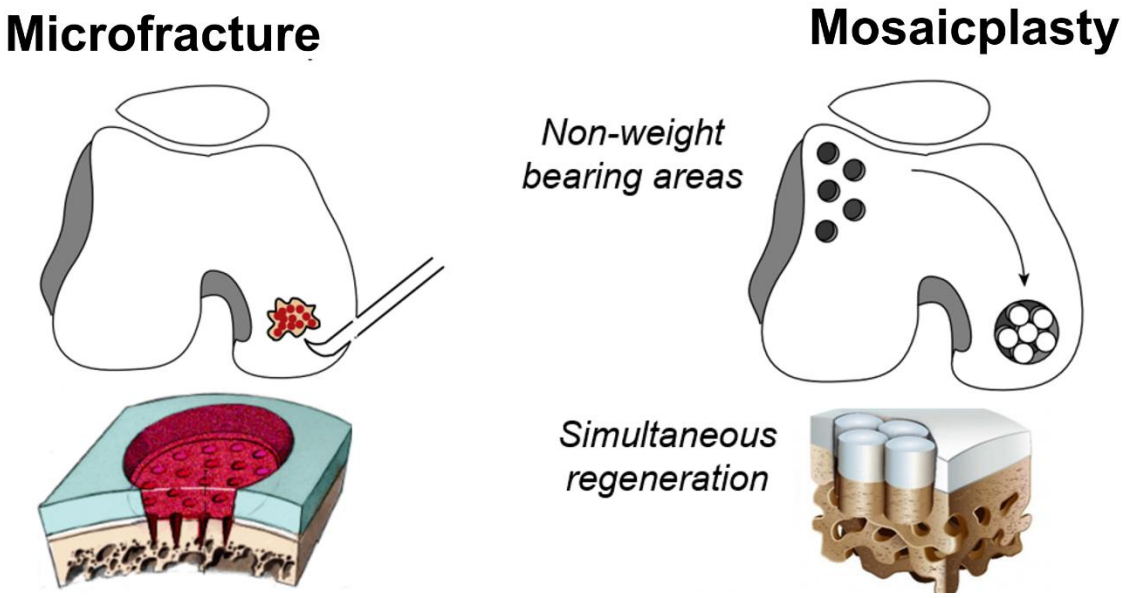

Fig.1.4 Illustration of microfracture and mosaicplasty [20]. Image taken with permission from [20]

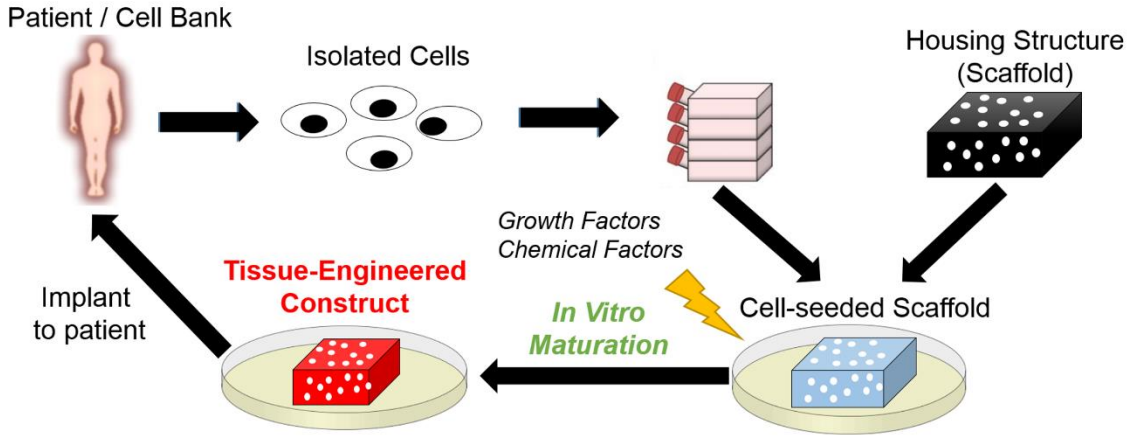

Fig.1.5 Illustration of tissue engineering [27-30].

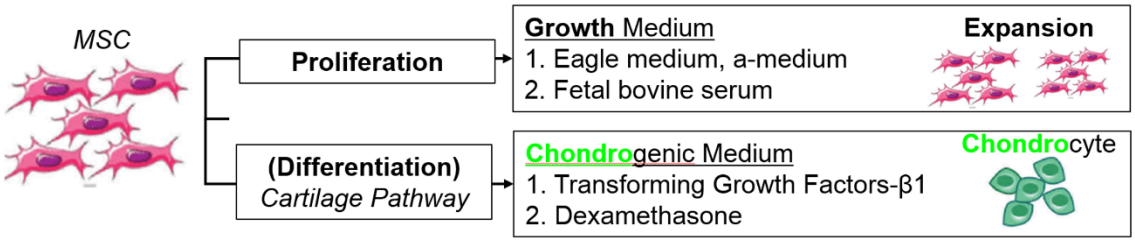

Fig.1.6 Schematic diagram of describing the proliferation and differentiation of MSC [34-40].

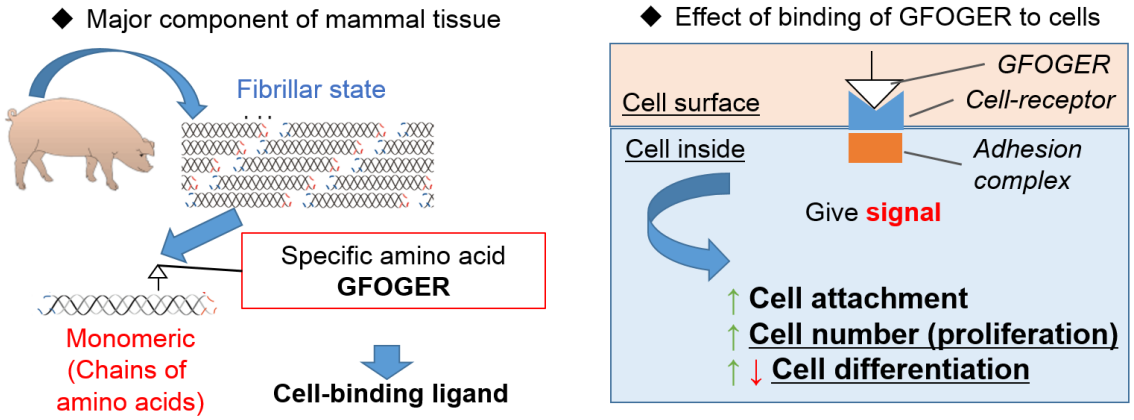

Fig.1.7 Schematic diagram of describing the structure of collagen (left figure) and the signaling induced by attachment of collagen and cell [69-74].

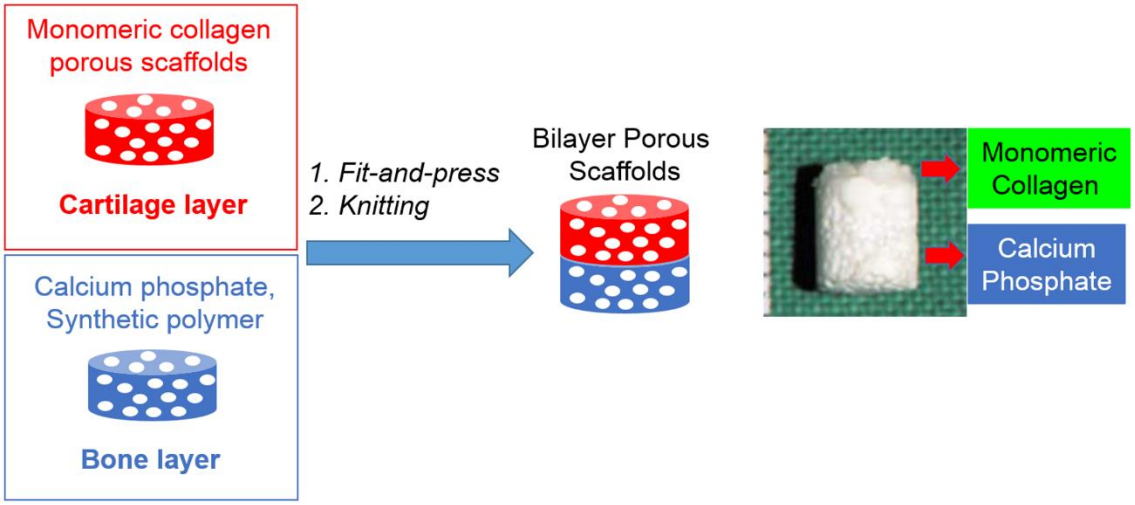

Fig.1.8 Illustration of fabrication of bilayer scaffolds from two different scaffolds [75]. Image taken with permission from [75].

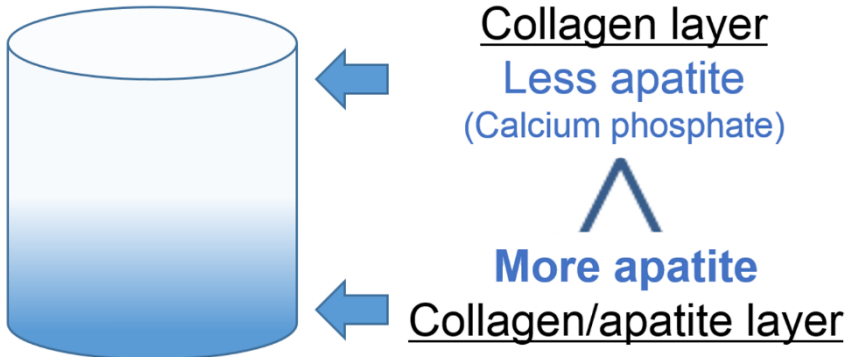

Fig.1.9 Illustration of a continuous bilayer scaffold consisting of collagen sponge with gradient apatite content

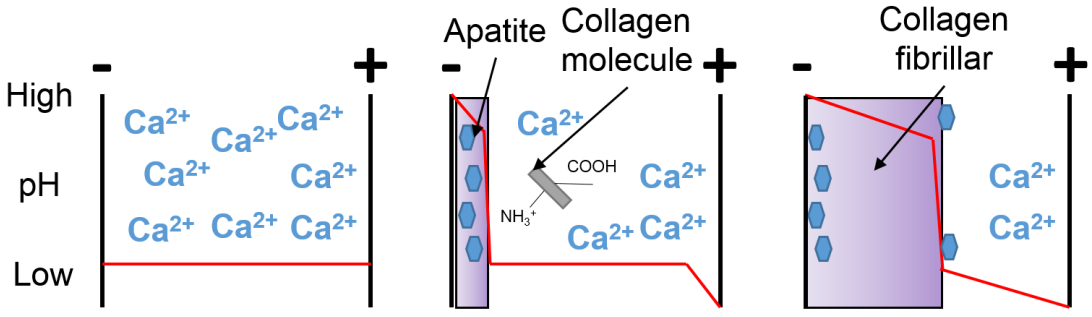

Fig.1.10 Schematic drawing of fabrication of continuous bilayer scaffolds by electrolysis [82].

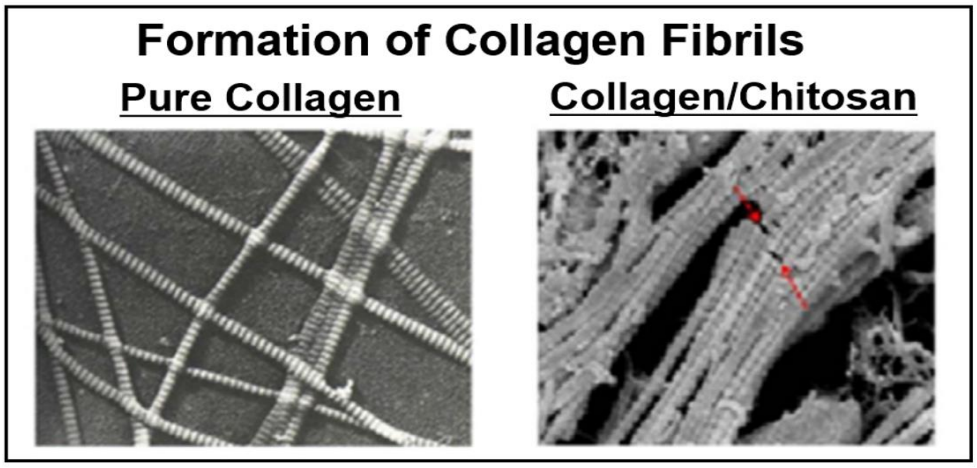

Fig.1.11 Collagen fibril appearance without and with addition of chitosan [93]. Image was taken with permission from [93].

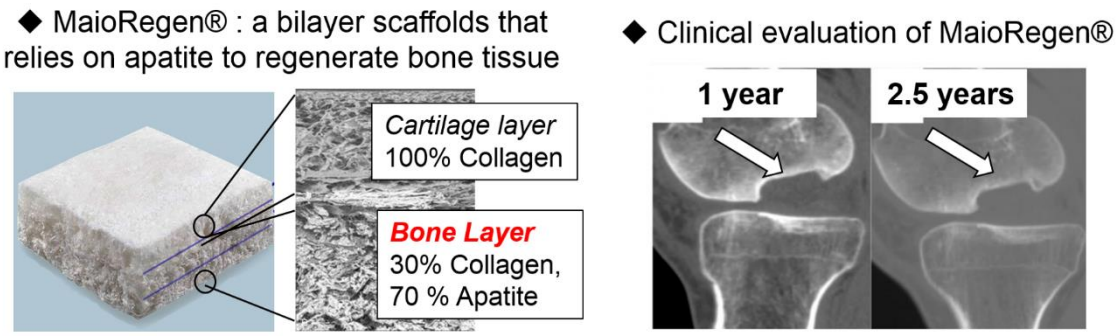

Fig.1.12 Appearance of MaioRegen [83] and the result of MRI imaging 1 and 2.5 years after implantation [94]. Image was taken with permission from [83].

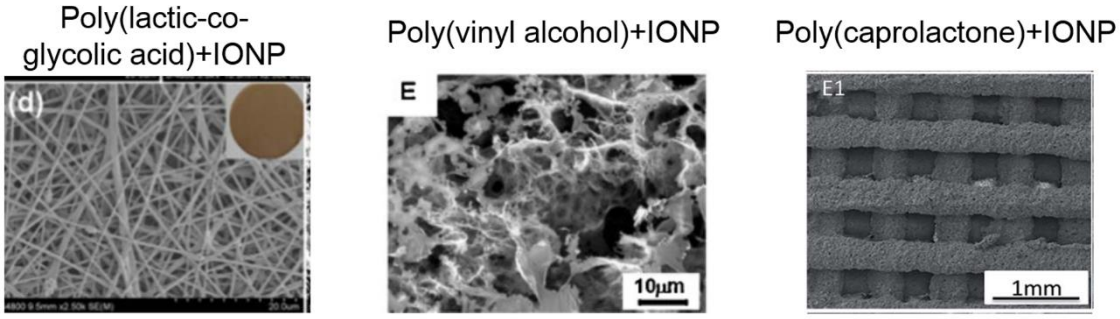

Fig.1.13 Microstructure of various types of porous scaffolds impregnated with IONP [102-104]. Image was taken with permission from [102-104].

References

1 Life expectancy around the world has increased steadily for nearly 200 years. | Learn Science at Scitable, https://www.nature.com/scitable/content/life-expectancy-around-the-world-has-increased-19786%0A, (accessed 20 September 2007).

2 I. J. Wallace, S. Worthington, D. T. Felson, R. D. Jurmain, K. T. Wren, H. Maijanen, R. J. Woods and D. E. Lieberman, *Proc. Natl. Acad. Sci.*, 2017, **114**, 9332–9336.

3 T. J. Levingstone, E. Thompson, A. Matsiko, A. Schepens, J. P. Gleeson and F. J. O'brien, *Acta Biomater.*, 2016, **32**, 149–160.

4 A. D. Pearle, R. F. Warren and S. A. Rodeo, *Clin. Sports Med.*, 2005, **24**, 1–12.

5 A. Aspberg, in *Cartilage*, Springer International Publishing, Cham, 2016, vol. 12, pp. 1–22.

6 I. Gadjanski, K. Spiller and G. Vunjak-Novakovic, *Stem Cell Rev. Reports*, 2012, **8**, 863–881.

7 B. J. Huang, J. C. Hu and K. A. Athanasiou, *Biomaterials*, 2016, **98**, 1–22.

8 B. Johnstone, M. Alini, M. Cucchiarini, G. R. Dodge, D. Eglin, F. Guilak, H. Madry, A. Mata, R. L. Mauck, C. E. Semino and M. J. Stoddart, *Eur. Cell. Mater.*, 2013, **25**, 248–67.

9 A. H. Gomoll, H. Madry, G. Knutsen, N. van Dijk, R. Seil, M. Brittberg and E. Kon, *Knee Surgery, Sport. Traumatol. Arthrosc.*, 2010, **18**, 434–447.

10 A. K. Lynn, S. M. Best, R. E. Cameron, B. A. Harley, I. V. Yannas, L. J. Gibson and W. Bonfield, *J. Biomed. Mater. Res. - Part A*, 2010, **92**, 1057–1065.

11 I. Martin, S. Miot, A. Barbero, M. Jakob and D. Wendt, *J. Biomech.*, 2007, **40**,

750–765.

12 J. Zhou, C. Xu, G. Wu, X. Cao, L. Zhang, Z. Zhai, Z. Zheng, X. Chen and Y. Wang, *Acta Biomater.*, 2011, **7**, 3999–4006.

13 H. J. Mankin, *J. Bone Joint Surg. Am.*, 1982, **64**, 460–6.

14 S. W. O'Driscoll, *J. Bone Joint Surg. Am.*, 1998, **80**, 1795–812.

15 V. Irawan, T.-C. Sung, A. Higuchi and T. Ikoma, *Tissue Eng. Regen. Med.*, 2018, **15**, 673–697.

16 G. Pisanu, U. Cottino, F. Rosso, D. Blonna, A. G. Marmotti, C. Bertolo, R. Rossi and D. E. Bonasia, *Joints*, 2018, **6**, 42–53.

17 C. N. van Dijk, M. L. Reilingh, M. Zengerink and C. J. A. van Bergen, *Knee Surgery, Sport. Traumatol. Arthrosc.*, 2010, **18**, 570–580.

18 R. B. Jakobsen, L. Engebretsen and J. R. Slauterbeck, *J. Bone Jt. Surg. - Ser. A*, 2005, **87**, 2232–2239.

19 C. L. Camp, M. J. Stuart and A. J. Krych, *Sports Health*, 2014, **6**, 265–273.

20 K. Ye, C. Di Bella, D. E. Myers and P. F. M. Choong, *ANZ J. Surg.*, 2014, **84**, 211–217.

21 L. Hangody, P. Fules and P. Füles, *J Bone Jt. Surg Am*, 2003, **85-A Suppl**, 25–32.

22 L. Hangody, G. Vásárhelyi, L. R. Hangody, Z. Sükösd, G. Tibay, L. Bartha and G. Bodó, *Injury*, 2008, **39**, 32–39.

23 D. C. Crawford, T. M. DeBerardino and R. J. Williams, *J. Bone Jt. Surgery-American Vol.*, 2012, **94**, 979–989.

24 T. Takato, Y. Mori, Y. Fujihara and Y. Asawa, 2014, **11**, 45–51.

25 T. M. O'Shea and X. Miao, *Tissue Eng. Part B. Rev.*, 2008, **14**, 447–464.

26 M. G. Haugh and S. C. Heilshorn, *Curr. Opin. Solid State Mater. Sci.*, 2016, **20**, 171–179.

27 N. Kawazoe, C. Inoue, T. Tateishi and G. Chen, *Biotechnol. Prog.*, 2010, **26**, 819–826.

28 G. Chen, T. Sato, T. Ushida, R. Hirochika, Y. Shirasaki, N. Ochiai and T. Tateishi, *J. Biomed. Mater. Res. - Part A*, 2003, **67**, 1170–1180.

29 R. Lanza, J. Gearhart, B. Hogan, D. Melton, R. Pedersen, D. Thomas, J. Thomson and I. Wilmut, Eds., *Essentials of Stem Cell Biology*, Academic Press, San Diego, CA, 2009.

30 D. W. Hutmacher, *Scaffolds in tissue engineering bone and cartilage*, Woodhead Publishing Limited, 2006, vol. 21.

31 W. Knudson and R. F. Loeser, *Cell. Mol. Life Sci.*, 2002, **59**, 36–44.

32 J. Wang, J. De Boer and K. De Groot, *J. Dent. Res.*, 2008, **87**, 650–654.

33 A. Higuchi, Q. D. Ling, S. T. Hsu and A. Umezawa, *Chem. Rev.*, 2012, **112**, 4507–4540.

34 I. Ullah, R. B. Subbarao and G. J. Rho, *Biosci. Rep.*, 2015, **35**, 1–18.

35 A. Higuchi, Q.-D. Ling, Y.-A. Ko, Y. Chang and A. Umezawa, *Chem. Rev.*, 2011, **111**, 3021–3035.

36 A. Higuchi, Q. Ling, Y. Chang, S. Hsu and A. Umezawa, *Chem. Rev.*, 2013, **113**, 3297–3328.

37 A. Higuchi, Q. D. Ling, Y. Chang, S. T. Hsu and A. Umezawa, *Chem. Rev.*, 2013, **113**, 3297–3328.

38 H. Y. Lin, W. C. Tsai and S. H. Chang, *J. Biomater. Sci. Polym. Ed.*, 2017, **28**, 664–678.

39 L. F. Fernandes, M. A. Costa, M. H. Fernandes and H. Tomás, *Connect. Tissue Res.*, 2009, **50**, 336–346.

40 R. A. Somoza, J. F. Welter, D. Correa and A. I. Caplan, *Tissue Eng. Part B Rev.*, , DOI:10.1089/ten.teb.2013.0771.

41 X. Li, Y. Teng, J. Liu, H. Lin, Y. Fan, X. Zhang, R. L. Mauck, A. R. Horwitz, A. B. Tekinay, M. O. Guler, W. K. Aicher, J. P. Stegemann, M. L. Hart, B. Kurz, G. Klein and B. Rolauffs, *J. Mater. Chem. B*, 2017, **5**, 5109–5119.

42 A. J. Engler, S. Sen, H. L. Sweeney and D. E. Discher, *Cell*, 2006, **126**, 677–689.

43 V. Irawan, T. Sugiyama and T. Ikoma, *Key Eng. Mater.*, 2016, **696**, 121–128.

44 A. Higuchi, Q.-D. Ling, S. S. Kumar, Y. Chang, A. A. Alarfaj, M. A. Munusamy, K. Murugan, S.-T. Hsu and A. Umezawa, *J. Mater. Chem. B*, 2015, **3**, 8032–8058.

45 A. Higuchi, S. S. Kumar, G. Benelli, A. A. Alarfaj, M. A. Munusamy, A. Umezawa and K. Murugan, *Trends Biotechnol.*, 2017, **35**, 1102–1117.

46 G. M. Harbers and K. E. Healy, *J. Biomed. Mater. Res. - Part A*, 2005, **75**, 855–869.

47 X. Wang, C. Yan, K. Ye, Y. He, Z. Li and J. Ding, *Biomaterials*, 2013, **34**, 2865–2874.

48 E. Schuh, J. Kramer, J. Rohwedel, H. Notbohm, R. Müller, T. Gutsmann and N. Rotter, *Tissue Eng. Part A*, 2010, **16**, 1281–1290.

49 C. M. Murphy, A. Matsiko, M. G. Haugh, J. P. Gleeson and F. J. O'Brien, *J. Mech. Behav. Biomed. Mater.*, 2012, **11**, 53–62.

50 N. Huebsch, E. Lippens, K. Lee, M. Mehta, S. T. Koshy, M. C. Darnell, R. M. Desai, C. M. Madl, M. Xu, X. Zhao, O. Chaudhuri, C. Verbeke, W. S. Kim, K.

Alim, A. Mammoto, D. E. Ingber, G. N. Duda and D. J. Mooney, *Nat. Mater.*, 2015, **14**, 1269–1277.

51 O. Chaudhuri, L. Gu, D. Klumpers, M. Darnell, S. A. Bencherif, J. C. Weaver, N. Huebsch, H. Lee, E. Lippens, G. N. Duda and D. J. Mooney, *Nat. Mater.*, 2016, **15**, 326–334.

52 Q. Zhang, H. Lu, N. Kawazoe and G. Chen, *Acta Biomater.*, 2014, **10**, 2005–2013.

53 D. W. Hutmacher, *Biomaterials*, 2000, **21**, 2529–2543.

54 N. Davidenko, C. F. Schuster, D. V. Bax, N. Raynal, R. W. Farndale, S. M. Best and R. E. Cameron, *Acta Biomater.*, 2015, **25**, 131–142.

55 L. H. Bernstein, Integrins, Cadherins, Signaling and the Cytoskeleton.

56 M. Barczyk, S. Carracedo and D. Gullberg, *Cell Tissue Res.*, 2010, **339**, 269–280.

57 Z. Lu, B. Z. Doulabi, C. Huang, R. a Bank and M. N. Helder, *Tissue Eng. Part A*, 2010, **16**, 81–90.

58 P. Nykvist, H. Tu, J. Ivaska, J. Ka and T. Pihlajaniemi, *J. Biol. Chem.*, 2000, **275**, 8255–8261.

59 H. Zhu, N. Mitsuhashi, A. Klein, L. W. Barsky, K. Weinberg, M. L. Barr, A. Demetriou and G. D. Wu, *Stem Cells*, 2006, **24**, 928–935.

60 Y. Takeuchi, M. Suzawa, T. Matsumoto and J. B. Chem, *J. Biol. Chem*, 1997, **272**, 29309–29316.

61 S. V. Plotnikov, A. M. Pasapera, B. Sabass and C. M. Waterman, *Cell*, 2012, **151**, 1513–1527.

62 M. Guvendiren and J. A. Burdick, *Nat. Commun.*, 2012, **3**, 792–799.

63 J. H. Wen, L. G. Vincent, A. Fuhrmann, Y. S. Choi, K. C. Hribar, H. Taylor-Weiner, S. Chen and A. J. Engler, *Nat. Mater.*, 2014, **13**, 979–987.

64 C. R. Lee, A. J. Grodzinsky and M. Spector, *Biomaterials*, 2001, **22**, 3145–3154.

65 L. Galois, S. Hutasse, D. Cortial, C. F. Rousseau, L. Grossin, M. C. Ronziere, D. Herbage and A. M. Freyria, *Biomaterials*, 2006, **27**, 79–90.

66 M. G. Haugh, C. M. Murphy, R. C. McKiernan, C. Altenbuchner and F. J. O'Brien, *Tissue Eng. Part A*, 2011, **17**, 1201–1208.

67 M. Ngiam, S. Liao, A. J. Patil, Z. Cheng, C. K. Chan and S. Ramakrishna, *Bone*, 2009, **45**, 4–16.

68 M. Tamaddon, M. Burrows, S. A. Ferreira, F. Dazzi, J. F. Apperley, A. Bradshaw, D. D. Brand, J. Czernuszka and E. Gentleman, *Sci. Rep.*, 2017, **7**, 43519.

69 M. D. Shoulders and R. T. Raines, *Annu. Rev. Biochem.*, 2009, **78**, 929–958.

70 L. Cao, V. Lee, M. E. Adams, C. Kiani, Y. Zhang, W. Hu and B. B. Yang, *Matrix Biol.*, 1999, **18**, 343–355.

71 A. K. Kundu and A. J. Putnam, *Biochem. Biophys. Res. Commun.*, 2006, **347**, 347–357.

72 J. Farjanel, G. Schürmann and P. Bruckner, *Osteoarthr. Cartil.*, , DOI:10.1053/joca.2001.0445.

73 D. Bosnakovski, M. Mizuno, G. Kim, S. Takagi, M. Okumura and T. Fujinaga, *Biotechnol. Bioeng.*, 2006, **93**, 1152–1163.

74 M. Kino-Oka, S. Yashiki, Y. Ota, Y. Mushiaki, K. Sugawara, T. Yamamoto, T. Takezawa and M. Taya, *Tissue Eng.*, 2005, **11**, 597–608.

75 S. Liu, J. Wu, X. Liu, D. Chen, G. L. Bowlin, L. Cao, J. Lu, F. Li, X. Mo and C.

Fan, *J. Biomed. Mater. Res. - Part A*, 2015, **103**, 581–592.

76 G. Chen, T. Sato, J. Tanaka and T. Tateishi, *Mater. Sci. Eng. C*, 2006, **26**, 118–123.

77 S. Zhang, L. Chen, Y. Jiang, Y. Cai, G. Xu, T. Tong, W. Zhang, L. Wang, J. Ji, P. Shi and H. W. Ouyang, *Acta Biomater.*, 2013, **9**, 7236–7247.

78 A. M. Yousefi, M. E. Hoque, R. G. S. V. Prasad and N. Uth, *J. Biomed. Mater. Res. - Part A*, 2015, **103**, 2460–2481.

79 C. Csaki, U. Matis, A. Mobasheri, H. Ye and M. Shakibaei, *Histochem. Cell Biol.*, 2007, **128**, 507–520.

80 W. Dai, N. Kawazoe, X. Lin, J. Dong and G. Chen, *Biomaterials*, 2010, **31**, 2141–2152.

81 T. J. Levingstone, A. Matsiko, G. R. Dickson, F. J. O'Brien and J. P. Gleeson, *Acta Biomater.*, 2014, **10**, 1996–2004.

82 V. Irawan, Y. Sasaki and T. Ikoma, *J. Mater. Chem. B*, , DOI:10.1039/C9TB00791A.

83 A. Tampieri, M. Sandri, E. Landi, D. Pressato, S. Francioli, R. Quarto and I. Martin, *Biomaterials*, 2008, **29**, 3539–3546.

84 B. A. Harley, A. K. Lynn, Z. Wissner-Gross, W. Bonfield, I. V. Yannas and L. J. Gibson, *J. Biomed. Mater. Res. - Part A*, 2010, **92**, 1066–1077.

85 G. S. Kumar and E. K. Girija, *Ceram. Int.*, 2013, **39**, 8293–8299.

86 Y. Fan, K. Duan and R. Wang, *Biomaterials*, 2005, **26**, 1623–1632.

87 J. Zhuang, J. Lin, J. Li, W. Weng, K. Cheng and H. Wang, *Colloids Surfaces B Biointerfaces*, 2015, **136**, 479–487.

88 F. Jiang, H. Hörber, J. Howard and D. J. Müller, *J. Struct. Biol.*, 2004, **148**, 268–

278.

89 F. Chicatun, C. E. Pedraza, N. Muja, C. E. Ghezzi, M. D. McKee and S. N. Nazhat, *Tissue Eng. Part A*, 2013, **19**, 2553–2564.

90 A. Sionkowska and J. Kozłowska, *Int. J. Biol. Macromol.*, 2013, **52**, 250–259.

91 Z. Chen, X. Mo, C. He and H. Wang, *Carbohydr. Polym.*, 2008, **72**, 410–418.

92 X. Wang, L. Sang, D. Luo and X. Li, *Colloids Surfaces B Biointerfaces*, 2011, **82**, 233–240.

93 X. Liu, N. Dan, W. Dan and J. Gong, *Int. J. Biol. Macromol.*, 2016, **82**, 989–997.

94 B. B. Christensen, *Dan. Med. J.*, 2016, **63**, 1–27.

95 T. Hayakawa, C. Mochizuki, H. Hara, T. Fukushima, F. Yang, H. Shen, S. Wang and M. Sato, *J. Hard Tissue Biol.*, 2009, **18**, 7–12.

96 W. W. Thein-Han and R. D. K. Misra, *Acta Biomater.*, 2009, **5**, 1182–1197.

97 J. Barralet, S. Best and W. Bonfield, *J. Biomed. Mater. Res.*, 1998, **41**, 79–86.

98 M. Hott, B. Noel, D. Bernache-Assolant, C. Rey and P. J. Marie, *J. Biomed. Mater. Res.*, 1997, **37**, 508–516.

99 D. Septiadi, F. Crippa, T. L. Moore, B. Rothen-Rutishauser and A. Petri-Fink, *Adv. Mater.*, 2018, **30**, 1–30.

100 N. Tran and T. J. Webster, *Acta Biomater.*, 2011, **7**, 1298–1306.

101 Q. Wang, B. Chen, F. Ma, S. Lin, M. Cao, Y. Li and N. Gu, *Nano Res.*, 2017, **10**, 626–642.

102 R. Hou, G. Zhang, G. Du, D. Zhan, Y. Cong, Y. Cheng and J. Fu, *Colloids Surfaces B Biointerfaces*, 2013, **103**, 318–325.

103 K. Lai, W. Jiang, J. Z. Tang, Y. Wu, B. He, G. Wang and Z. Gu, *RSC Adv.*, 2012, **2**, 13007–13017.

104 J. Zhang, S. Zhao, M. Zhu, Y. Zhu, Y. Zhang, Z. Liu and C. Zhang, *J. Mater. Chem. B*, 2014, **2**, 7583–7595.

Chapter 2-Effect of Collagen Structures on Biological Properties of Hydroxyapatite and Collagen Scaffolds

Chapter 2 describes the investigation of influence of collagen structures (monomeric / fibrillar) to the biological properties of collagen/HAp scaffold (attached cells morphology, proliferation, cell-exerted forces). Monomeric scaffolds (sponge porous body) was fabricated by direct freeze-drying of collagen/HAp suspension; whereas, fibrillar sponges were fabricated by phosphate-buffered saline (PBS) neutralization of collagen/HAp suspension of similar concentration as to induce formation of collagen fibrls. All of the fabricated sponges showed similar initial condition (chemical composition, crosslinking degree, HAp/collagen ratio). However, monomeric sponge showed smooth appearance of pore walls in contrast to fibrous pore walls of fibrillar sponge. Monomeric sponge exhibited lower compressive modulus and strength (albeit at the same order of magnitude) and lower water-retaining capacity to fibrous pore walls suggesting the monomeric and fibrillar characteristic for each sponge. Fibroblast exhibited flattened morphology when attached on monomeric sponge and elongated morphology on fibrillar sponge. Cell numbers of fibroblast cultured on monomeric sponge was significantly lower at day 1, 3, 6 to fibrillar sponge. Furthermore, high fibrillar sponge exhibited larger scaffold shrinkage to monomeric sponge after 6 day of culture, suggesting the extensive cell-exerted contraction for fibrillar sponge. This study provides the initial proofs that collagen structures (monomeric/fibrillar) of collagen/HAp scaffolds are the important parameter in modulating cell activities (cell morphology, proliferation, cell-exerted contraction).

2.1. Introduction

As explained in Chapter 1, physical and chemical properties of collagen scaffolds (pore

size [1], compressive modulus [2,3], biopolymer blending [4,5]) was widely known to influence the biological properties of scaffolds (attached cells morphology, proliferation, differentiation, and modulation of cell-exerted forces), which provides significant insights for the designs of important parameters for tissue-engineering scaffolds applications. Nonetheless, influences of collagen structures (monomeric / fibrillar) to cell activities are the rarely investigated relationship.

Collagen-based scaffolds are generally fabricated from collagen precursors exhibiting either monomeric or fibrillar structures [6–8]. Monomeric collagen is triple-helices molecule (width size 5 nm) which are stably suspended in low pH aqueous solution (pH 3-5) owing to the electrostatic repulsion imparted by the positively charged molecules [9,10]. The liquid state of monomeric collagen permits flexible modification of composition and rapid processing into the porous bodies by freeze-drying or electrospinning methods [11]. On the other hand, fibrillar structures of collagen could be achieved by neutralizing the pH or increasing the ionic strength of monomeric collagen solution; this in turn causes the monomeric collagen to self-assemble to fibrillar structure with finite width size (30-200 nm) [9,12]. The fibrillar structures form the network which bind water molecules, causing the change of liquid into gel-like state material which could be further transformed into porous bodies by freeze-drying [13]. The transition is less desired from the material fabrication perspective, as it involves additional step to induce fibril formation; gel-like state is also more difficult to process compared to liquid state (e.g., unable to fully fill the mold space) [11,14]. Nonetheless, native structure of collagen in mammalian tissue is fibrillar form [15], thereby collagen scaffold fabricated from fibrillar collagen was expected to support cell basic activities, namely cell proliferation, superior to monomeric collagen scaffold.

The main goal of the current study was to investigate the influences of collagen fibrillar state (monomeric/fibrillar) in collagen/HAp sponges to the proliferation capacity of fibroblast cultured on the corresponding sponges. Initially, the physical, chemical, and cross-linking degree of sponges were confirmed to be identical as to exclude the factors that might confound the fibroblast proliferation rate. Next, the monomeric and fibrillar characteristic of sponges were assessed by mechanical and swelling capacity characterization. Lastly, cell culture experiment with fibroblast was conducted on each sponge as to elucidate the influence of collagen structure to cell morphology and proliferation capacity. Mechanism on how collagen structures influence cell activities was also discussed based on the obtained data.

2.2. Methods and Experiments

Porcine skin collagen dissolved in HCl (0.62 wt%) was kindly supplied by Nitta Gelatin Co., Ltd. (Osaka, Japan). 6 M HCl, NaOH pellet, $CaCO_3$ powder, 85% H_3PO_4, 99.5% ethanol, and 99% *t*-butanol were purchased from Wako Pure Chemical Industries, Ltd. (Tokyo, Japan). Phosphate Buffered Saline (PBS) Dulbecco's formula (without Calcium and Magnesium) tablets were purchased from DS Pharma Biomedical, Ltd. (Osaka, Japan).

Hydroxyapatite (HAp, $Ca_{10}(PO_4)_6(OH)_2$) powder was prepared by a wet chemical method [16]. $CaCO_3$ powder was calcined at 1050°C for 3 hours to obtain CaO powder; appropriate amount of CaO powder was mixed with ion-exchanged water to obtain 0.5 mol/L of $Ca(OH)_2$ suspension. pH of suspension was adjusted to 7.8 by addition of 0.6 mol/L H_3PO_4. The suspension was spray-dried with a mini-spray drier (B-290, Büchi, Switzerland) under the inlet and outlet temperatures of 180°C and 60°C. The crystalline phase of the spray-dried particles heated at 1200°C for 30 minute were identified by using

X-ray diffractometry (XRD: X'Pert PRO, Philips, Netherlands).

The starting suspension of collagen/HAp was prepared by adding a particular amount of HAp powder to 0.62 wt% collagen to obtain 0.125 wt %. The solution was stirred at low temperature until all the powder was homogeneously dispersed in the solution. pH after stirring was 5.7 and the pH was adjusted to 5.0 with addition of 6 M HCl.

2.2.1 Fabrication of monomeric sponges

0.5wt% collagen/ 0.1wt% HAp suspension was obtained by adding dilute HCl (pH 5.0) to the previously prepared 0.62 wt% collagen/ 0.125 wt% HAp suspension. The diluted suspension was poured into square polycarbonate mold (length = 2.5 cm, height = 1.0 cm). The sample at this stage was named collagen/HAp solution. The mold was put onto freezer for rapid cooling to -20°C, and subsequently held at -20°C for 24 hours before subjected to freeze-drying overnight.

2.2.2 Fabrication of fibrillar sponges

0.62 wt% Collagen/ 0.125 wt% HAp suspension was mixed with x10 PBS in 9 : 1 volume ratio and subsequently adjusted to 0.5 wt% Collagen/ 0.1 wt% HAp by addition of HCl solution (pH 5.0). pH of the solution after addition of x10 PBS was 6.3. The collagen/HAp suspension was quickly hand-stirred and poured into square polycarbonate mold (length = 2.5 cm, height = 1.0 cm). Next, the mold was held at 28°C for 12 hours in order to complete fibril formation process. The resulting samples was gel-like state and the gel was subjected to freezing and freeze-drying in the exact manner with samples fabricated by direct-freeze drying method. The obtained sponges were subsequently washed with 75% ethanol as to remove the precipitated salt and subsequently re-

lyophilized. pH universal indicator was added to collagen/HAp suspension in order to observe final pH before the freezing stage.

2.2.3 Crosslinking of collagen/HAp sponge

All of the collagen sponges were crosslinked twice, firstly by dehydrothermal and secondly by carbodiimide chemistry. For dehydrothermal crosslinking, collagen was held at temperature 105°C for 24h in a vacuum of 0.05 bar. Next, sponges were subjected to carbodiimide crosslinking; 1-ethyl-3-3-dimethyl aminopropyl carbodiimide (EDC) was used to crosslink adjacent collagen molecules and *N*-Hydroxysuccinimide (NHS) was added as a crosslink catalyst. The concentration of EDC was 6 mM per gram of scaffold; a molar ratio of 2.5M EDAC/M NHS was used for all EDAC crosslinking [17,18]. These concentrations were prepared in 8 mL of 75% ethanol and the samples were crosslinked at room temperature for 4 hours. Samples were washed with 75% ethanol for 2x, ion-exchanged water for 3x, and subsequently re-lyophilized. Characterizations of sponges were all conducted for crosslinked samples. Samples obtained by freeze-drying collagen/HAp solution and gel-like state were named as monomeric and fibrillar sponges.

2.2.4 Characterization of fibril formation

The fibril formation on PBS-neutralized samples was observed by initially subjecting the hydrogel to dehydration series as follow: soaking in 50%, 60%, 70%, 80%, 90% ethanol for 1 hour each and followed by soaking in 99% ethanol for 1 hour (3 times). Lastly, sample was soaked in t-butanol for 12 hours (3 times), frozen at 0°C and freeze-dried. The fibril size of hydrogel was measured with JSmile view software; 20 instances of fibers were measured from section of dehydrated gel. The final fibril size was the

average of fibril from four different sections for each condition (n=4).

The denaturation temperature of collagen was determined by differential scanning calorimetry (DSC: DSC-8230, Rigaku, Japan). Sample of monomeric collagen was prepared by air-drying collagen/HAp solution, whereas sample for fibrillar collagen was obtained from dehydrated gel [19]. ~3 mg samples were initially hydrated with PBS by vortex mixing and subsequently sealed in the hermetic aluminum pan. An empty hermetic aluminum pan was used as a reference. Sample pan was equilibrated at 25°C for 20 minutes, and subsequently heated to 120°C at cooling rate 3°C/min. The minima point of endothermic peak observed at 40-55°C was determined as denaturation temperature.

2.2.5 Analysis of physical dimensions of sponges

The gross appearance of sponges was recorded with digital camera. Chemical groups of sponges were characterized with Fourier Transform Infra-red. Small cut of sponge was mixed with KBr pellet and hand-pressed to obtain transparent disk; measurement was conducted in transmission mode. Pure KBr disk was used as background.

The dry weight of as-crosslinked sponges was measured with a mass balance; the diameter and thickness were measured with a vernier caliper. Porosity was defined as the percentage of void space in a 3D-sponge and was calculated by the relative density:

$$\text{Porosity (\%)} = (1-\boldsymbol{\rho}_{\text{scaffold}} / \boldsymbol{\rho}_{\text{solid}}) \times 100$$

where, $\boldsymbol{\rho}_{\text{scaffold}}$ is the density of collagen sponges post-crosslinking, the fraction of collagen and HAp form the total mass was measured by TG-DTA data as will be explained later section. $\boldsymbol{\rho}_{\text{solid}}$ is the theoretical composite density of non-porous collagen (0.5

wt%)/HAp(0.1 wt%). Density of 1.3 g ml and 3.2 g ml were selected for collagen and HAp, respectively.

2.2.6 Analysis of microstructures of sponges

The structure of sponges was analyzed using scanning electron microscopy (SEM) (JEOL 840 73, Joel, Japan). Transversal sections of were sputter coated with platina before observation under SEM. Pore size of sponges was measured with JSMILE view, by averaging 50 instances of measured pore size taken from four random sections (n = 4).

2.2.7 Analysis of HAp/collagen ratio of sponges

Fraction of collagen/HAp was determined by TG-DTA (TG-8120, Rigaku, Japan). Sample weight of 3 - 5 mg was heated (15 K/min) from room temperature to 700°C in a static air condition. Alumina (α-A_2O_3) of similar mass was used as a reference sample. Burned masses up to 600°C were determined as collagen part whereas remaining masses was determined as HAp.

2.2.8 Analysis of crosslinking degree of sponges

Crosslinking degree of collagen/HAp sponges was determined using a 2,4,6-trinitro-benzene- sulfonic acid (TNBS) assay with a protocol similar to previous reports [20]. Each sample (2– 4 mg) was added into the solution of 0.5 ml of a 4% (w/v) $NaHCO_3$ and 0.5 ml 0.05% (w/v) TNBS. After 2 h at 40 °C, 1.5 ml of 6 M HCl was added and the samples were further heated at 60 °C for 90 min. The reaction mixture was diluted with ion-exchanged water (2.5 ml) and cooled to room temperature. Absorbance of solution at 320 nm was measured using a ultraviolet-visible spectrophotometer (UV-VIS: UV2450,

Shimadzu, Japan). Blank samples were prepared using the same procedure, except that HCl was added before introducing the TNBS solution. The concentration of free amine groups was calculated by the following equation:

$$[NH_2] = \frac{A \text{ x } V}{\varepsilon \text{ x } l \text{ x } m}$$

where $[NH_2]$ is the free amine group concentration (mol g^{-1}), A is the absorbance, V is the solution volume (ml), ε = 14.600 (ml $mmol^{-1}$ cm^{-1}), l is the path length (cm), m is the weight of the sample (mg). The free amine concentration of crosslinked and non-crosslinked collagen were used to determine the degree of crosslinking which calculated with the following formula:

$$D = \left(\frac{[NH_2]_{non-crosslinked} - [NH_2]_{crosslinked}}{[NH_2]_{non-crosslinked}}\right) \text{ x } 100\%$$

Comparison of means between samples was analyzed by two-tail Student's *T*-test ($p<0.05$).

Chemical composition was determined with Fourier-Transform Infrared (FTIR: DR-81, JASCO). Briefly, thin slice of collagen sponge was pressed with KBr to obtain the transparent disk. The disk was subsequently analyzed with FTIR in transmission mode. Background spectrum was initially measured by using KBr purchased from Wako Pure Chemical Industries, Ltd (Japan) at the wavenumber range of 4,000 - 400 cm^{-1}, resolution of 4.0 cm^{-1}, and accumulation times at 256. FTIR spectra of the mixture of KBr and composites were mixed at 100:1 in weight was subsequently measured under the same condition.

2.2.9 Analysis of mechanical properties of sponges

Compressive modulus and strength of sponges were determined by compressive testing (TA-XT2, Stable Micro Systems, UK) fitted with a 5-N load cell. Samples of 8 mm diameter and 4 mm height (n = 4 per group) were punched from the as-crosslinked sponges. Mechanical testing was conducted in wet conditions. Wet samples were prehydrated in PBS at 4°C for 24 h before testing. Amount of PBS was dropped onto samples during testing to keep the hydrated state of samples. Testing was conducted at a strain rate of 6 mm/min to achieve a strain of 60% The modulus was defined as the slope of a linear fit to the stress–strain curve over 1%–5% strain. Stress at a strain of 30% was employed as compressive strength [21]. Comparison of means between samples was analyzed by two-tail Student's *T*-test ($p<0.05$).

2.2.10 Analysis of swelling properties of sponges

Cylindrical samples (diameter 5 mm, thickness 2 mm) were punched from crosslinked samples and the corresponding dry weight (m_d) was measured by electronic balance. Sponge was submerged in 1 ml PBS and incubated at 37°C for up to 48 hours. Sponges were taken at regular intervals (1 h, 24 h, 48h); the water-uptake capacity (m_w) were measured directly, whereas the water-retaining (m_s) was measured after blotting the submerged sponges on filter paper. Two different measurements of swelling capacity to retain water were made [22]:

1. The ability of the scaffold structure to absorb fluid (the material and the pores)

Water-uptake (%) = $\frac{M_w - M_d}{M_d}\ x\ 100$

2. Fluid retaining by scaffold material (PBS from pores is removed):

Water-retaining (%) = $\frac{M_s - M_d}{M_d}$ x 100

Comparison of means between groups was analyzed by one-way ANOVA ($p<0.05$).

2.2.11 Cell Culture Experiment

NIH3T3 (Wako Pure Chemicals Ltd., Japan) were expanded on 90 mm dishes using DMEM (DMEM; Wako Pure Chemicals Ltd., Japan) supplemented with 10% fetal bovine serum (FBS; CELLect, MP Biomedicals Inc., France) and 1% penicillin/ streptomycin (Wako Pure Chemicals Ltd., Japan). Cells were passaged at 80% confluence by using trypsin–ethylene diamine tetraacetic acid (Trpysin-EDTA; Wako Pure Chemicals Ltd., Japan) and cells below passage 20 were used for in vitro analysis

(37°C, 5% CO2)

Collagen/HAp sponges were sterilized in 70% ethanol for 1 hour, 2 times. Sponges were washed with autoclaved PBS and conditioned overnight in serum-free DMEM. Before cell seeding, sponges were dried with sterilized filter paper. Sponges were placed in the non-treated well plate; 100 μL of the cell suspension ($2.5x10^5$ cells) were dropped on top of the dried sponges. The well plate was returned to incubator and left for 3 hours to allow cell attachment. Following incubation, 400 μL of complete DMEM was added to each well and the plate was returned to the incubator. To assess the cell morphology, a number of cell-seeded sponges at day 6 were rinsed with PBS and fixed with 2.5% glutaraldehyde. Samples were sequentially dehydrated with ethanol series (50%, 70%, 90%, 95%, 100%) and t-butanol. The specimens were re-lyophilized and observed with SEM.

The cell number was measured at day 1, day 3, and day 6 after cell seeding by using Cell Counting Kit-8 (CCK-8: Dojindo Laboratories, Japan). Briefly, 50 μL of CCK-8 was added to each well and the plate was incubated at 37°C for another 2 h. An aliquot of 100 μL was taken from each well and transferred to fresh 96-well plate. The absorbance of these samples was measured at 450 nm with a spectrophotometric microplate reader (Bio-Rad 680, USA). The absorbance value was converted to cell numbers by using calibration curve of known NIH3T3 cell numbers vs absorbance of CCK-8. Proliferation rate was obtained by the following equation:

$$Proliferation\ rate = \frac{Cell\ number\ substracted\ at\ day\ 6\ to\ 1}{Total\ Cell\ Culture\ Days}\ x\ 100$$

To assess the shrinkage of cell-seeded sponges, diameter of sponge at day 0, day 1, day 3, day 6 was continuously measured with a vernier caliper. The shrinkage was expressed in % original diameter, as given in the following equation:

$$\%\ change\ of\ diameter\ = \frac{Diameter\ at\ day\ 1,day\ 3,day\ 6}{Diameter\ at\ day\ 0}\ x\ 100$$

All of the results are expressed as mean ± standard deviation of four-different sponges. Comparison of means between samples was analyzed by two-tail Student's *T*-test ($p<0.05$). All of the previous statistical calculation was conducted with Microsoft Excel.

2.3. Results and Discussion

The appearance and optical density value of collagen/HAp solution and hydrogel was shown in Fig. 2-1. Collagen/HAp solution was clearly translucent (optical density (OD):

0.37± 0.01) and subsequently transformed into turbid gel-like state (OD: 1.61± 0.02) after PBS-addition and heat treatment. The formation of turbid gel-like state (hydrogel) is the characteristic of collagen fibrils formation [23,24]. Collagen fibrils form network structure which attract water, resulting in the gel-like state (hydrogel) material. The formed fibrils exist in nanometer range (30-200 nm), which inhibit the transmittance of optical light, resulting in the turbid structure [10,25].

Microstructure observation further confirmed this notion (Fig. 2-2). Membrane obtained by air-drying of collagen/HAp solution showed the absence of fibrillar structures whereas dehydrated collagen/HAp hydrogel exhibited mainly the large sized collagen fibril (94 ± 10 nm), indicating complete fibrilogenesis. Molecules of collagen monomers (width size<5 nm) are stably suspended in aqueous solution at low pH (3-5) due to the electrostatic repulsion of positively charged monomers [9]. By increasing the pH value (6-9) and ionic strength of aqueous solution, collagen monomers lost the electrostatic stability and begin to aggregate and self-assemble into fibrillar structure [23,25]. In the current study, the initial pH of collagen/HAp solution was 5.0 and the pH was increased to 6.3 after addition of 10x PBS, thus justifying the initiation of collagen fibrils self-assembly.

The monomeric and fibrilllar properties were further investigated by characterizing the temperature of endothermic peak (denaturation temperature) with DSC analysis (Fig. 2-3). Air dried membrane of collagen/HAp solution exhibited endothermic temperature at 47.1 ± 0.2°C, whereas collagen/HAp hydrogel showed significantly higher endothermic temperature at 52.4 ± 0.3°C. Denaturation temperature was associated with the destruction of triple helix structure of collagen monomer. Observed temperature of collagen/HAp solution (47.1 ± 0.2°C) was slightly higher to previously reported value for

pure monomeric collagen (~40°C) [26], likely to originate from presence of Ca^{2+} and PO_4^{3-} ions from the dissolved HAp which stabilize the bond in the triple helix structure [27]. Formation of collagen fibril in collagen/HAp hydrogel was associated with the increasing of non-covalent bonds (e.g. hydrogen bonds) between adjacent collagen monomers, resulting in the improved thermal stabilizations, which in turn increase the denaturation temperature [27]. Taken together, these results suggested that monomeric and fibrillar collagen was successfully obtained for collagen/HAp solution and hydrogel.

2.3.1 Characterization of obtained sponges

Chemical properties of sponges

As mentioned in experimental section, samples obtained by freeze-drying collagen/HAp solution and hydrogel were respectively named as monomeric and fibrillar sponges.

Fig. 2.4 exhibited the gross appearance of the sponges in wet condition. Monomeric was more transparent compared to the turbid appearance of fibrillar sponges. Table 2-1 summarized the density, porosity, and crosslinking degree of the fabricated sponges. All samples exhibited about similar level of density (0.25 – 0.33 g/cm^3) and porosity (~98%), owing to the same initial conditions of solution and the freeze-drying parameters. Moreover, crosslinking degree of all sponges lied at the similar level (21-22%), as the similar concentrations of EDC/NHS were used.

FTIR analysis of all sponges was shown in Fig. 2-5. Porcine skin collagen showed the bands at 671 cm^{-1} (Amide I), 1535 cm^{-1} (Amide II), and 1225 cm^{-1} (Amide III), consistent with previous study [28]. Monomeric and fibrillar sponge exhibited additional peaks at 1032 cm^{-1}/1080 cm^{-1} and clear doublets at 550 and 580 cm^{-1}, attributable to PO_4^{3-} peaks of HAp [29]. These results indicated the formation of collagen/HAp composite in all of the sponges.

Representative of TG-DTA analysis for fibrillar sponge was shown in Fig. 2-6. The figure showed mass loss up to 250°C (10.2%) accompanied with two endothermic peaks at 73°C and 230°C, which were attributed to water desorption. Further heating showed continuous mass loss up to 600°C (71.2%) accompanied with exothermic peaks at 312°C and 368°C, which were assigned to thermal degradation and combustion of collagen fraction [14,30]. The leftover mass after heating was ~13% which correspond to the inorganic fraction of sponge. FTIR analysis of the leftover mass showed peak characteristic of HAp (data not shown). Other sponges were subjected to similar thermal analysis and each sponge showed similar pattern of TG-DTA curve. HAp (inorganic)/collagen (organic) ratio for each sponge was calculated from the TG-DTA results and summarized in Fig. 2-7. Theoretical inorganic/organic fraction referred to the ratio calculated by assuming ideal composition of 0.5%wt collagen and 0.1wt% HAp. All of sponges exhibited similar level of inorganic/organic ratio (0.16-0.17); albeit, at the value much lower to theoretical ratio. The results were expected as the initially added HAp was slightly dissolved during mixing with collagen solution.

Taken together, these data suggested the similar initial condition for sponges fabricated through direct freeze-drying or/and through hydrogels intermediate.

Microstructure of obtained sponges

Fig. 2.8 showed the microstructure of the fabricated sponges. All samples exhibited elongated pore structures; however, monomeric sponge showed slightly broken pore structure in contrast to the well-defined pore structure of fibrillar sponge. Pore is the negative replica of ice crystal formed during freezing step. The random and stochastic nature of ice formation might cause a numbers of ice crystal to encapsulate the solute

particles (collagen monomers), thus introducing the broken pores [31]. On the other hand, larger size of collagen fibrils prevents the solute encapsulation by ice crystals [32]. As a result, collagen fibrils were densified into the channel between ice crystals, forming well-defined pore structures and prevalent collagen fibers presence on pore wall. Pore size for monomeric and fibrillar sponge was 231 ± 49 nm and 241 ± 39 nm, respectively. The results were expected as the pore size of sponge is determined by the final freezing temperature; which was set to -20°C in the current study.

Characterization of the mechanical and swelling properties of obtained sponges

Compressive modulus and strength of all sponges were given in Fig. 2.9. Fibrillar sponge showed significantly higher compressive modulus to monomeric sponge. Compressive stress also exhibited similar trend, in which fibrillar sponge were stronger to monomeric sponge. The results can be explained by considering the microstructure of sponges. For the fibrous sponges, HAp precipitates (2-3 μm) were closely incorporated inside the pore walls, as evidenced from tight encapsulation of HAp precipitates by collagen fibrils, thus enhancing the load distribution between rigid HAp particles and mechanically weak collagen matrix (5 μm). On the other hand, HAp precipitates were simply embedded in the pore walls, resulting in the mechanically inferior structure.

Swelling properties (water-uptake and -retaining capacity) of monomeric and fibrillar sponge were measured. Water-uptake capacity corresponds to total amount of fluid bound by the pores and pore walls; whereas, water-retaining capacity represents the quantity of fluid retained by the pore walls after fluid in pores was removed.

Fig. 2.10 showed that both of monomeric and fibrillar sponges had similar water-uptake capacity at 1h, 24h, 48h [33,34]. The results were expected as monomeric and fibrillar

sponges has similar dimension, pore size, and porosity, resulting in the identical water-uptake capacity. Interestingly, fibrillar sponge exhibited significantly higher of water-retaining capacity to monomeric sponge at all-time points of measurement. Collagen is a hydrophilic molecule as it contains high amount of polar amino acids (aspartic acid / glutamic acid) capable of binding water molecules. Collagen fibrils in pore walls of fibrillar sponge might form structural network which are more effective in retaining water molecules to monomeric sponge, thereby increasing the water-retaining capacity of fibrilar sponges.

Taken together, these results suggested the successful formation of monomeric and fibrillar sponges.

2.3.2 Characterization of biocompatibility

Morphology of cells (Fig. 2-11) attached on sponges at day 6 showed the flattened morphology for monomeric sponges; in contrast to the elongated morphology for fibrillar sponges. Previous studies associated the different morphology of fibroblast with the distribution of cell-binding sites. The diffuse distribution of cell-binding sites causes the formation of cell receptor-binding site complex at perimeter of cells, resulting in the flattened fibroblast morphology [35,36]. In contrast, the concentrated binding sites causes attachment to occur at particular spots near the perimeter of cells, resulting in the elongated morphology [35,36]. Collagen monomers were randomly distributed on the pore walls of monomeric sponge, implying the diffuse distribution of binding motif (GFOGER), and thus causing cells to assume lamellopodia morphology. On the other hand, binding motif in collagen fibrils was arranged in orderly manner [37]; the fibrils were also closely packed on the pore walls of fibrillar sponges, as evidenced from the SEM

results, suggesting the concentrated distribution of binding site. As a result, fibrillar sponges modulated cells to assume elongated morphology.

Analysis of cell numbers were given in Fig. 2.12. Cells for all of the sponges were increased from day 1 to day 6; however, fibrillar sponge showed significantly larger cell number at all-time points compared to monomeric sponge, implying the higher proliferation rate of cells in fibrillar sponge to monomeric sponge. Analysis of sponge shrinkage was given in Fig. 2.13. Fibrillar sponge showed the insignificantly larger decreasing of original diameter to monomeric sponge at day 3 and 6, suggesting the more extensive shrinkage for fibrillar sponge.

At early days after cell attachment (<day 7), fibroblast with elongated morphology implied the more extensive formation of stress fibers to cells with flattened morphology [35,36]. The higher degree of stress fibers formation was associated with more active proliferation [38]. Furthermore, attached cells exerted the contraction force to the underlying substrate during proliferation or migration; with the magnitude of contraction force dependent on the extent of stress fibers formation [39,40]. In turn, the cell-mediated contraction causes the shrinkage of scaffold. The current data suggested that fibrillar sponge primed cells to assume elongated morphology and subsequently promoted proliferation of fibroblast, likely through the stress fiber-mediated mechanism.

The schematic drawing of distribution of binding sites in monomeric and fibrillar collagen sponges and the subsequent effect on fibroblast were given in Fig. 2.14.

2.4. Summary

Collagen showed two different kinds of structure that is monomeric and fibrillar. In the current study, monomeric and fibrillar sponges were obtained by directly freeze-drying the collagen/HAp suspension and hydrogel, respectively. All sponges exhibited similar

initial conditions, that is pore size, porosity, inorganic/organic ratio, and crosslinking degree. Characteristic of monomeric and fibrillar collagen in the corresponding sponges was confirmed by microstructure observation, mechanical characterization, and swelling properties characterization.

Cell-culture experiment revealed that morphology of fibroblast was dependent on the type of collagen sponges, namely flattened and elongated morphology for monomeric and fibrillar sponge, respectively. The differences in morphology was likely to originate from the different manner of collagen binding site distribution in monomeric and fibrillar collagen. Furthermore, fibrillar collagen exhibited higher cells proliferation and larger sponge shrinkage to monomeric sponge, with the underlying mechanisms linked to morphological differences.

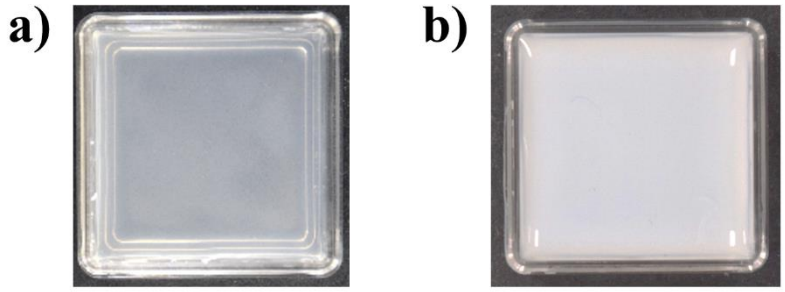

Fig. 2.1 (a) Collagen / HAp solution (pH 5.0 and optical density: 0.37± 0.01) and (b) Collagen/HAp gel-like state after PBS-neutralization and heat treatment at 28°C for 12 h (pH 6.3 and optical density: 1.61± 0.02)

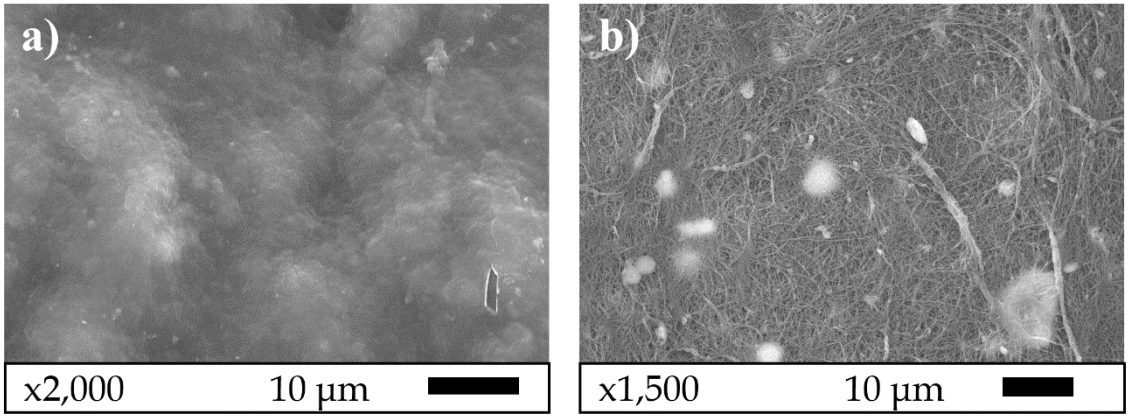

Fig. 2.2 Microstructures of (a) air-dried collagen/HAp membrane, (b) dehydrated collagen/HAp hydrogel

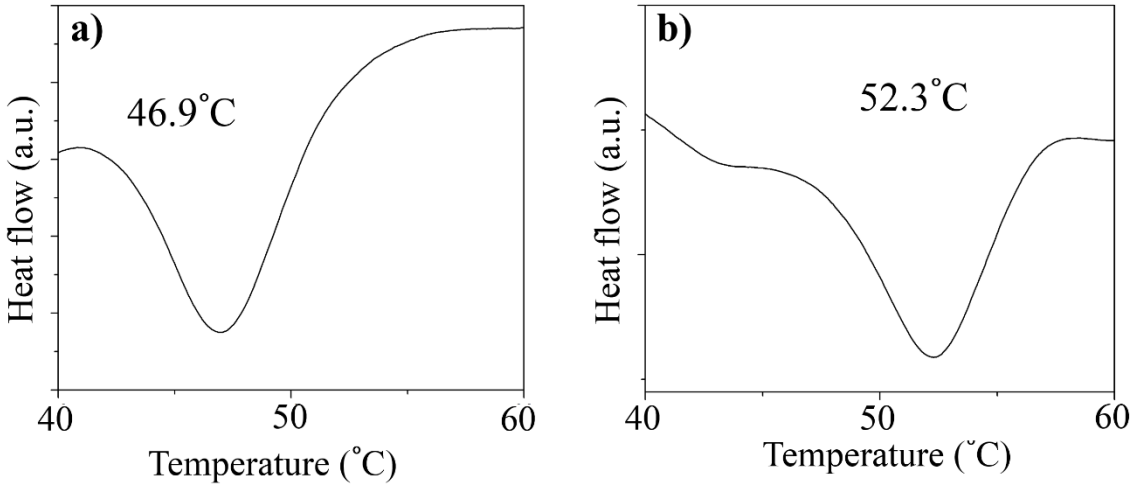

Fig. 2.3 Representative DSC curve and endothermic temperature of (a) air-dried collagen/HAp membrane, (b) dehydrated collagen/HAp hydrogel

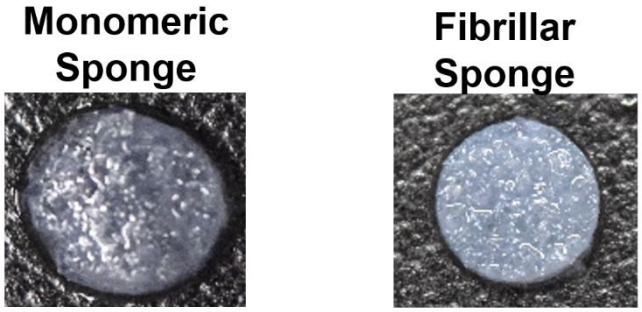

Fig. 2.4 Gross appearance of wetted sponges and associated physical properties

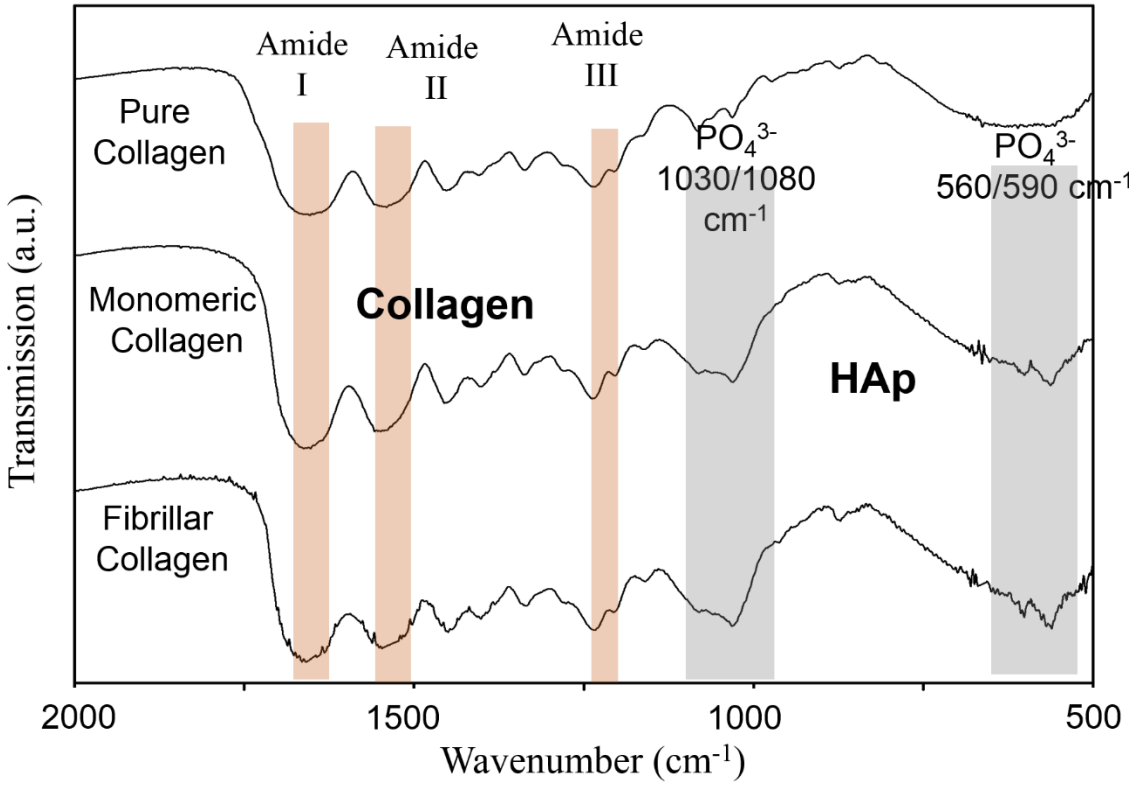

Fig. 2.5 FTIR spectra of fabricated sponges; the brown box indicated the amide peaks associated with collagen whereas the gray box indicated peaks associated with phosphate group of HAp.

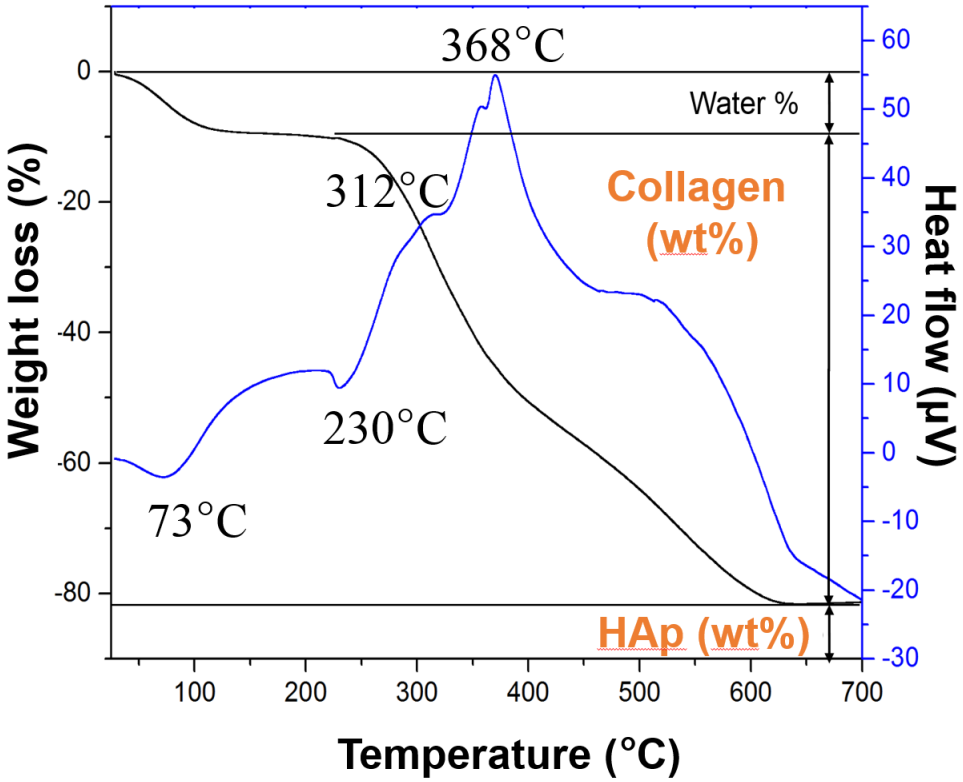

Fig. 2.7 Representative TG-DTA plot of fibrillar spong

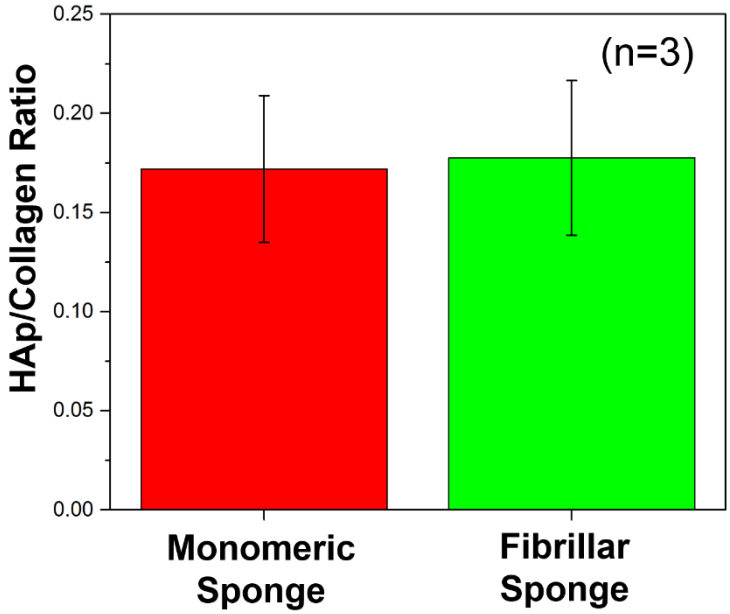

Fig. 2.6 HAp/collagen ratio of fabricated sponges

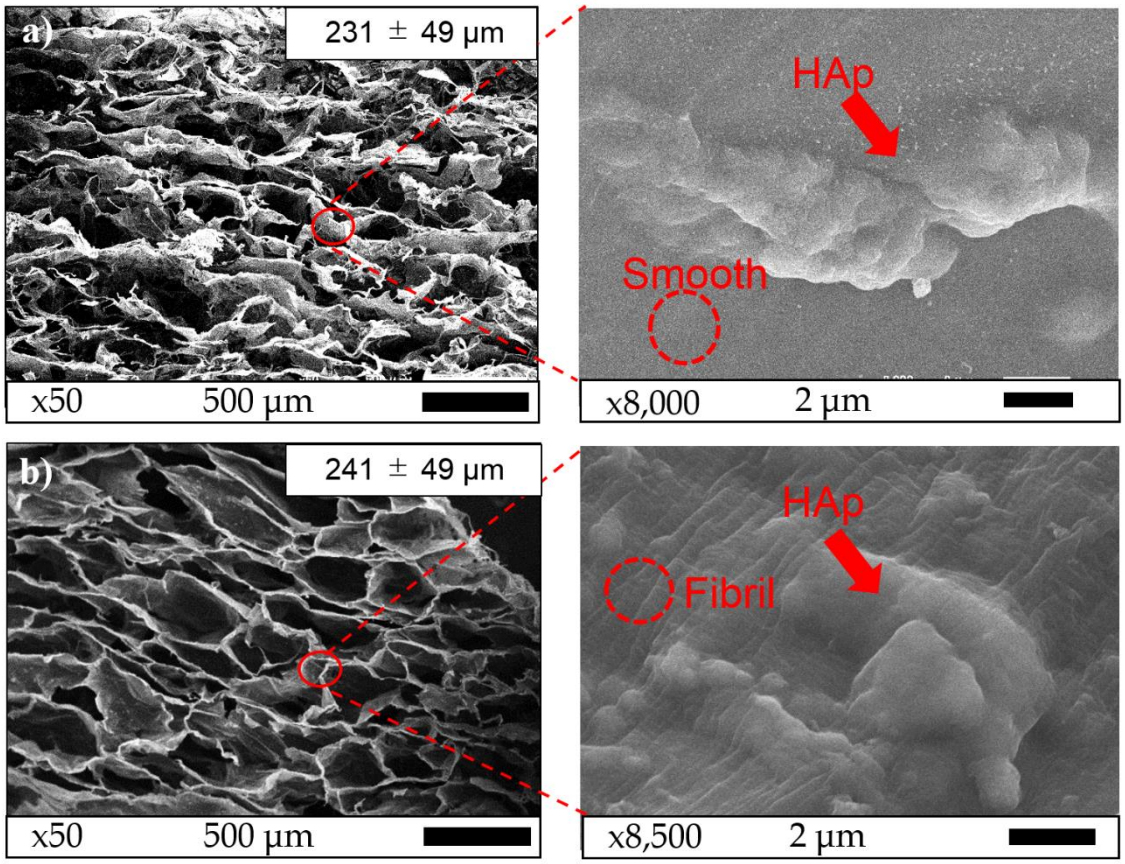

Fig. 2.8 Microstructures images at low and high magnification for (a) monomeric sponges, (b) fibrillar sponges

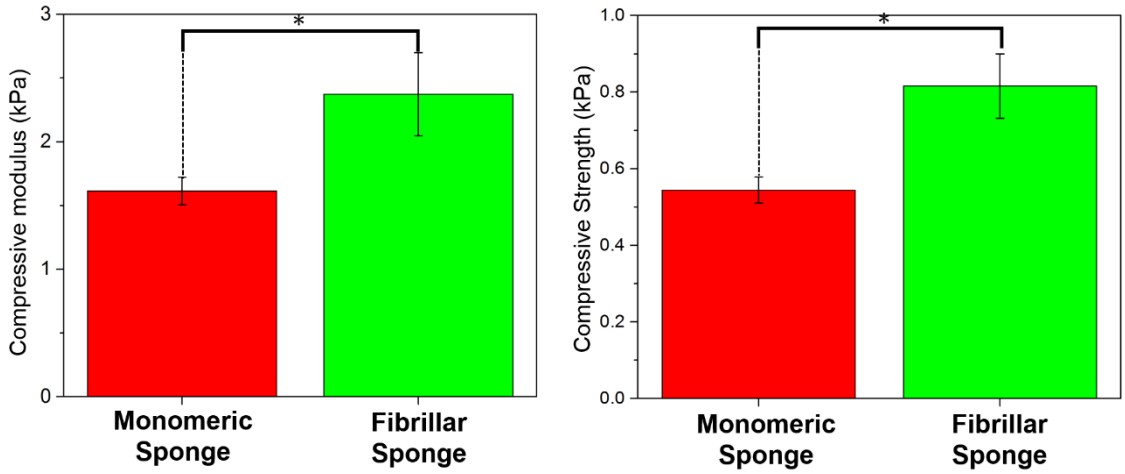

Fig. 2.9 Compressive modulus of compressive strength of the fabricated sponges. n =4, p<0.05

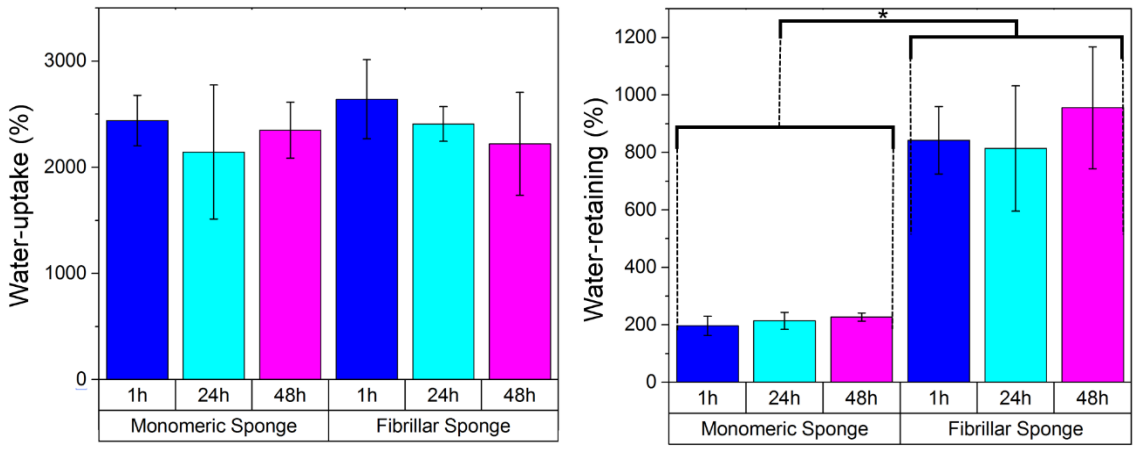

Fig. 2.10 Swelling capacity of scaffolds after 1, 24, 48h immersion in PBS solution. Swelling consist of water-uptake and water-retaining. n =4, $p<0.05$

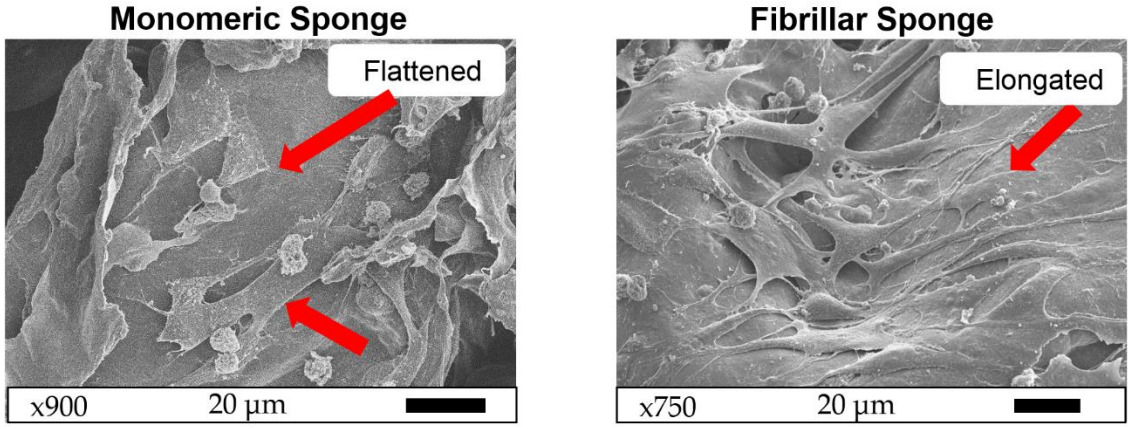

Fig. 2.11 Morphology of cells after 6 days of cell culture

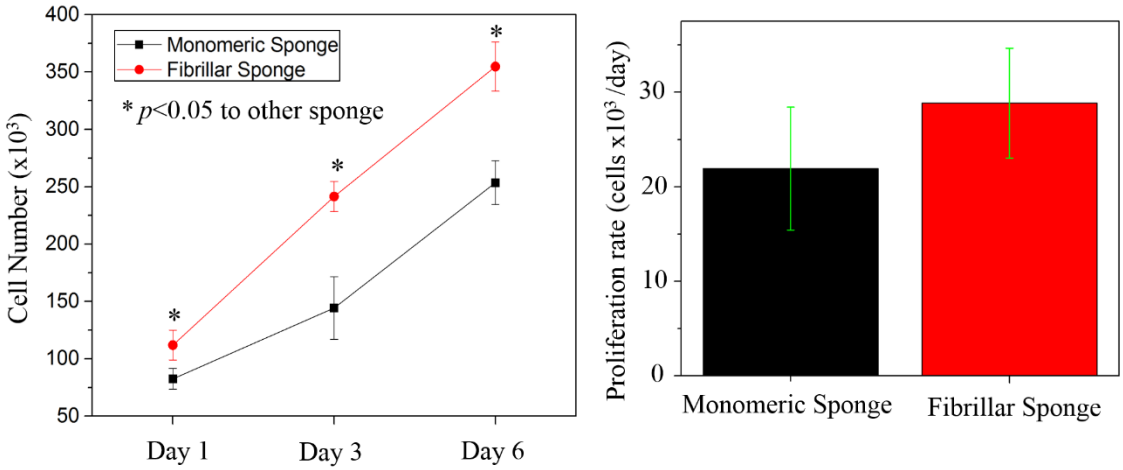

Fig. 2.12 Cells numbers and proliferation rate of fibroblast cultured on the sponges, n =3, *$p<0.05$ to other type of sponges

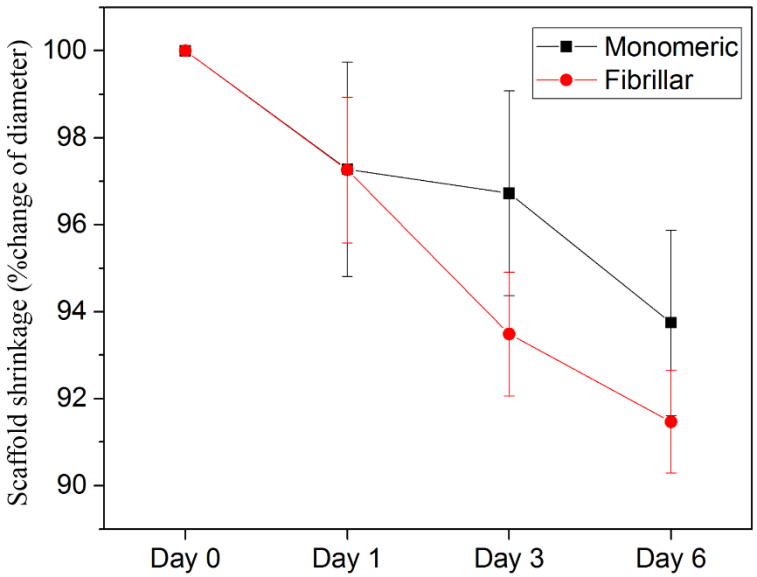

Fig. 2.13 Scaffold shrinkage as expressed in % change of diameter for fabricated sponges

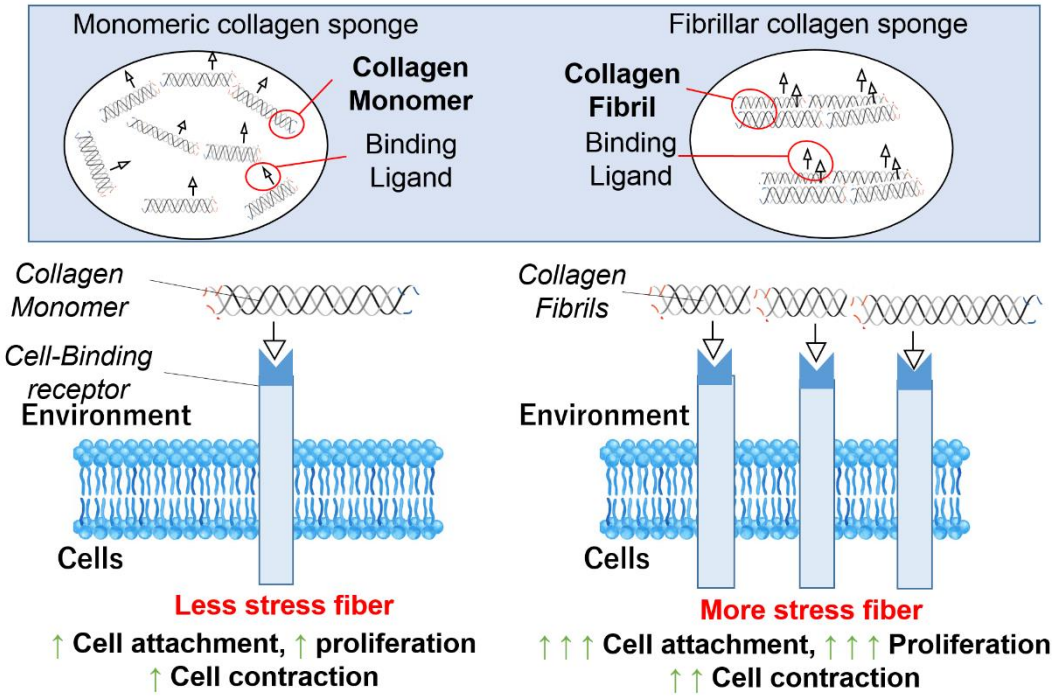

Fig. 2.14 (Blue box figure) Schematic drawing depicting the distribution of binding sites for monomeric and fibrillar collagen sponges. (Bottom figure) Binding between collagen (monomer / fibrils) and cells initiates the formation of isolated/clustered binding complex, which in turn determine the degree of stress fibers formation (red words) and the associated cell activities (cell attachment, proliferation, contraction). Number of green arrow indicates magnitude of the corresponding activities

Table 2.1 Density, porosity, and cross-linking degree of fabricated sponges

	Monomeric	**Fibrillar**
Density (g/cm^3)	0.033± 0.002	0.032± 0.003
Porosity (%)	97.8± 8.8	97.6± 10.8
Cross-linking degree	22.6 % ± 3.9 %	21.3 % ± 5.2 %

References

1 S. M. Lien, L. Y. Ko and T. J. Huang, *Acta Biomater.*, 2009, **5**, 670-679.

2 C. M. Murphy, A. Matsiko, M. G. Haugh, J. P. Gleeson and F. J. O'Brien, *J. Mech. Behav. Biomed. Mater.*, 2012, **11**, 53-62.

3 M. G. Haugh, C. M. Murphy, R. C. McKiernan, C. Altenbuchner and F. J. O'Brien, *Tissue Eng. Part A*, 2011, **17**, 1201-1208.

4 A. Di Martino, M. Sittinger and M. V. Risbud, *Biomaterials*, 2005, **26**, 5983-5990.

5 V. Irawan, T.-C. Sung, A. Higuchi and T. Ikoma, *Tissue Eng. Regen. Med.*, 2018, **15**, 673-697.

6 S. Zhang, L. Chen, Y. Jiang, Y. Cai, G. Xu, T. Tong, W. Zhang, L. Wang, J. Ji, P. Shi and H. W. Ouyang, *Acta Biomater.*, 2013, **9**, 7236-7247.

7 G. Chen, T. Sato, J. Tanaka and T. Tateishi, *Mater. Sci. Eng. C*, 2006, **26**, 118-123.

8 M. Tamaddon, M. Burrows, S. A. Ferreira, F. Dazzi, J. F. Apperley, A. Bradshaw, D. D. Brand, J. Czernuszka and E. Gentleman, *Sci. Rep.*, 2017, **7**, 43519.

9 G. C. Wood, *Biochem. J.*, 1960, **75**, 598-605.

10 Y. Li, A. Asadi, M. R. Monroe and E. P. Douglas, *Mater. Sci. Eng. C*, 2009, **29**, 1643-1649.

11 X. Wang, L. Sang, D. Luo and X. Li, *Colloids Surfaces B Biointerfaces*, 2011, **82**, 233-240.

12 K. Gelse, E. Pöschl and T. Aigner, *Adv. Drug Deliv. Rev.*, 2003, **55**, 1531-1546.

13 V. Irawan, T. Sugiyama and T. Ikoma, *Key Eng. Mater.*, 2016, **696**, 121-128.

14 V. Irawan, Y. Sasaki and T. Ikoma, *J. Mater. Chem. B*, , DOI:10.1039/C9TB00791A.

15 A. Higuchi, Q.-D. Ling, Y.-A. Ko, Y. Chang and A. Umezawa, *Chem. Rev.*, 2011, **111**, 3021-3035.

16 T. Ikoma, A. Yamazaki, S. Nakamura and M. Akao, *J. Solid State Chem.*, 1999, **144**, 272-276.

17 M. Safandowska and K. Pietrucha, *Int. J. Biol. Macromol.*, 2013, **53**, 32-37.

18 A. Sionkowska and J. Kozłowska, *Int. J. Biol. Macromol.*, 2013, **52**, 250-259.

19 S. Chen, T. Ikoma, N. Ogawa, S. Migita, H. Kobayashi and N. Hanagata, *Sci. Technol. Adv. Mater.*, , DOI:10.1088/1468-6996/11/3/035001.

20 D. V Bax, N. Davidenko, D. Gullberg, S. W. Hamaia, R. W. Farndale, S. M. Best

and R. E. Cameron, *Acta Biomater.*, 2017, **49**, 218-234.

21 S. Yunoki, T. Ikoma, A. Monkawa, K. Ohta, M. Kikuchi, S. Sotome, K. Shinomiya and J. Tanaka, *Mater. Lett.*, 2006, **60**, 999-1002.

22 C. N. Grover, R. E. Cameron and S. M. Best, *J. Mech. Behav. Biomed. Mater.*, 2012, **10**, 62-74.

23 H. W. Kim, L. H. Li, E. J. Lee, S. H. Lee and H. E. Kim, *Jol. H. W. Kim, L. H. Li, E. J. Lee, S. H. Lee, H. E. Kim, J. Biomed. Mater. Res. - Part A 75, 629 (2005).urnal Biomed. Mater. Res. - Part A*, 2005, **75**, 629-638.

24 Y. Guo, T. Yuan, Z. Xiao, P. Tang, Y. Xiao, Y. Fan and X. Zhang, *J. Mater. Sci. Mater. Med.*, 2012, **23**, 2267-2279.

25 G. C. Wood and M. K. Keech, *Biochem. J.*, 1960, **75**, 588-598.

26 R. G. Paul and A. J. Bailey, *ScientificWorldJournal.*, 2003, **3**, 138-155.

27 Y. Li and E. P. Douglas, *Colloids Surfaces B Biointerfaces*, 2013, **112**, 42-50.

28 J. H. Muyonga, C. G. B. Cole and K. G. Duodu, *Food Chem.*, 2004, **86**, 325-332.

29 S. Koutsopoulos, *J. Biomed. Mater. Res.*, 2002, **62**, 600-612.

30 J. Wang, Q. Yang, N. Cheng, X. Tao, Z. Zhang, X. Sun and Q. Zhang, *Mater. Sci. Eng. C*, 2016, **61**, 705-711.

31 F. J. O'Brien, B. A. Harley, I. V. Yannas and L. Gibson, *Biomaterials*, 2004, **25**, 1077-1086.

32 H. Schoof, J. Apel, I. Heschel and G. Rau, *J. Biomed. Mater. Res.*, 2001, **58**, 352-357.

33 T. Kondo, D. Kumon, A. Mieno, Y. Tsujita and R. Kose, *Mater. Res. Express*, , DOI:10.1088/2053-1591/1/4/045016.

34 F. F. Felician, C. Xia, W. Qi and H. Xu, *Chem. Biodivers.*, , DOI:10.1002/cbdv.201700557.

35 M. J. Dalby, S. Childs, M. O. Riehle, H. J. H. Johnstone, S. Affrossman and A. S. G. Curtis, *Biomaterials*, 2003, **24**, 927-935.

36 M. J. Dalby, M. O. Riehle, H. J. H. Johnstone, S. Affrossman and A. S. G. Curtis, *Tissue Eng.*, 2003, **8**, 1099-1108.

37 J. P. R. O. Orgel, O. Antipova, I. Sagi, A. Bitler, D. Qiu, R. Wang, Y. Xu and J. D. San Antonio, *Connect. Tissue Res.*, 2011, **52**, 18-24.

38 J. S. Park, J. S. Chu, A. D. Tsou, R. Diop, Z. Tang, A. Wang and S. Li, *Biomaterials*, 2011, **32**, 3921-3930.

39 C. R. Lee, A. J. Grodzinsky and M. Spector, *Biomaterials*, 2001, **22**, 3145-3154.

40 S. T. Kreger and S. L. Voytik-Harbin, *Matrix Biol.*, 2009, **28**, 336-346.

Chapter 3-Effect of Chitosan Addition on Collagen Structures and Stem Cell Activity for Hydroxyapatite and Collagen Scaffolds

Chapter 3 describes the fabrication of fibrillar and monomeric sponge consisting of collagen, chitosan, and hydroxyapatite (HAp) and the evaluation of influence of collagen structures in the sponges to the proliferation, chondrogenic differentiation, and matrix secretion capacity of human mesenchymal stem cells (MSC). Initially, fibrillar sponge was fabricated through electrolysis of suspension of collagen, chitosan, and HAp. Four different ratio of chitosan/collagen were selected for electrolysis: 100/0 (Chi-0), 87.5/12.5 (Chi-12.5), 75/25 (Chi-25), 50/50 (Chi-50); whereas concentration of HAp was kept constant (0.2 wt%) for all samples. Final thickness of gel obtained by electrolysis was found to decrease with the increasing ratio of chitosan. Moderate addition of chitosan (Chi-12.5) showed the improvement of collagen fibril formation; as evidenced from microstructure and denaturation temperature analysis. Chi-12.5 was subsequently used to fabricate monomeric and fibrillar sponges wherein chondrogenic differentiation of MSC for 28 days was conducted. It was showed that fibrillar sponges supported rapid proliferation of MSC, reaching the maximum cell number at 14 days, at the cost of slight inhibition of chondrogenic differentiation, as evidenced from the lower gene expression of *SOX9* and *COLII*. Nonetheless, rapid proliferation of MSC in fibrillar sponges was beneficial for earlier and larger accumulation of matrix molecule (aggrecan / sulfated glycosaminoglycan (sGAG)) compared to monomeric sponges. Lastly, fibrillar sponges underwent more significant improvement of mechanical properties to monomeric sponges, likely due to the larger amount of accumulated aggrecan / sGAG.

3.1 Introduction

In chapter 1, electrolysis of collagen/HAp solution was aimed to be used to fabricate a continuous bilayer scaffold consisting of fibrillar collagen sponges and gradient HAp content. Nonetheless, electrolysis of collagen solution occasionally produce structure without complete formation of collagen fibrils [1]. One of the reason is high pH region occurring near the negatively charged electrode rapidly eliminates the electrostatic repulsion between collagen monomers, causing the abrupt collagen monomers aggregation [2,3]. As a result, proper self-assembly of collagen fibrils fail to occur.

Chitosan had been known to form polyionic complex with collagen monomers [4–6], which in turn might inhibit the rapid aggregation of collagen monomers. The moderate amount of added chitosan had been reported to improve degree of collagen fibril formation (increasing of the fibril width and the amount of precipitated fibrils) [6,7]. It was hypothesized that addition of chitosan into collagen could improve the fibrilogenesis of electrolyzed collagen.

In Chapter 2, it was shown that the presence of collagen fibril on sponge (fibrillar sponge) could improve the proliferation capacity of fibroblast compared to monomeric sponge. The proposed mechanism was as followed: cell-binding ligands were clustered for collagen fibrils, which in turn strongly activate ligand-receptor signaling responsible for promoting proliferation. Nonetheless, the influence of fibrillar state of collagen sponges to the proliferation, differentiation (chondrogenic), and matrix secretion capacity of human mesenchymal stem cells are unknown.

The goals of the Chapter 3 were (1) to optimize ratio of collagen/chitosan as to obtain electrolyzed gel with sufficient thickness and improved collagen fibrilogenesis. (2) To utilize the optimized composition ratio of collagen/chitosan to fabricate monomeric and fibrillar sponge. (3) To conduct cartilage tissue-engineering with the fabricated

monomeric and fibrillar sponge. The suitability of sponges to tissue engineering was evaluated in terms of sponge capacity to support cell proliferation, differentiation and secretion of related matrix.

3.2 Experimental and Methods

Porcine skin collagen dissolved in HCl (0.62 wt%) was kindly supplied by Nitta Gelatin Co., Ltd. (Osaka, Japan). 6 M HCl, NaOH pellet, $CaCO_3$ powder, 85% H_3PO_4, 99.5% ethanol, chitosan (low molecular weight) and 99% *t*-butanol were purchased from Wako Pure Chemical Industries, Ltd. (Tokyo, Japan). Phosphate Buffered Saline (PBS) Dulbecco's formula (without Calcium and Magnesium) tablets were purchased from DS Pharma Biomedical, Ltd. (Osaka, Japan).

Universal indicator solution pH 3-10 was purchased from Fluka Chemie GmbH (Deisenhofen, Germany). Platina plates (0.25×10×10 mm, 99.98%) as an electrode were purchased from the Nilaco Corp. (Tokyo, Japan). The cylindrical electrolysis mold (ø = 24 mm, h = 10 mm) was custom-made from polycarbonate materials.

3.2.1 Preparation of collagen and chitosan suspensions

Hydroxyapatite (HAp) powder was prepared by spray-drying in a similar manner to experimental section of previous Chapter. Chitosan solution was prepared initially in 2wt%. Appropriate amount of chitosan (low molecular weight) was dissolved in 0.1 M HCl and vigorously stirred for 30 minutes at 50°C. The obtained solution was yellow and clear (pH 3.2) and subsequently adjusted to 0.62wt% by addition of ion-exchanged water. The final pH of 0.62wt% chitosan was 5.1.

Collagen (Col: 0.62wt%) /chitosan (Chi: 0.62wt%) solution was mixed at the following ratio (Col/Chi): 1.0, 0.875, 0.75, 0.50, 0.25. The mixture was stirred at room temperature

and into it was added 0.2wt% HAp powder. The stirring was continued until HAp was homogeneously distributed in the solution; the final pH of each ratio was measured to be 5.7.

3.2.2 Fabrication of gels of various Col/Chi ratio

Electrolysis of Col/Chi solution was conducted at square-silicon mold (length = 2 cm, width = 3 cm, height = 1 cm). Electrolysis was applied by initially positioning the platina plates on length side and connecting each plate to negative and positive potentials. The used current density was i = 1.5 mA/cm^2 and the electrolysis time was 12 minutes. After electrolysis, the final thickness of gel (n = 3) was recorded. The change of pH during electrolysis was recorded by adding pH universal to Chi-0 solution before electrolysis. At each time point (3, 6, 12 minutes) the photograph of electrolysis system was taken. The gels were subjected to ethanol dehydration for gel characterization.

3.2.3 Characterization of gels of various Col/Chi ratio

Chemical composition of dehydrated gel was characterized by FTIR, with the parameter of measurement similar to section 2. Thin slice of collagen hydrogel was pressed with KBr to obtain the transparent disk. The disk was subsequently analyzed with FTIR in transmission mode. Background spectrum was initially measured by using KBr purchased from Wako Pure Chemical Industries, Ltd (Japan) at the wavenumber range of 4,000 - 400 cm^{-1}, resolution of 4.0 cm^{-1}, and accumulation times at 256. FTIR spectra of the mixture of KBr and composites were mixed at 100:1 in weight was subsequently measured under the same condition.

To assess the fibril formation, microstructure and denaturation temperature of dehydrated gel was characterized. Microstructure was observed with SEM to assess the

fibril formation. Fibril size was measured correspondingly by using JSmile software (n = 40). The denaturation temperature of collagen was determined by differential scanning calorimetry (DSC: DSC-8230, Rigaku, Japan). Sample of monomeric collagen was prepared by air-drying collagen/HAp solution, whereas sample for fibrillar collagen was obtained from dehydrated gel [8]. ~3 mg samples were initially hydrated with PBS by vortex mixing and subsequently sealed in the hermetic aluminum pan. An empty hermetic aluminum pan was used as a reference. Sample pan was equilibrated at 25°C for 20 minutes, and subsequently heated to 120°C at cooling rate 3°C/min. The freezing point was determined as the onset temperature of exothermic peak. The minima point of endothermic peak observed at 40-55°C was determined as denaturation temperature.

3.2.4 Fabrication of Monomeric and Fibrillar Collagen Sponges

Solution of Col/Chi with the ratio 0.875 was used to fabricate monomeric and fibrillar collagen sponges. Monomeric sponge was fabricated by directly freezing the solution at -20°C for 24 hours and freeze-drying at -10°C for 36 hours. Fibrillar sponge was fabricated by initially electrolyzing the Col/Chi solution in cylinder polycarbonate mold (diameter = 2.3 cm, height = 3 cm), with I = 1.5 mA/cm^2 for 24 minutes. The electrolyzed gels were subsequently frozen and freeze-dried in the similar manner with monomeric sponge. The appearance, density, and porosity of fabricated sponges were measured. The microstructure of sponges was observed to assess the fibrillar nature of sponges. The pore size of sponges was measured with JSmile software (n=40).

3.2.5 Cell Culture Experiment

Crosslinking of Monomeric and Fibrillar Collagen Sponges

The fabricated sponges were crosslinked with EDC/NHS as to impart the stability during cell culture experiment and to control the initial compressive modulus of sponges. The protocol to select the concentrations of EDC/NHS was as followed: 90 mg of electrolyzed collagen sponges was prepared in polypropylene weighing boat, 1.2 mmol carboxylate per gram of collagen was presumed from previous study[9]; amount of EDC was prepared accordingly to obtain mole ratio of EDC/COO^-: 10x, 30x. NHS was also prepared with the mole ratio adjusted to 2.5x lower than the respective EDC mole. The crosslinking was conducted in 15 ml 75% ethanol for 2 hours at room temperature before washing 2x with excessive ion-distilled water. Monomeric and fibrillar sponge was crosslinked with 30x and 10x EDC, respectively. Different crosslinking degree was used to ensure that both of monomeric and fibrillar sponge showed similar value of compressive modulus and strength.

3.2.5.1 Cell Isolation and Culture

Two different kinds of cell-culture medium were prepared for the study. **1.** Growth medium, consisting of DMEM low glucose, supplemented with 1% Penicilin, and 10% fetal bovine serum. **2.** Chondrogenic-inducing medium (chondrogenic medium), consisting of DMEM-low glucose supplemented with 20 ng/mL human TGF-β3 (Fuji Chemical, Japan), 40 mg/mL proline (Sigma-Aldrich), 100nM dexamethasone (Sigma-Aldrich), 1 ug/ml ITS (insulin, transferrin, and selinium) (BD Biosciences).

Primary cells human bone marrow mesenchymal stem cells (MSC) were purchased from Riken Cell Bank.Cells were expanded in the tissue culture flask with growth medium. Cells were expanded up to fourth passage before used for chondrogenic study.

3.2.5.2 Cell Seeding and Chondrogenic Differentiation Protocol

Each sponge was seeded with total cell numbers 9 x 10^5 cells. Expanded MSC was detached with trypsin and was suspended in growth medium at a density of 6 x 10^6 cells per mL. Sterilized sponge was washed with PBS and conditioned in serum-free DMEM low glucose; sponge was subsequently dried with sterilized filter paper, as to remove the liquid in pore water and to ensure good cell penetration, and placed in 24-well non-tissue culture plate. Cell suspension was carefully sucked with the syringe; needle of syringe was used to pierce sponges at the center part of sponge and 150 μl of cell suspension was subsequently injected into the sponges. The well-plate was placed back into the incubator for 3 hours to allow initial cell attachment; 700 μl of cell medium was added afterwards. The well was subsequently incubated for a further 28 days with medium being changed at 3-day intervals.

3.2.5.3 Analysis of Cell Morphology and Sponge Microstructure

Cell morphology was assessed using scanning electron microscopy (SEM) after 24 h of seeding. Constructs were washed with PBS for 10min and subsequently fixed with 2.5% glutaraldehyde for 1 h at room temperature. The constructs were then dehydrated using a series of washes with ethanol from 50% to 100% concentration followed by ethanol exchange by t-butanol and freeze-drying at 0°C.

3.2.5.4 Analysis of Gene Expression

To determine gene expression on the cultured cells within the sponges, real-time reverse transcription polymerase chain reactions (RT-PCR) were carried out[10]. Briefly, sponges were frozen in liquid nitrogen and electric crushed to obtain the powder sample. RNA was extracted from powder sample by using Sepasol-RNA Super II (Nacalai Tesque,

Japan). One hundred nanograms of total RNA was reverse transcribed to cDNA using a MuLV reverse transcriptase (Applied Biosystems, USA). Real-time PCR were run on a QuantStudio®3 real-time PCR System (Applied Biosystems). Real-time PCR was used to amplify Glyceraldehyde-3-phosphate dehydrogenase (GAPDH), sex determining region Y-box 9 (SOX-9), type II collagen (COL2A1) and aggrecan (ACAN). These target genes were chosen, as they are expressed in cells differentiating in chondrogenic pathway. The RT-PCR reactions were performed with 0.2 µl cDNA, 18 mM forward / reverse primers, 5 mM PCR probe and qPCR Master Mix (Eurogentec, Seraing, Belgium).

3.2.5.5 Analysis of Cell Proliferation

Cell number was quantified using a Hoechst dye 33258 assay previously described [11] Briefly, cell-seeded were taken out of culture at day 14 and day 28 and washed in PBS before digestion in a solution prepared from papain enzyme solution containing 0.5M EDTA, cysteine-HCL, and 1mg/mL papain enzyme (Carica papaya; Sigma- Aldrich). Measurements were taken using a UV-VIS (Jasco, Japan) at an emission of 460 nm and an excitation of 355 nm. A standard curve was established by using a known amount of bovine DNA. The DNA was converted to number of cells by assuming a single cell has 7 picogram of DNA.

3.2.5.6 Analysis of Sulfated GAG (sGAG) Production

Digested scaffolds were assessed for sulfated GAG production that was synthesized by seeded cells using a solution of Blyscan sGAG assay kit [12], according to the manufacturer protocol. Absorbance was measured at 656 nm and sGAG concentration was extrapolated from a standard curve generated using a sGAG standard.

3.2.5.7 Analysis of Mechanical Properties of Sponges after 28 days of cell culture

Compressive modulus and strength of sponges were determined by compressive testing (TA-XT2, Stable Micro Systems, UK) fitted with a 5-N load cell. Testing was conducted at a strain rate of 6 mm/min to achieve a strain of 60% The modulus was defined as the slope of a linear fit to the stress–strain curve over 1%–5% strain. Stress at a strain of 20% was employed as compressive strength [13]. Compressive testing was conducted on the cell-free sponge (day 0) and cell-seeded sponge (day 28). Comparison of means between samples was analyzed by two-tail Student's *T*-test ($p<0.05$).

3.3 Results and Discussion

3.3.1 Characterization of The Electrolyzed Hydrogel

Electrolysis was conducted on various ratio of collagen/chitosan as to obtain the composition that fulfill two criteria: (1) sufficient thickness (<4 mm) of electrolyzed hydrogel, (2) complete formation of fibrillar gel.

Visual representation of electrolysis of Chi-0 solution was given in Fig. 3.1. The suspension was yellow-colored by pH universal indicating pH around 5.0. After 3 minutes of electrolysis, purplish collagen gel appeared at cathode area; whereas collagen solution near anode turned into red color. The purple and red color implied the pH>11 and pH<3, respectively. Initial, addition of HAp particles to porcine skin collagen solution increased the pH from 3.0 to 5.7, indicating slight dissolution of HAp into its constituting species (calcium, phosphate, hydroxide) [14]. The released ionic spesies subsequently mediated the electrolysis reactions of water at cathode (eq. (1.1)) and anode (eq. (1.2)):

Cathode: $2H_2O+2e^- \rightarrow 2OH^-+H_2$ (1-1)
Anode: $2H_2O \rightarrow 4H^+ +4e^-+O_2$ (1-2)

The produced OH^- and H^+ corresponded to formation of high and low pH regions. The rapid increasing of pH initiated the aggregation / or self-assembly of collagen fibril, which in turn form water-binding network of the hydrogel structure.

Collagen gel grew in thickness during 12 minutes of electrolysis; however, the gel growth was stopped as it was in contact with low pH region. The final thickness of gel with varying chitosan ratio was given in Fig 3.2. As can be seen, the thickness of electrolyzed gel was reduced with the increasing concentration of chitosan. The formation of electrolyzed gel was originated from precipitation of collagen fibrils due to the rapid increasing of pH near cathode area [14,15]. On the other hand, chitosan existed in protonated state at low pH [16]; which in turn might act as an acid that neutralize cathode-produced OH^-. As the result, the progression of OH^- was inhibited, resulting in the reduction of gel width with concentration of chitosan.

FTIR analysis of dehydrated gels was shown in Fig. 3-3. Pure collagen sample (Chi-0) showed the bands characteristic of collagen: amide I (1650 cm^{-1}), amide II (1540-1450 cm^{-1}), amide III regions (1235-1160 cm^{-1}) [17,18]. Pure chitosan showed characteristic peak of glycosylic bond at 1152 cm^{-1} and carboxylic bond at 1430 cm^{-1} [18]. These two peaks become more prominent as the ratio of chitosan was increased from 0.125 to 0.5, suggesting the successful formation of collagen/chitosan composite.

Microstructure observation of dehydrated gel was shown in Fig. 3.4. Chi-0 showed formation of non-fibrillar region and fibril region (width: 30.2 ± 6.1 nm). Increasing ratio of chitosan to 0.125 (Chi-12.5) eliminated non-fibrillar region. At this ratio, collagen

fibril was slightly reduced to 29.3 ± 4.1 nm. Collagen fibril become more broken with the increasing chitosan ratio (Chi-25 and Chi-50). The results were explained as follow: the formation of collagen fibril originated from the continual aggregation of collagen monomers [19]. At high pH, numerous amount of collagen nucleus was formed simultaneously, resulting in the small size collagen fibril size or non-fibrillar collagen [20]. Chitosan form polyionic complex with collagen monomer, thereby inhibiting rapid formation of collagen nucleus [6,7]. Moderate amount of chitosan is beneficial to allow proper growth of collagen nucleus into finite sized fibrils. Nonetheless, large amount of chitosan (Chi-50) greatly inhibited collagen nucleus formation, resulting in the inhibited collagen fibril formation.

DSC curve of hydrogel was shown in Fig. 3.5. Chi-0 showed the lowest denaturation temperature 47.8°C, followed by Chi-12.5 and Chi-25 (48.9 and 50.7°C); the denaturation temperature was decreased for Chi-50 (48.4°C). The average of denaturation temperature (n = 3) was given in Fig. 3.5(b). As can be seen, addition of chitosan up to Chi-25 increased the denaturation temperature, suggesting the improved formation of collagen fibrils. The lowering of denaturation temperature observed for Chi-50 was attributed to the inhibition of collagen fibril formation by the prevalent formation of collagen/chitosan complex at high amount of chitosan addition.

Based on the aforementioned two criteria, (1) sufficient thickness (<4 mm) of electrolyzed hydrogel, (2) complete formation of fibrillar gel, it was taken that the optimum concentration of collagen/chitosan was 87.5/12.5 (wt%/wt%).

3.3.2 Characterization of The Fabricated Monomeric and Fibrillar Sponges

Gross appearance of monomeric and fibrillar sponges were shown in Fig. 3.6 and

physical properties of sponges were summarized in Table 3.1. Relatively turbid appearance of fibrillar sponges was attributed to the presence of collagen on the pore wall, which scattered the transmitted light. Density and porosity of both sponges were similar due to the identical initial concentration and processing parameters (freezing temperature, freeze-drying).

Microstructure observation of monomeric and fibrillar sponge was shown in Fig. 3.7 Both sponges showed similar pore size, that is 237± 56 μm for monomeric sponge and 242± 53 μm for fibrillar sponge. Higher magnification of pore walls revealed the smooth appearance for monomeric sponge and fibrillar appearance for fibrillar sponge. It has been shown that the presence of fibrillar collagen influence the swelling capacity of sponges particularly the material swelling of sponge. The swelling capacity for monomeric and fibrillar collagen sponges were given in Fig. 3.8. As can be seen, the total swelling was similar for both of sponges; whereas, the material swelling was significantly higher for fibrillar sponges to monomeric sponges.

Taken together, these results suggested the successful fabrication of monomeric and fibrillar sponges.

3.3.3 Influence of collagen fibrillar state on morphology of MSC

Morphology of cells (Fig. 3.9) attached on monomeric sponge showed the flattened structure; whereas, cells on fibrillar sponge exhibited elongated structure. As previously explained, the flattened and elongated structures were associated with the spread and concentrated ligand distribution, respectively. The flattened structure showed diffuse formation of stress fiber; whereas the elongated structure exhibited thick formation of stress fiber at the initial time point of attachment [21,22].

3.3.4 Effect of fibrillar state of collagen on gene expression

Gene expression analysis showed that fibrillar state of collagen sponges significantly influenced chondrogenic gene expression. Monomeric sponge stimulated approximately two-fold and three-fold higher SOX9 gene (Fig. 3.10a) expression than fibrillar sponge at day 14 and 28, respectively. Nonetheless, both sponges showed the trend of increasing SOX9 gene expression for both sponges from day 14 to day 28. Similar trend of increasing gene expression from day 14 to day 28 was also observed for expression of ACAN gene (Fig. 3.10b) for MSC cultured in the monomeric and fibrllar sponge. Unlike SOX9, there was no significant difference of ACAN expression for cells cultured in both sponge at similar time point. Lastly, monomeric sponge promoted three-fold higher COLII expression (Fig. 3.11) compared to fibrillar sponge, suggesting the higher chondrogenicity of monomeric to fibrillar sponge. The results suggested that MSC in monomeric sponge undergo extensive chondrogenice differentiation to fibrillar sponge.

3.3.5 Effect of fibrillar state of collagen on proliferation of MSC

Fibrillar sponge showed significantly higher cell number (~5.8 x 10^6 cells) compared to monomeric sponge (~4.2 x 10^6 cells) at day 14 (Fig. 3.12). The cell number seemed to be unchanged at day 28 for fibrillar sponge, in contrast, monomeric sponge underwent rapid increasing of cell number approaching ~5.8 x 10^6 cells DNA value. These data suggested that ~5.8 x 10^6 cells DNA was the confluence limit of the sponges. In the proliferation step, cells continue to divide until it fully occupies the available spaces and eventually come into contact with other cells [23]. At this point, cells stopped divided and reached the confluent limit of sponges. In chapter 2, fibrillar sponge was likely to promote proliferation rate of cells compared to monomeric sponge, through the stress fiber-

mediated mechanism. Fibrillar sponge encouraged formation of cells with thick stress fibers which in turn favor proliferation of cells [21,22] at the cost of inhibiting chondrogenic differentiation [24]..

3.3.6 Effect of fibrillar state of collagen on sGAG secretion by MSC

Fibrillar sponge showed significantly higher amount of sGAG at day 14 and 28 compared to monomeric sponge (Fig. 3.13). sGAG molecules in the form of chondroitin sulfate or keratin sulfate were known to be assembled with core protein and hyaluronic acid, by chondrocyte-related cells, as to obtain aggrecan proteoglycan [25–27]. The assembly of these smaller molecules into aggrecan were largely governed by the expression of *ACAN* gene [28]. It was clear that expression level of *ACAN* was relatively similar for cells cultured on monomeric and fibrllar sponge, suggesting almost equal rate of sGAG production for cells in monomer and fibrillar sponge. Thereby, the higher cell number in fibrillar sponge at day 14 translate to the larger amount of sGAG accumulation compared to monomeric sponge.

3.3.7 Effect of synthesized matrix to the mechanical properties of sponges

Microstructure of sponges after 28-days of culture was shown in Fig. 3.14. Both samples showed presence of net-like structures, attributable to the newly secreted matrix. The net like structures was strongly embedded on the pore walls, suggesting the close interaction of newly secreted matrix and scaffolds. Compressive modulus and strength of non-tissue engineered sponges (Day-0) and tissue-engineered sponges (Day-28) was shown in Fig. 3.15. Non-tissue engineered sponges exhibited similar mechanical properties: monomeric sponge showed compressive modulus at 1.13 ± 0.09 kPa and strength at 1.19 ± 0.22 kPa which is similar to the fibrillar sponge: compressive modulus

1.19 ± 0.22 kPa; compressive strength 0.45 ± 0.02 kPa. After 28 days of culture, monomeric sponge underwent increasing of compressive modulus to 1.50 ± 0.16 kPa; whereas fibrillar sponge showed significantly higher compressive modulus at 2.14 ± 0.29 kPa. Compressive strength of both sponges also showed the higher increasing value for fibrillar sponge to monomeric sponge. The enhancement of mechanical properties was associated with the greater synthesized amount of matrix in the scaffold. In the chondrogenic pathway, there are two major secreted matrix molecules, that is aggrecan and type II collagen[29,30]. Aggrecan mainly function to resist compressive load [27]; concentrated aggrecan provide osmotic pressure which in turn counter the applied compressive load, resulting in the more robust structure. The significantly higher improvement of mechanical properties observed for fibrillar sponge was likely to originate from the larger amount of accumulated sGAG (aggrecan).

3.4 Summary

Electrolysis of collagen (0.62wt%)-HAp (0.2 wt%) solution caused imperfect collagen fibrilogenesis. Addition of small amount of chitosan (Col/Chi: 87.5 / 12.5) successfully improved the fibrilogenesis of the obtained electrolyzed gel at the cost of slight reduction in collagen gel thickness.

Collagen-chitosan solution with the following ratio: Col87.5/Chi12.5-HAp0.2wt% was successfully translated into monomeric and fibrillar sponges by direct freeze-drying and electrolysis.

Cartilage tissue-engineering was conducted on monomeric and fibrillar sponges by employing human bone marrow mesenchymal stem cells (MSC) differentiated in the chondrogenic pathway. Fibrillar sponge supported higher proliferation of stem cells, which in turn favor earlier and larger accumulation of matrix, responsible for enhancing

the compressive properties of structure. The mechanism used by fibrillar sponge to accelerate cell proliferation inadvertently inhibit the chondrogenic differentiation of MSC, resulting in the apparent higher degree of chondrogenic differentiation for MSC cultured in monomeric sponge.

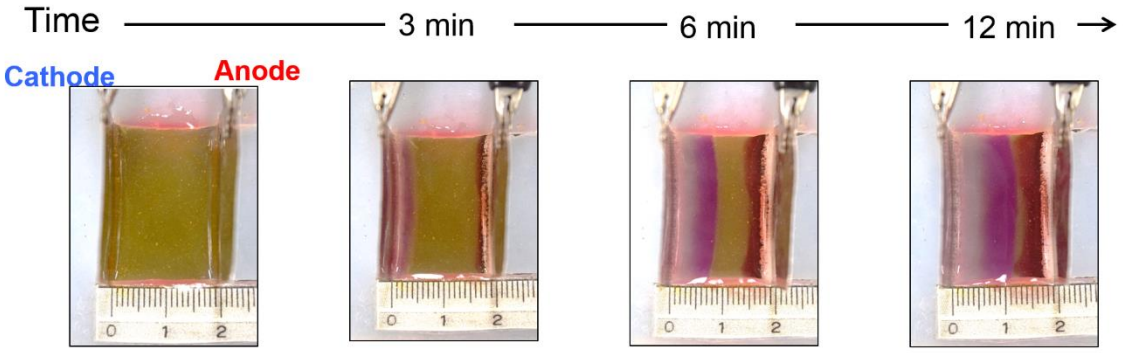

Fig. 3.1 Visual representation of electrolysis of Chi-0 solution. Yellow, purple, and red color indicated pH at 5, 11, 2, respectively.

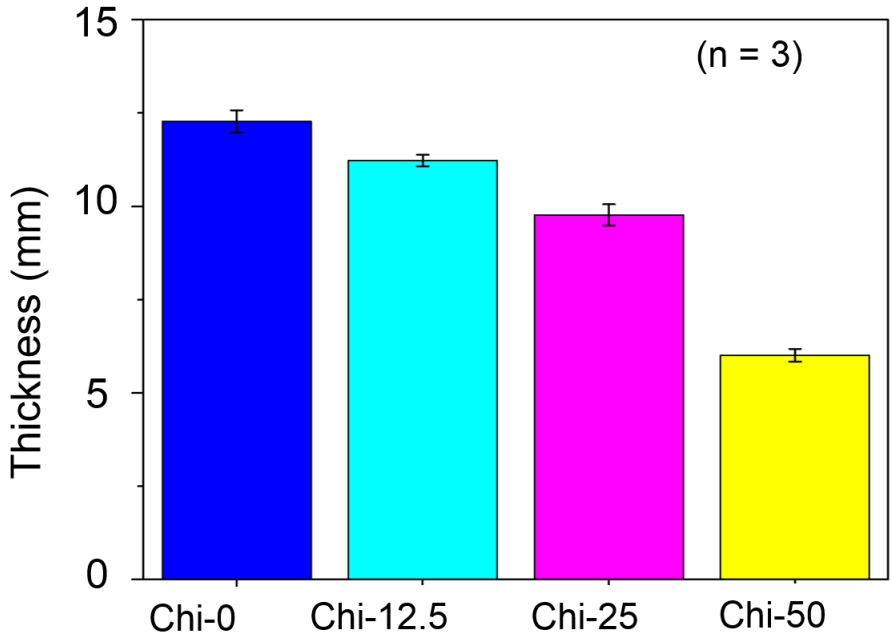

Fig. 3.2 Final thickness of gel obtained by electrolysis of Col-Chi of varying ratio (HAp 0.2 wt%).

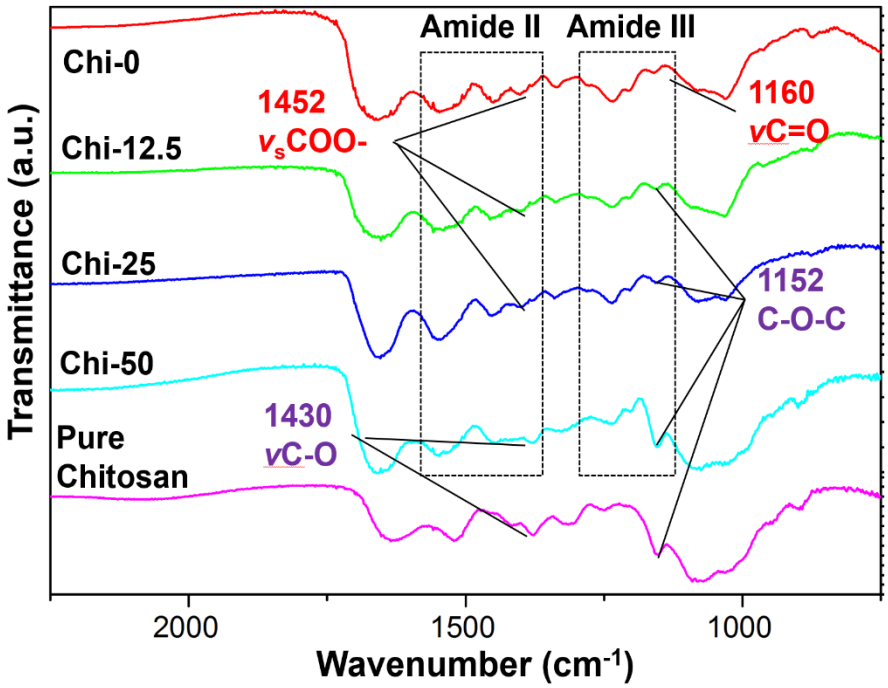

Fig. 3.3 FTIR evaluation of dehydrated gel obtained by electrolysis of Col-Chi of varying ratio (HAp 0.2 wt%).

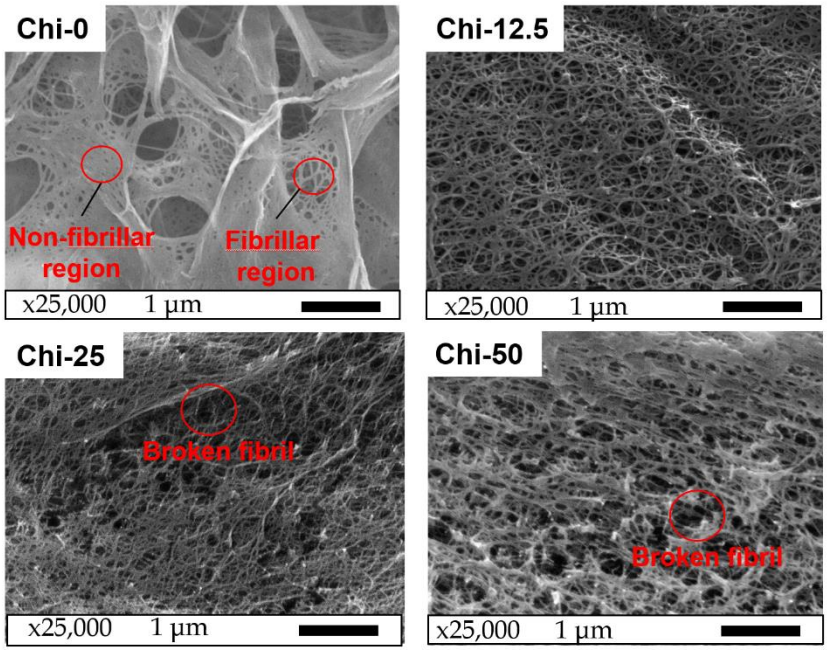

Fig. 3.4 SEM imaging of dehydrated gel obtained by electrolysis of Col-Chi of varying ratio (HAp 0.2 wt%).

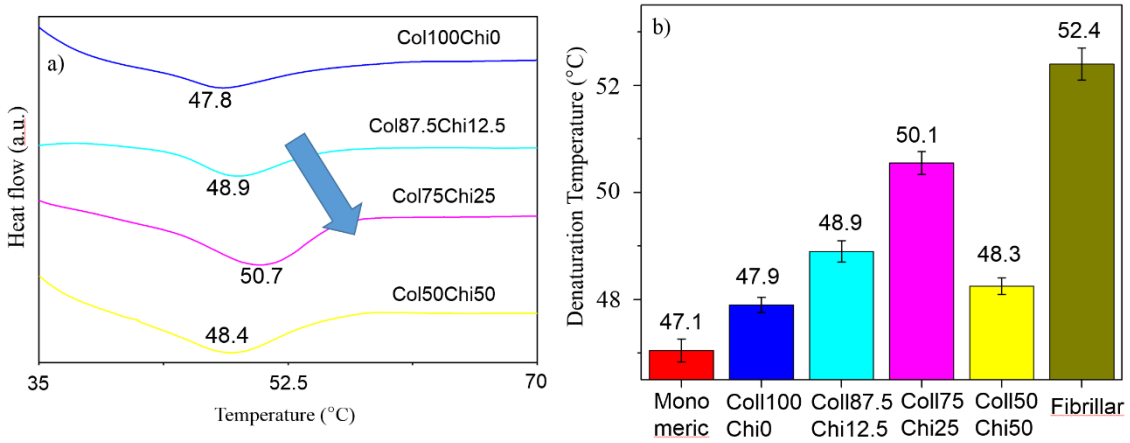

Fig. 3.5 (a) DSC curve of dehydrated hydrogel, (b) Denaturation temperature of dehydrated hydrogel. Monomeric and fibrillar were the samples fabricated in chapter 2 (n=3, mean ± standard deviation).

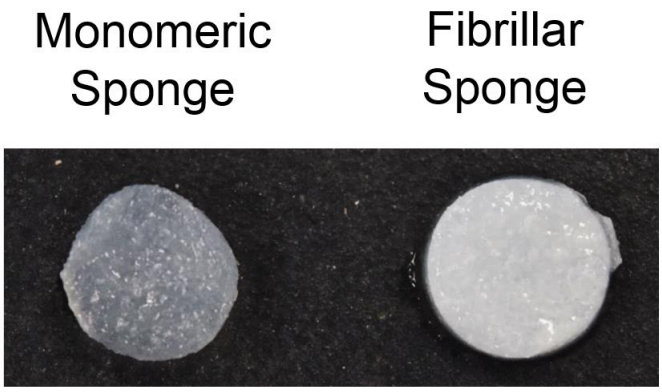

Fig. 3.6 SEM imaging of dehydrated gel obtained by electrolysis of Col-Chi of varying ratio (HAp 0.2 wt%)

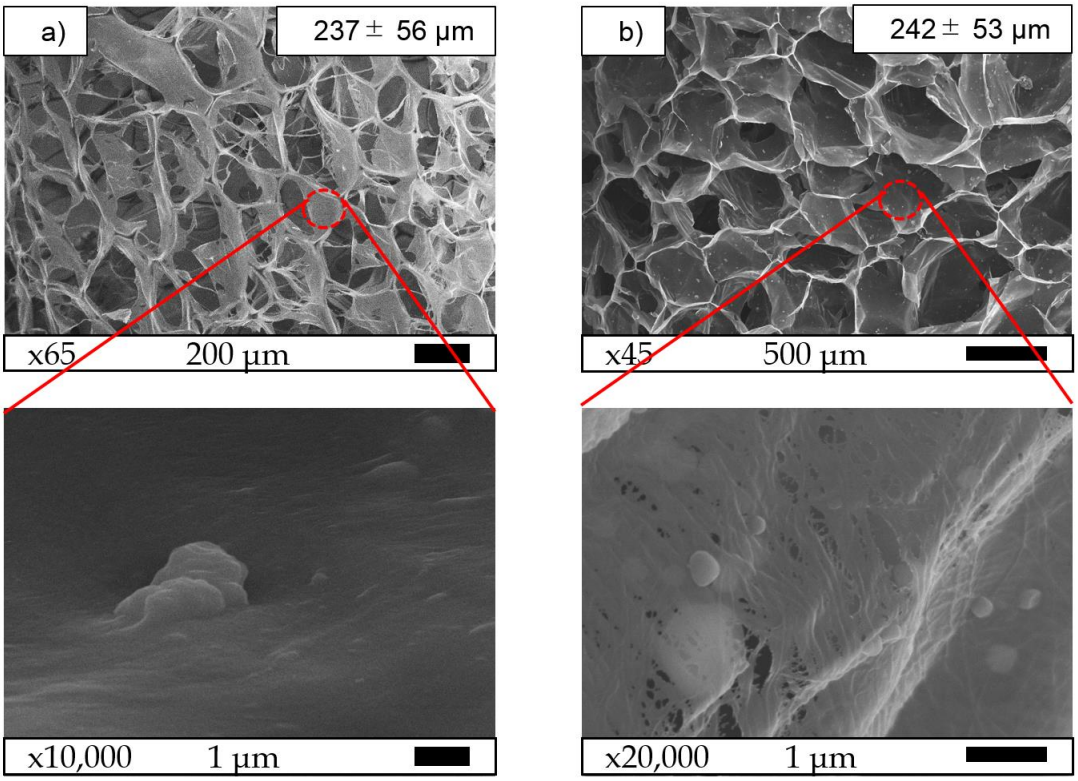

Fig. 3.7 Pore structure and pore walls morphology of monomeric and fibrillar sponge

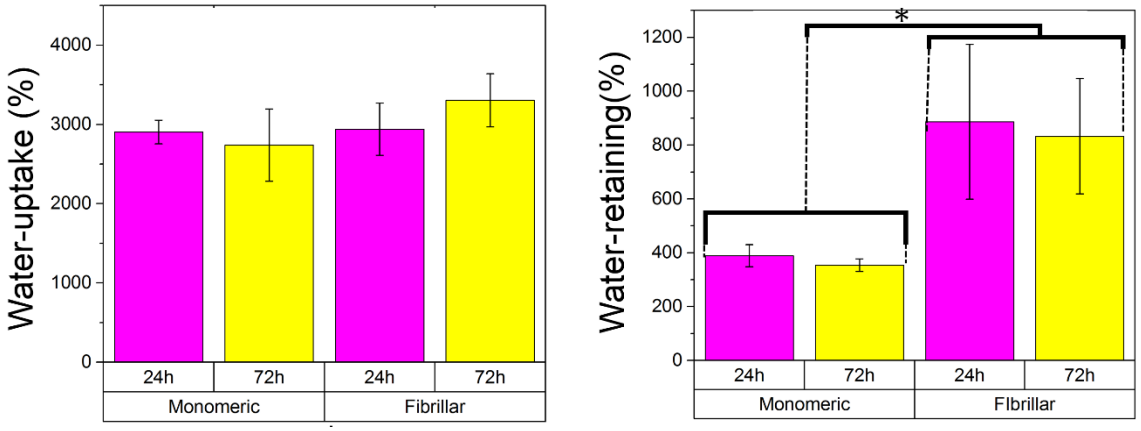

Fig. 3.8 Total swelling and material swelling for monomeric and fibrillar sponges. * $p <$ 0.05, n= 3

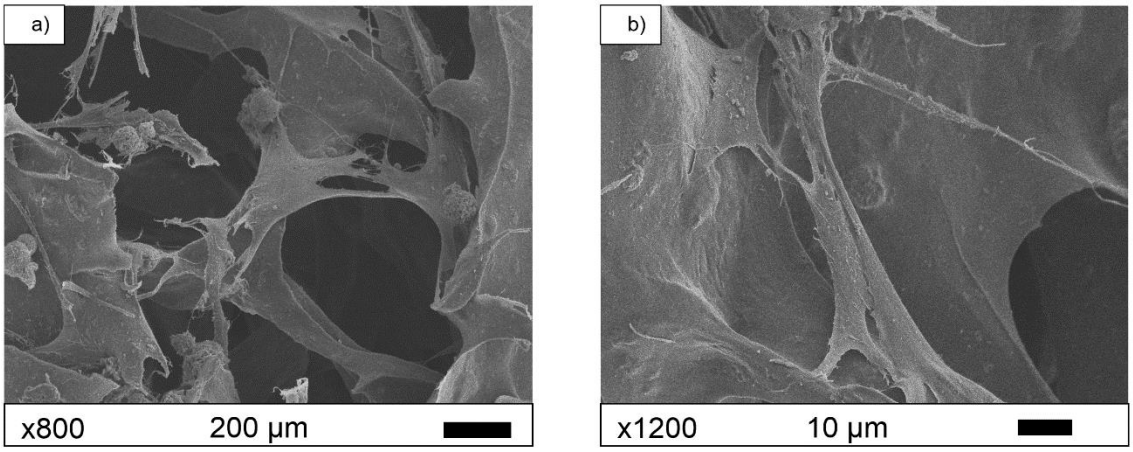

Fig. 3.9 Morphology of attached MSC in monomeric (a) and fibrillar sponges (b)

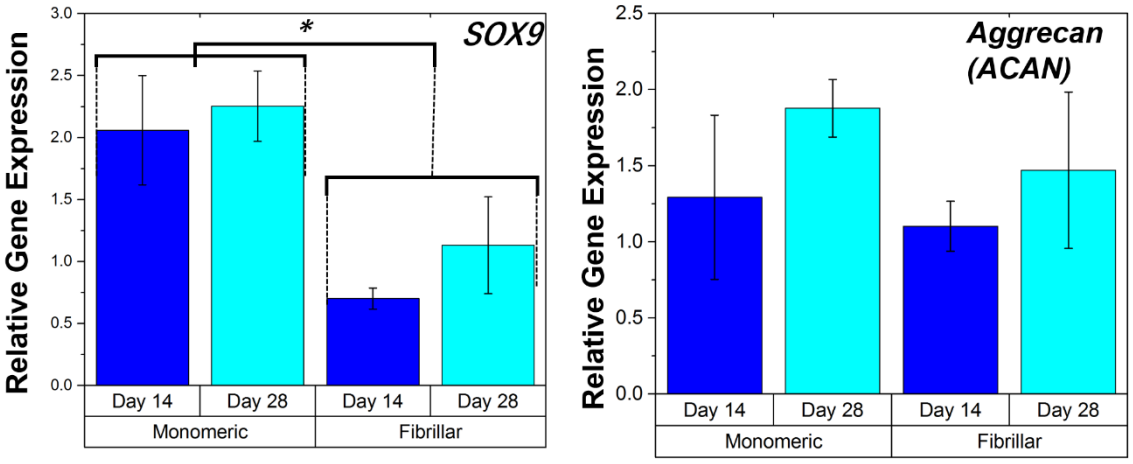

Fig. 3.10 Relative gene expression of *SOX9* and *ACAN* for MSC cultured in monomeric and fibrillar sponges at Day-14 and Day-28 of cell culture. * $p < 0.05$, n= 3

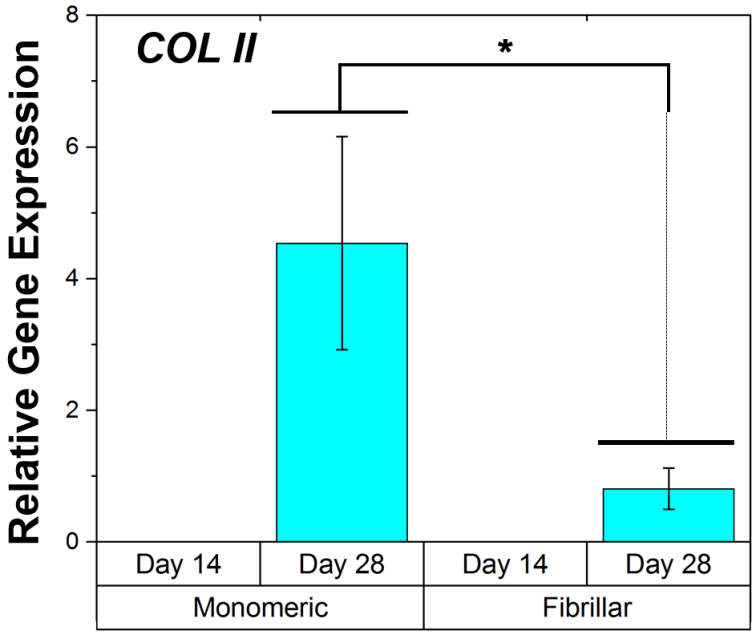

Fig. 3.11 Relative gene expression of *COLII* sponges for MSC cultured in monomeric and fibrillar sponges at Day-14 and Day-28 of cell culture. * $p < 0.05$, n= 3

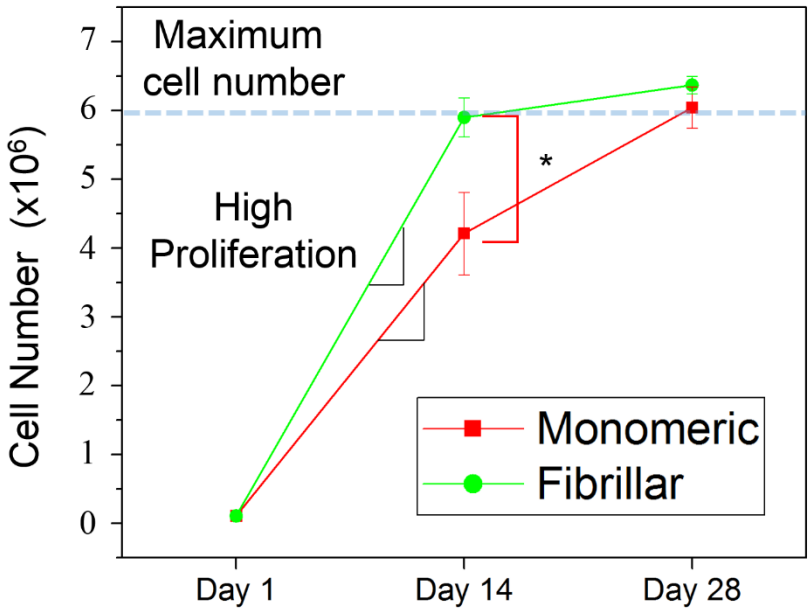

Fig. 3.12 Cell number for MSC cultured in monomeric and fibrillar sponges at Day-14 and Day-28 of cell culture. * $p < 0.05$, n= 3

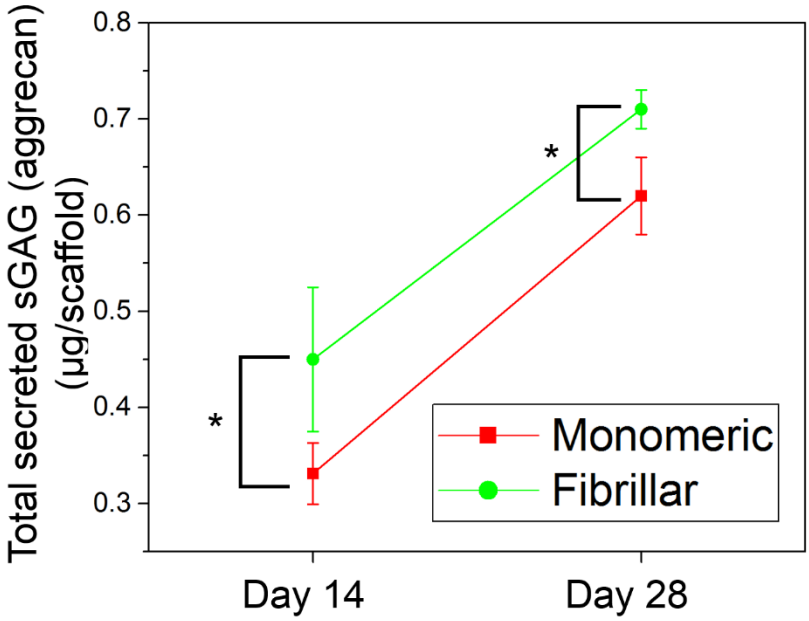

Fig. 3. 13 Total accumulation of sGAG (aggrecan) for MSC cultured in monomeric and fibrillar sponges at Day-14 and Day-28 of cell culture. * $p < 0.05$, n=3

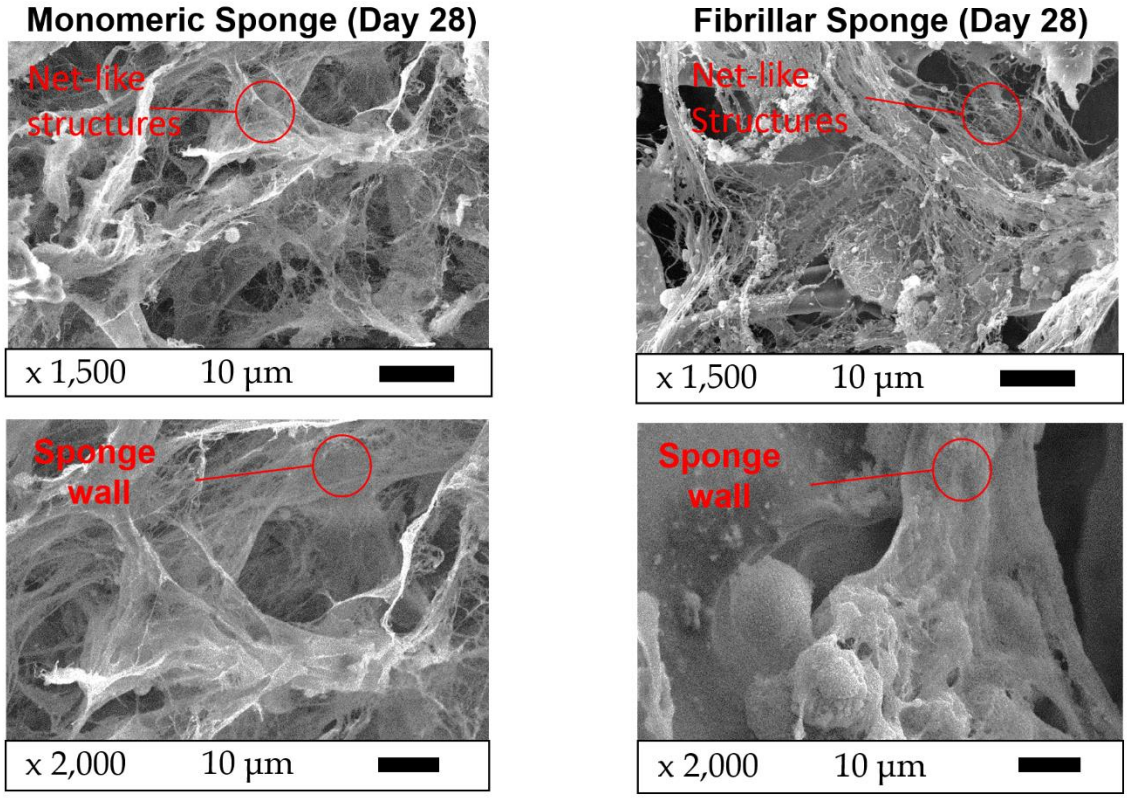

Fig. 3. 14 Appearance of cross-section for sponges after 28-days cell culture. Net-like structures correspond to newly secreted matrix

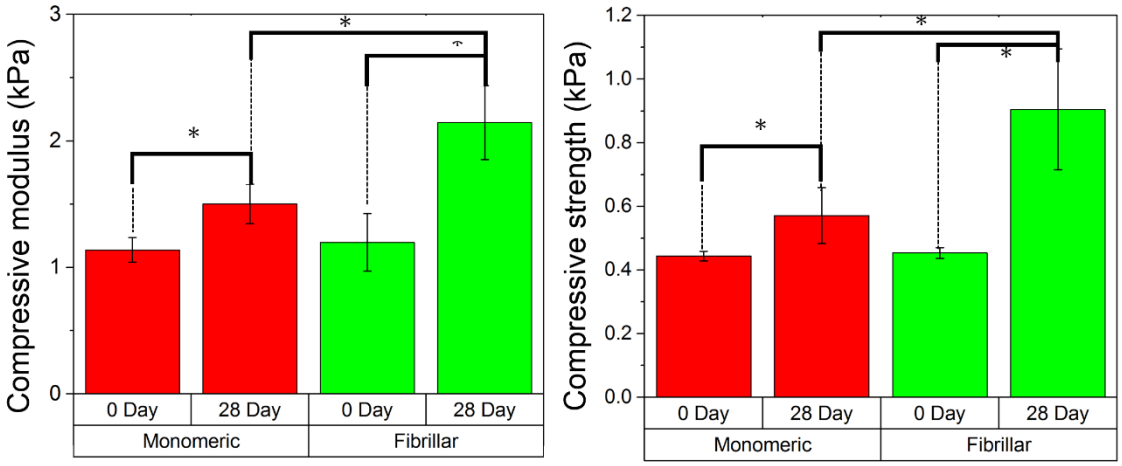

Fig. 3. 15 Compressive modulus and strength of non-tissue engineered sponge (day 0) and tissue-engineered sponge (day 28 after chondrogenic cell culture). * $p < 0.05$, n= 3

Table 3.1. Physical properties of monomeric and fibrillar sponges

	Monomeric	**Fibrillar**
Density (g/cm^3)	0.010 ± 0.001	0.018 ± 0.002
Porosity (%)	99.2 ± 0.03	98.6 ± 0.02

References

1 H. Kamata, S. Suzuki, Y. Tanaka, Y. Tsutsumi, H. Doi, N. Nomura, T. Hanawa and K. Moriyama, *Mater. Trans.*, 2011, **52**, 81-89.

2 A. A. Marino and R. O. Becker, *Calcif. Tissue Res.*, 1969, **4**, 330-338.

3 Y. Li, A. Asadi, M. R. Monroe and E. P. Douglas, *Mater. Sci. Eng. C*, 2009, **29**, 1643-1649.

4 F. Chicatun, C. E. Pedraza, N. Muja, C. E. Ghezzi, M. D. McKee and S. N. Nazhat, *Tissue Eng. Part A*, 2013, **19**, 2553-2564.

5 A. Sionkowska, *Prog. Polym. Sci.*, 2011, **36**, 1254-1276.

6 X. Wang, L. Sang, D. Luo and X. Li, *Colloids Surfaces B Biointerfaces*, 2011, **82**, 233-240.

7 X. Liu, N. Dan, W. Dan and J. Gong, *Int. J. Biol. Macromol.*, 2016, **82**, 989-997.

8 S. Chen, T. Ikoma, N. Ogawa, S. Migita, H. Kobayashi and N. Hanagata, *Sci. Technol. Adv. Mater.*, , DOI:10.1088/1468-6996/11/3/035001.

9 M. G. Haugh, C. M. Murphy, R. C. McKiernan, C. Altenbuchner and F. J. O'Brien, *Tissue Eng. Part A*, 2011, **17**, 1201-1208.

10 F. Meng, A. He, Z. Zhang, Z. Zhang, Z. Lin, Z. Yang, Y. Long, G. Wu, Y. Kang and W. Liao, *J. Biomed. Mater. Res. - Part A*, 2014, **102**, 2725-2735.

11 A. Matsiko, T. J. Levingstone, F. J. O'Brien and J. P. Gleeson, *J. Mech. Behav. Biomed. Mater.*, 2012, **11**, 41-52.

12 L. Galois, S. Hutasse, D. Cortial, C. F. Rousseau, L. Grossin, M. C. Ronziere, D. Herbage and A. M. Freyria, *Biomaterials*, 2006, **27**, 79-90.

13 S. Yunoki, T. Ikoma, A. Monkawa, K. Ohta, M. Kikuchi, S. Sotome, K. Shinomiya and J. Tanaka, *Mater. Lett.*, 2006, **60**, 999-1002.

14 V. Irawan, Y. Sasaki and T. Ikoma, *J. Mater. Chem. B*, , DOI:10.1039/C9TB00791A.

15 G. C. Wood, *Biochem. J.*, 1960, **75**, 598-605.

16 J. K. Suh and H. W. Matthew, *Biomaterials*, 2000, **21**, 2589-98.

17 J. H. Muyonga, C. G. B. Cole and K. G. Duodu, *Food Chem.*, 2004, **86**, 325-332.

18 Z. Chen, X. Mo, C. He and H. Wang, *Carbohydr. Polym.*, 2008, **72**, 410-418.

19 G. C. Wood and M. K. Keech, *Biochem. J.*, 1960, **75**, 588-598.

20 F. Jiang, H. Hörber, J. Howard and D. J. Müller, *J. Struct. Biol.*, 2004, **148**, 268-278.

21 M. J. Dalby, M. O. Riehle, H. J. H. Johnstone, S. Affrossman and A. S. G.

Curtis, *Tissue Eng.*, 2003, **8**, 1099-1108.

22 M. J. Dalby, S. Childs, M. O. Riehle, H. J. H. Johnstone, S. Affrossman and A. S. G. Curtis, *Biomaterials*, 2003, **24**, 927-935.

23 C. R. Lee, A. J. Grodzinsky and M. Spector, *Biomaterials*, 2001, **22**, 3145-3154.

24 A. Woods, G. Wang and F. Beier, *J. Biol. Chem.*, 2005, **280**, 11626-11634.

25 J. T. Connelly, C. G. Wilson and M. E. Levenston, *Osteoarthr. Cartil.*, 2008, **16**, 1092-1100.

26 V. Irawan, T.-C. Sung, A. Higuchi and T. Ikoma, *Tissue Eng. Regen. Med.*, 2018, **15**, 673-697.

27 A. Aspberg, in *Cartilage*, Springer International Publishing, Cham, 2016, vol. 12, pp. 1-22.

28 C. Csaki, U. Matis, A. Mobasheri, H. Ye and M. Shakibaei, *Histochem. Cell Biol.*, 2007, **128**, 507-520.

29 A. M. Freyria, M. C. Ronzière, D. Cortial, L. Galois, D. Hartmann, D. Herbage, F. Mallein-Gerin, M. C. Ronziere, D. Cortial, L. Galois, D. Hartmann, D. Herbage and F. Mallein-Gerin, *Tissue Eng Part A*, 2009, **15**, 1233-1245.

30 A. Higuchi, Q. D. Ling, Y. Chang, S. T. Hsu and A. Umezawa, *Chem. Rev.*, 2013, **113**, 3297-3328.

Chapter 4-Electrolysis Preparation and Osteoblast Proliferation of Bilayer Scaffolds with Gradient Hydroxyapatite and Collagen Contents including Chitosan and Magnetite

Chapter 4 describes the development of electrolysis as a method to fabricate a continuous bilayer structure consisting of fibrillar collagen/chitosan sponge with the gradient HAp content and the subsequent evaluation of the influence of IONP addition to the mechanical properties and osteoblast-proliferation supporting capacity of fibrillar bilayer structure. Initially, formation of collagen sponge with gradient HAp content was investigated by electrolyzing collagen solution with three different HAp concentration (0.1, 0.2, 0.3 wt%). 0.1wt% electrolyzed sponge showed that the region closest to cathode exhibited the ratio of HAp/collagen 0.25 ± 0.05, which gradually decreased with distance from cathode to 0.21 ± 0.04, 0.14 ± 0.03, and 0.07 ± 0.02. On the other hand, gradual decreasing of HAp content was absent for 0.2 and 0.3 wt% samples. Next, bilayer structure consisting of fibrillar collagen sponge with gradient HAp content was fabricated by electrolyzing collagen-chitosan-HAp solution. Lastly, IONP (20 mg / ml) was incorporated into the collagen-chitosan-HAp sponge, without and with pre-magnetic treatment and to accumulate IONP at the side closest to cathode. Incorporation of IONP without pre-magnetic treatment (Col-Chi-HAp/IONP) successfully enhanced the compressive modulus and strength of the bilayer structure; whereas, incorporation of IONP with pre-magnetic (Col-Chi-HAp/IONP/Magnet) treatment diminished the mechanical properties of bilayer structure. Cell attachment was slightly reduced for osteoblast cultured in the Col-Chi-HAp/IONP compared to structure without IONP addition Col-Chi-HAp/IONP/Magnet, resulting in the lower initial cell number. Nonetheless, IONP-added samples exhibited higher increasing of cell number, suggesting the improved proliferation

capacity.

4.1 Introduction

The previous chapters described fabrication of fibrillar collagen sponge with electrolysis and investigation of a fibrillar collagen-based sponges as a tissue-engineering scaffold compared to the monomeric collagen sponge. It was concluded that fibrillar collagen sponge was suitable as a tissue-engineering scaffold, particularly for cartilage tissue-engineering.

As mentioned in the chapter 1, electrolysis was hypothesized as a tool to fabricate a continuous bilayer scaffold consisting of fibrillar collagen sponge with gradient HAp content. The layer intended for cartilage-tissue engineering should show lower HAp content as to avoid chondrocyte hypertrophy; whereas the layer intended for bone tissue regeneration should exhibit the gradually increasing amount of HAp content as to promote bone matrix deposition [1]. In this way, the necessity to use knitting or gluing for joining two different kinds of scaffolds is eliminated, thereby reducing the risk of delamination after implantation [2,3]. To further improve the bone regeneration capacity of bilayer scaffolds, iron-oxide nanoparticles (IONP) were introduced to the scaffold as a potential agent to induce bone cells proliferation [4–6].

The goals of the chapter 3 were (1) to investigate electrolysis as a method to fabricate collagen sponges with gradient HAp content (continuous bilayer scaffold), (2) to fabricate collagen/chitosan sponge with gradient HAp content and investigate the influence of iron-oxide nanoparticles (IONP) addition to the capacity of bilayer scaffold to support osteoblast proliferation.

4.2 Experimental and Methods

Freeze-dried type I collagen from tilapia scales was purchased from Taki Chemical

Co., Ltd (Japan). 6 M hydrochloric acid, $CaCO_3$, 85% H_3PO_4, 99.5% ethanol, and *t*-butyl alcohol were bought from Wako Pure Chemical Industries, Ltd (Japan). Universal indicator solution pH 3-10 was purchased from Fluka Chemie GmbH (Germany). Platina plates (0.25×10×10 mm, 99.98%) as an electrode were purchased from the Nilaco Corp. The cylindrical electrolysis mold (ø = 24 mm, *h* = 20 mm) was custom-made from polycarbonate materials. HydroxyHAp was prepared in a similar manner as mentioned in the previous Chapters.

4.2.1 Fabrication of collagen sponge with gradient HAp content

4.2.1.1 Preparation of collagen/HAp solutions

0.015 mol/L of HCl solution was used to completely dissolved HAp particles at three different concentrations (0.1, 0.2, 0.3 wt%) . Next, collagen was subsequently dissolved in the HAp solution at a concentration of 1.0 wt%. The pH of final solution was adjusted to 3.0-3.2 by addition of small amount of 6 M HCl solution.

4.2.1.2 Electrolysis of solutions and fabrication of porous bodies

Two platina plates with 30 mm × 10 mm × 0.25 mm as electrodes were set on the opposite sides of cylindrical mold into which sufficient volume of collagen/HAp solution was poured. A power source (P4K36-0.1, Matsuda Sangyo, Ltd, Japan) was used, and a constant current at 6.6 mA (22 A/m^2) was applied to the electrodes. The electrolyzed hydrogels were washed in ultrapure water and placed in -20°C freezer as to induce rapid freezing and subsequently subjected to freeze-drying over-night. Sponges obtained by electrolysis of collagen - HAp (0.1, 0.2, 0.3 wt%) were named as ColHAp0.1, ColHAp0.2, ColHAp0.3, respectively.

4.2.1.3 Chemical analysis of the sponges

FTIR analysis with a diffuse reflectance attachment (DR-81, JASCO) was performed on the freeze-dried sponges to determine chemical composition. Background spectrum was initially measured by using KBr purchased from Wako Pure Chemical Industries, Ltd (Japan) at the wavenumber range of 4,000 - 400 cm^{-1}, resolution of 4.0 cm^{-1}, and accumulation times at 256. FTIR spectra of the mixture of KBr and composites were mixed at 100:1 in weight was subsequently measured under the same condition.

XRD analysis was conducted to confirm the inorganic phase of the sponges under the conditions as follow; step width at 0.02° and 2θ range from 20 to 60°, X-ray source of Cu, and power at 40 kV and 15 mA.

4.2.1.4 Analysis of gradient composition of collagen/HAp sponges

To assess the compositional difference in the sponges, thermal gravimetry-differential thermal analysis (TG-DTA: TG8120, Rigaku-Denki Co., Japan)) was performed. The entire part of the collagen sponge was evenly cut into four sections of equal thickness based on the normalized distance (Figure 4.1). Normalized distance was defined as the distance measured from cathode side. Each section was termed as (i). (ii), (iii), (iv) corresponding to the normalized distance and was analyzed by TG-DTA : under the following conditions; sample weight of 3 - 5 mg, heating ratio of 7 K/min, temperature range from room temperature to 600°C, and in a static air. Alumina (α-A_2O_3) was used as a reference. In each region, burned and leftover fraction were determined as organic (collagen) and HAp (inorganic) fraction, respectively.

Repeated measure one-way ANOVA was used to analyze inorganic/organic fraction of

each section from the same sample and significant difference between two means was analyzed by Tukey's test ($p<0.05$). Comparison of means between sample from different condition was analyzed by one-tail Student's *t*-test ($p<0.05$).

4.2.2 Fabrication of fibrillar collagen/chitosan sponge with gradient HAp content

4.2.2.1 Preparation of collagen-chitosan/HAp solution

Chitosan (low molecular weight) is prepared in stock solution in 2wt% in freshly prepared 0.1 M HCl. The solution was continuously mixed in 50°C for 1 hour and cooled down to room temperature. The solution was diluted to 0.62wt% by addition of ion-exchanged water to give clear solution at pH 5.1. Next, porcine skin collagen (HCl, pH 3.0, 0.62 wt%) was mixed with 0.62wt% chitosan solution in the 0.875 ratio. Spray-dried HAp particles (0.1 wt%) was dissolved in the collagen-chitosan solution and the pH was adjusted to 3.0 by addition of 6M HCl.

4.2.2.2 Electrolysis of solutions and fabrication of porous bodies

Electrolysis was conducted in the similar parameter with electrolysis of collagen/HAp solution, albeit cylindrical mold was used. The electrolyzed hydrogels were washed in ultrapure water and placed in -20°C freezer as to induce rapid freezing and subsequently subjected to freeze-drying over-night.

4.2.2.3 Analysis of the gradient composition of collagen-chitosan/HAp sponges

Chemical composition was conducted in the similar manner as in previous section. Microstructure of sponge pore walls was analyzed by SEM. Cross-section of sponge was taken, placed on the carbon tape, and coated with platina before SEM observation.

Gradient composition analysis of sponges (n=3) were conducted in the similar manner as in Chapter 2 section. Slight modification was conducted for gradient composition analysis. Two regions of interest were selected for the current analysis, that is (i-ii) and (iii-iv) regions.

4.2.3 Fabrication of fibrillar collagen-chitosan-iron oxide nanoparticles (IONP) /HAp sponge

4.2.3.1 Fabrication of IONP

IONPs were synthesized according to previous study [7]. 2.33 g of $FeCl_2 \cdot 4H_2O$ and 6.49 g of $FeCl_3 \cdot 6H_2O$ were added into 120 ml of nitrogen-purged ion exchanged water. The solution was rigorously stirred under N_2 gas, into which 120 ml of 0.8 mol/L of NaOH solution was added at a dropwise rate of 1.0 ml/min. The stirring was continued for 2 hours after complete addition of base and IONPs were washed with ion-exchanged water for three times.

4.2.3.2 Coating of IONP with carboxylate groups (citric acid)

Coating of IONPs with citric acid was conducted according to previous study [8]. 150 ml of citric acid solution (3.0 g) with pH adjusted to 4.6 was added into the IONPs agglomerate. The mixture was heated at 60°C in water bath for 30 minutes and rigorously stirred for another 90 minutes. Citric acid-coated IONPs (COO-IONPs) were repeatedly washed for five times by water and acetone. Lastly, CA-IONPs were dried in a vacuum oven for 12 hours. The particles were suspended in ion-exchanged water in concentration (10 mg/ml).

4.2.3.3 Preparation and electrolysis of collagen-chitosan-IONP/HAp solution

2 ml of COO-IONPs (20 mg/ml) was mixed with 8 ml of previously prepared collagen-chitosan/HAp solution. The mixture was hand-stirred to give homogeneous suspension; the suspension was poured into the cylindrical mold (diameter: 2.5 cm, height: 3.0 cm). Pre-magnetic treatment was applied as to fully accumulate COO-IONPs at the cathode side by placing neodymium magnet at the cathode side for 5 minutes. Next, electrolysis was conducted with the parameter similar to previous sections The electrolyzed gel was subsequently freeze-dried to obtain sponges. Other sponges were also prepared that is sponge without magnetic pre-treatment and sponge without COO-IONPs (0.9 ml of deionized water was added, instead of COO-IONPs suspension). The obtained sponges were crosslinked with dehydrothermal 105°C, for 24 hours.

4.2.3.4 Analysis of the fabricated sponges

The pore microstructure was observed with SEM in the backscattered-electron mode as to assess the distribution of IONP. Higher magnification of pore wall was observed in the secondary electron imaging mode. The mechanical properties of sponges was observed by compressive testing. Sample for compressive test was cut with biopsy punch for the diameter 8 mm and height 4 mm. Samples were immersed in PBS solution at 4° C for 24 hours and compressed with test speed 6 mm/min and strain target 60%. The modulus was defined as the slope of a linear fit to the stress–strain curve over 1%–5% strain. Stress at a strain of 10% was employed as compressive strength in. Three samples were prepared for each condition (n=3), and mean statistical differences for different condition was analyzed with Student`s t-test.

4.2.4 Cell-culture experiment

MC3T3-E1 (Riken Cell Bank) were expanded on 90 mm dishes using α-MEM (α-MEM; Wako Pure Chemicals Ltd., Japan) supplemented with 10% fetal bovine serum (FBS; CELLect, MP Biomedicals Inc., France) and 1% penicillin/ streptomycin (Wako Pure Chemicals Ltd., Japan). Cells were passaged at 80% confluence by using trypsin–ethylene diamine tetraacetic acid (Trpysin-EDTA; Wako Pure Chemicals Ltd., Japan) and cells below passage 10 were used for in vitro analysis.

Sponges were sterilized in 70% ethanol for 1 hour, 2 times. Sponges were washed with autoclaved PBS and conditioned overnight in serum-freeα-MEM. Sponges were placed in the non-treated well plate; 50 μL of the cell suspension ($6x10^4$ cells) were dropped on the cathode side of sponges. The well plate was returned to incubator and left for 3 hours to allow cell attachment. Following incubation, 450 μL of complete α-MEM was added to each well and the plate was returned to the incubator.

The cell number was measured at day 1, day 3, and day 5 after cell seeding by using Cell Counting Kit-8 (CCK-8: Dojindo Laboratories, Japan). Briefly, 50 μL of CCK-8 was added to each well and the plate was incubated at 37°C for another 2 h. An aliquot of 100 μL was taken from each well and transferred to fresh 96-well plate. The absorbance of these samples was measured at 450 nm with a spectrophotometric microplate reader (Bio-Rad 680, USA). The absorbance value was converted to cell numbers by using calibration curve of known MC3T3-E1 cell numbers vs absorbance of CCK-8. Cell seeding efficiency was obtained by the following equation:

$$Cell\ seeding\ efficiency = \frac{Cell\ number\ at\ day\ 1}{Initial\ cell\ number}\ x\ 100$$

To assess the cell attachment, sponge at day 6 was was rinsed with PBS and fixed with

2.5% glutaraldehyde and washed with PBS. Samples were sequentially dehydrated with ethanol series (50%, 70%, 90%, 95%, 100%) and t-butanol. The specimens were re-lyophilized before observed with SEM.

To assess the cell proliferation, fold-increase of cell numbers was calculated by using the following formula:

$$Fold - increase = \frac{Cell\ number\ at\ day\ 6}{Cell\ number\ at\ day\ 1}$$

4.3 **Results and Discussion**

4.3.1 Evaluation of feasibility to obtain double bilayer structure

Compositional characterization of Col1.0HAp0.1 by FTIR and XRD was given in Fig. 4.1. FTIR spectrum showed the mixture of three different peaks attributable to Col: 1671 cm^{-1} (Amide I), 1535 cm^{-1} (Amide II), and 1225 cm^{-1} (Amide III), which were matched to the previous report[9]. Moreover, additional peaks attributable to HAp was observed that is PO_4^{3-} at 1080 / 1030 cm^{-1} and doublets at 602 and 574 cm^{-1}. These peaks were attributable to the low-crystallized HAp[10]. XRD analysis of Col1.0HAp0.1 (Fig. 6(a)) showed broad peaks at 2θ: 21.7°, 26.2°, 28.4°, 31.9°, and 39.7°, which are attributable to HAp with low crystallinity[11]. The presence of low-crystallized HAp was beneficial for enhancing activity of pre-osteoblast cells *in vitro*[12] and supported the bone formation *in vivo*[13]. The formation of low-crystallized HAp would be attributed to the re-precipitation of dissolved Hap during electrolysis process.

Microstructure of region (i) and region (iv) for the freeze-dried Col1.0HAp0.1 was given in Fig. 4.2. Region (i) and (iv) exhibited similar pore size that is 213 μm ± 28 um

and 247μm ± 37 um, respectively. Higher magnification of pore walls for region (i) and (iv) revealed the presence of HAp precipitate seemingly encapsulated by Col fibrillar structure.

Analysis of gradient composition was conducted for Col1.0HAp0.1, Col1.0HAp0.2, and Col1.0HAp0.3 sponges (Fig. 4.3). The significant difference of HAp/Col ratio at (i) and (iv) regions for Apt concentration samples was only present for Col1.0Apt0.1 sponge and absent for Col1.0HAp0.2, and Col1.0HAp0.3 sponges. These data suggested the successful formation of continuously HAp-graded Col compositions as a sponge form for Col1.0Apt0.1, with the region closest to cathode (< 25 % of normalized distance) to be highly mineralized and region far from cathode to be less mineralized (> 75 % of normalized distance). It is worth to note that HAp/collagen ratio in the region (i) /`bone layer` of electrolyzed sponge is 1:5, still lower than composition for bone-like material (7:3). Nonetheless, presence of HAp at 20wt% of total scaffold mass had been reported to support the bone cells matrix secretion capacity [14]. Presence of HAp in the region (iv)/`cartilage layer` raised concerns regarding suitability as cartilage tissue-engineering scaffold, as HAp is not naturally existing in the native cartilage tissue [15]. Nonetheless, previous studies had reported no negative effect of HAp to cartilage-tissue formation capacity; instead, presence of HAp improved the mechanical properties of sponges [16,17].

The mechanism of formation of gradient HAp content in collagen was proposed by initially considering the relationship of electric field and ionic species distribution in the electrolysis system (Fig. 4.5). Initially, electrically charged electrode (negative for cathode and positive for anode) attract solvated counter-ions namely Ca^{2+} for cathode and HPO_4^{2-}, PO_4^{3-}, and Cl^- for anode. The counter-ions existed at particular distance from the electrode and forming the Stern layer [18–20]. The presence of counter-ions screened the

electric field cause the linear reduction of potential. Adjacent to the Stern layer, multiple cationic and anionic ions loosely compose a specific region named diffuse layer, which maintain the charge neutrality and exponentially reduce the magnitude of potential [18–20]. Stern and diffuse layer (electrical double layer) effectively screen the electrode potential, and as potential value determine the magnitude of electric field, the electric field at the bulk of electrolyte is essentially zero.

The water molecules are reduced and oxidized at cathode and anode according to the eq. 4-1 and 4-2:

Cathode : $2H_2O+2e^- \rightarrow 2OH^-+H_2$ $E° = -0.83$ V (4-1)

Anode : $2H_2O \rightarrow 4H^+ +4e^- +O_2$ $E° = +1.229$ V (4-2)

In the current electrolysis system, there are several ions identified: 1. Cationic: Ca^{2+}, 2. Anionic: $H_2PO_4^-$, Cl^-. Ca^{2+} and $H_2PO_4^-$ originate from the dissolve HAp ($Ca_{10}(PO_4)_6OH_2$); $H_2PO_4^-$ is the main form of inorganic phosphate at low pH. Out of these ions, only Cl^- that could compete with the electrolysis of water, particularly water oxidation at anode, owing to the high reduction potential $Cl_2 \rightarrow 2Cl^- +2e^-$ $E° = +1.36$ V. Nonetheless, as collagen formation occur mainly at cathode, it was presumed that the influence of Cl^- oxidation to the collagen formation is minimal [21].

Produced hydroxide ions (OH^-) causes deposition of collagen monomers into gel-like state material with the mechanism already explained in chapter 3; OH^- causes the increases of pH (<9), which in turn induces dissociation of $H_2PO_4^-$ into HPO_4^{2-} and PO_4^{3-}. These phosphoric acid species, together with Ca^{2+} and OH^-, precipitates into HAp according to the eq. 4-3:

$$_{10-x}Ca^{2+} + {}_xHPO_4^{2-} + {}_{6-x}PO_4^{3-} + {}_{2-x}OH^- \rightarrow Ca_{10-x}(HPO_4)_x(PO_4)_{6-x}OH_{2-x} \quad (4\text{-}3)$$

The mechanism of formation of gradient HAp content in collagen was schematically given in Fig. 4.6. Ionic species at Stern and diffuse layer are consumed at this reaction; which in turn removes the potential screening by electrical double layer. As a result, electric field extend and polarizes HAp particles, causing formation of electrical double layer at surface of HAp particles. Continuous production of OH^- at cathode cause further precipitation of HAp on electrical double layer of previously formed HAp particles, resulting in the large amount of precipitated HAp at area near cathode. As the electrolysis reaction proceeds, magnitude of electric field decreases linearly with distance, resulting in the absence or scarce existence of electrical double layer on a numbers of HAp particles at distance from cathode, which in turn cause less precipitation of HAp . Taken together, it was proposed that the changes of electric field magnitude throughout the electrolysis process causes gradient content of HAp.

At the current electrolysis system, initial voltage was 4.5 V and gradually increased to 6 V (~45 minutes of electrolysis) before rapidly jumping to 10 V (~45 – 60 minutes of electrolysis). The increasing of voltage was caused by accumulation of H_2 bubble gas at side of deposited collagen gel facing cathode side (data not shown), which in turn act to inhibit the electrolysis reactions. H_2 bubble gas could be removed from the gel by washing in water for several minutes, without significantly affecting the structures of obtained sponges.

It is worthy to note that Col1.0HAp0.3showed significantly higher ratio of HAp/Col ratio at (i) region at 0.42 ± 0.01 compared to the same region of Col1.0HAp0.1 (0.25±0.05) and Col1.0HAp0.2 (0.31±0.03), implying that the higher concentration of dissolved HAp (Ca^{2+} concentration) correlates with larger amount of re-precipitated HAp. However, the higher concentration of Ca^{2+} eliminates the gradient properties on the

electrolyzed sponges [21].

4.3.2 Evaluation of bilayer structure of collagen-chitosan/HAp

FTIR spectrum of Col-Chi-HAp was shown in Fig. 4.7. Bands attributable to amide of Col were observed at 1650-1450 cm^{-1}, peak characteristic of Chi was observed at 1152 cm^{-1}. Doublets characteristic of HAp PO_4^{3-} at 1069/1030 cm^{-1} and 606/562 cm^{-1}. Taken together, the composite of Col, Chi, and HAp was successfully obtained.

HAp/Col-Chi ratios for the cathode and anode sections was shown in Fig. 4.8. Region (i-ii), which was closest to cathode, possessed highest HAp/Col ratio at 0.20 ± 0.02 which was approximately two-fold ($p < 0.05$, n = 3) of region (iii-iv) (0.12 ± 0.01). These data suggested that addition of Chi did not interfere with the formation of structure with gradient HAp content.

4.3.3 Characterization of the Fabricated IONP

XRD characterization was shown in Fig. 4.9. XRD patterns (Fig. 4.9(a)) of of naked IONPs and COO-IONPs exhibited characteristic diffractions of magnetite (ICDD card # 88-0866) at 2θ = 30.1° (220), 35.5° (311), 43.2° (400), 53.6° (422), 56.9° (511), and 62.6° (400). Particle size for IONPs was 9.5 nm and for COO/IONP was 9.3 nm), as calculated with the Scherrer equation for (311) diffraction peak.

Presence of COO-coating on IONPs were confirmed with FTIR analysis (Fig. 4.9(b). All samples showed bands at 580 cm^{-1} and 800/890 cm^{-1}, attributable to Fe-O stretching of Fe_3O_4 and Fe-OH bonding of goethite (FeO(OH)), respectively [22,23]. COO/IONPs exhibited peaks at 1582 and 1378 cm-1, attributable to asymmetric and symmetric stretching of carboxylate group ($\nu_{asym}(COO^-)$ and $\nu_{sym}(COO^-)$) of citric acid [8], respectively.

Fig. 4.9(c) showed that COO/IONP was well-suspended in the deionized water at 5 mg/ml concentration and magnetically responsive in the presence of neodymium magnet. Zeta potential value for COO/IONP was -31.7 mV, attributable to the negative charge of COO groups of surface-chemisorbed citric acids. Taken together these results, suggested the successful functionalization of IONPs with COO^- groups by citric acid.

4.3.4 Evaluation of collagen-chitosan-IONP/HAp sponges

TG curve for all sponges were given in Fig. 4.10. Col and Chi was degraded up to 600°C; whereas the leftover mass was attributed to HAp and IONP. Col and Chi was assigned organic ratio; whereas HAp and IONP was attributed to inorganic ratio. The inorganic/organic ratio was summarized in Fig. 4.11. As can be seen, addition of IONP enhanced the inorganic ratio up to ten-fold for sample without and with magnetic pre-treatment. Distribution of IONP in the pore structure was analyzed with back-scattered electron imaging (Fig. 4.12). Col-Chi-HAp sample showed image with uniform brightness, whereas Col-Chi-HAp/IONP samples exhibited uniform bright area correspond to the presence of particles with heavier element (IONP). Col-Chi-HAp/IONP/Magnet sample showed segregation of dark area (Col) at the top part of sponge and bright area (IONP) at the bottom part of sponge, suggesting the successful formation of IONP-enriched layer. Application of magnetic treatment caused segregation of IONP at cathode area, and further application of electrolysis encapsulated the IONP. Higher magnification of Col-Chi-HAp sample exhibited smooth appearence of pore walls. In contrast, Col-Chi-HAp/IONP sample showed encapsulation of IONP by the pore walls. Pore walls of IONP-enriched area showed heavy aggregation of IONP which completely destroyed the pore structures.

Compressive modulus and strength of three sponges were shown in Fig. 4.13. Col-Chi-HAp/IONP sample showed the highest modulus compared to Col-Chi-HAp and Col-Chi-HAp/IONP/Magnet sample showed the lowest compressive modulus. Similar trend was also observed for compressive strength; IONP samples showed the highest strength to Col-Chi-HAp and Chi-HAp/IONP/Magnet. Nonetheless, the strength of Col-Chi-HAp and Col-Chi-HAp/IONP/Magnet was indifferent.

During compression of pure collagen sponge, pore strut (collagen) is the sole carrier of the load. Presence of HAp in the pore strut is beneficial as the relatively rigid HAp carrying the majority of the load, resulting in the stiffer structure. IONP, as the inorganic component, act in the similar manner when it exists in the pore struts. Thereby, addition of IONP is beneficial in enhancing the compressive properties of sponges, thereby presence of IONP is beneficial. Interestingly, Col-Chi-HAp/IONP/Magnet showed hampered compressive properties, despite exhibiting large inorganic/organic ratio. The segregated IONP destroyed the pore structures of sponges, which in turn diminish the integrity of sponges, and resulting in the lower mechanical properties.

Observation of cell morphology (Fig. 4.14) revealed that osteoblasts were completely attached on Col-Chi-HAp and Col-Chi-HAp/IONP; whereas osteoblasts underwent difficulty to properly attach on uneven surface of pore struts for Col-Chi-HAp/IONP/Magnet. Col has glycine-phenylalanine-hydroxyproline-glycine-glutamic acid-arginine (GFOGER) motif which is capable to directly bind the cells [15,24]. The presence of IONPs inside the Col pore struts might reduce the active binding site, thus reducing the initial cell attachment. Disturbance of cells binding to Col by IONP was translated to lower cell-seeding efficiency (Fig. 4.15a) for all of IONP-added sponges, Col-Chi-HAp/IONP (33.2% ± 1.8%) and Col-Chi-HAp/IONP/Magnet (17.8% ± 2.3%),

compared to sponge without IONP, Col-Chi-HAp (44.7 % ± 4.1 %). The cell number of all samples given in Fig. 4.15b; Col-Chi-HAp showed the highest cell number value at day 1, 3, day 6 compared to IONP-added sponges However, calculation of fold-increase (Fig. 4.16) revealed that both of Col-Chi-HAp/IONP and Col-Chi-HAp/IONP/Magnet underwent the significant increasing of cell number to Col-Chi-HAp, suggesting the positive effect of IONP onto osteoblast proliferation, consistent with previous studies [4,5]. In contrast, segregation of IONP in the sponge was detrimental to the mechanical and biological properties of sponge.

4.4 **Summary**

1. Electrolysis of Col/Apt solution successfully produced a continuous body of Col sponge with a gradually varying HAp content. During the electrolysis, the high and low pH pockets were formed at the vicinity of electrodes. The high pH region induced the gradual Col gelation and re-precipitation of HAp. The dimension of Col hydrogel could be adjusted by varying the electrode distance. Col sponges was obtained by freeze-drying the electrolyzed gel; sponges (Col1.0wt%/Apt0.1wt%) showed significantly higher HAp/Col ratio for area closest to cathode side (<25% of normalized distance) compared to area farthest from cathode (>75% of normalized distance). High concentration of dissolved Apt (0.2/0.3wt%) diminished the HAp-gradient properties. The mechanism of occurrence of gradient HAp properties was proposed as a relationship of electric-field and electrical double layer formation on precipitated HAp particles.

2. Electrolysis of Col-Chi-HAp solution successfully produced structure with gradient HAp composite. IONP was added to the Col-Chi-HAp sponge and IONP was incorporated in the pore walls of sponges. Addition of carboxylate-capped IONP into Col-

Chi-HAp composite increased the bulk compressive properties, possibly due to the enhanced crosslinking degree. Segregation of IONP at the region near cathode caused the destruction of pore walls. Presence of IONP slightly reduced the initial osteoblast attachment, resulting in the lower cell-seeding efficiency compared to Col-Chi-HAp sponge. Nonetheless, the similar cell number at day 6 of cell culture suggested that IONP promoted proliferation of osteoblast.

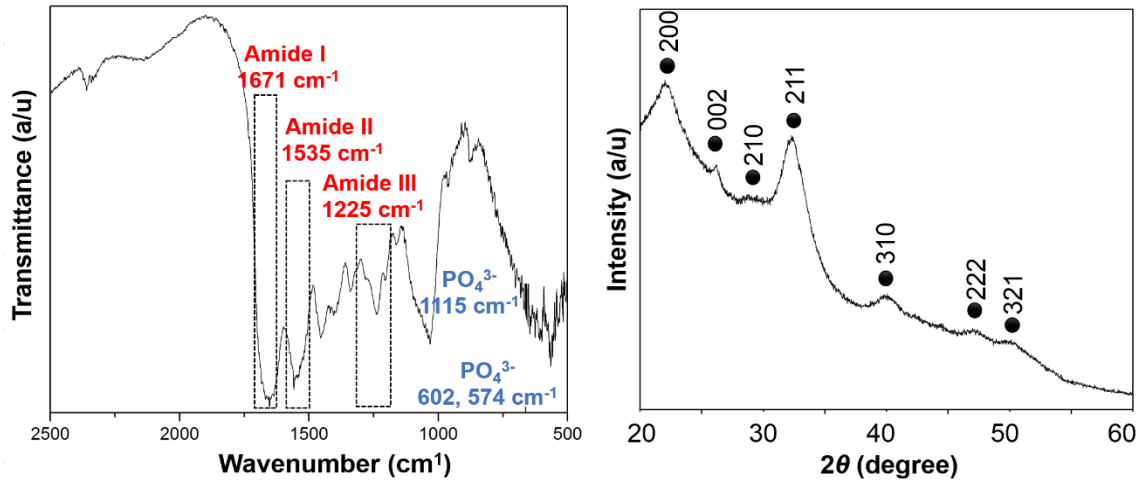

Fig. 4.1 (a) FTIR analysis and (b) XRD pattern of electrolyzed Col1.0HAp0.1

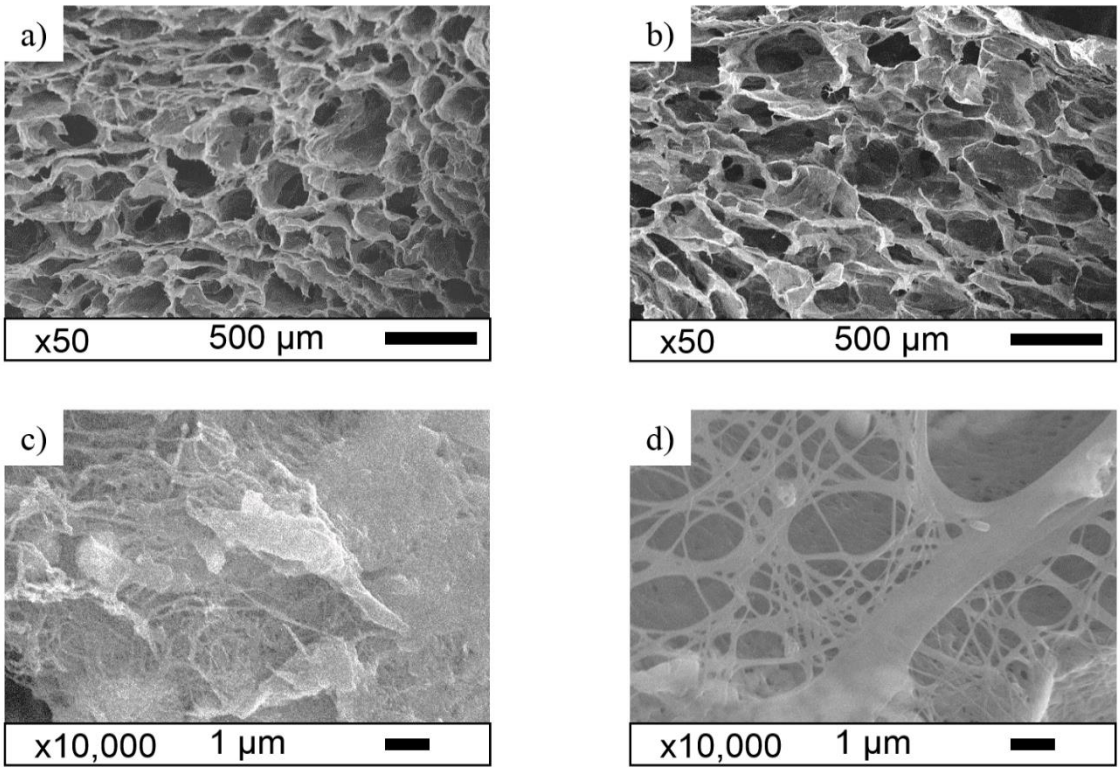

Fig. 4.2 (a, b) Pore structures of region (i) and (iv), respectively. (c, d) Pore wall appearance of region (i) and (iv), respectively

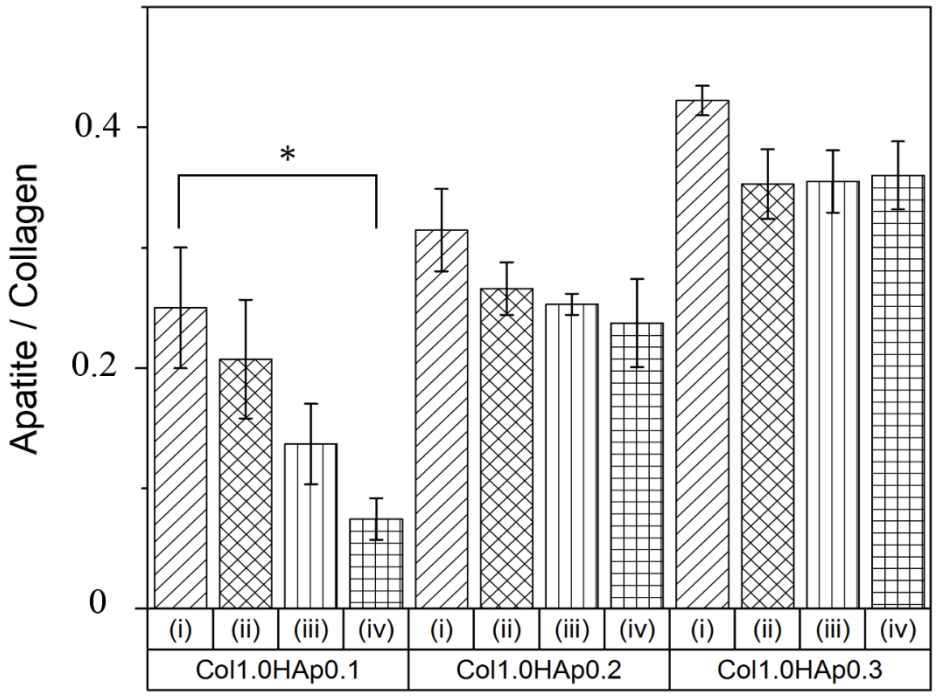

Fig. 4.3 Analysis of gradient composition for electrolyzed Col sponges with various HAp concentrations

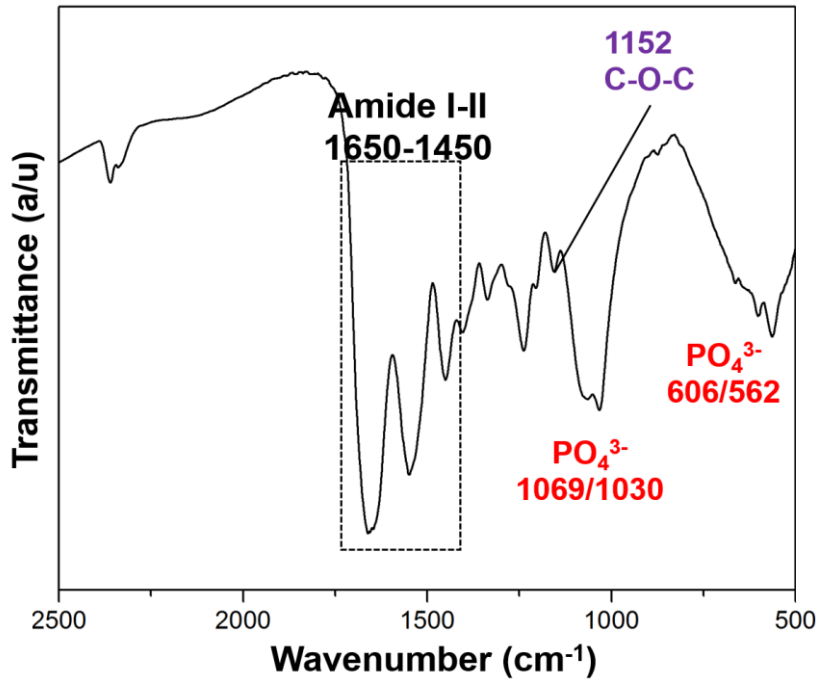

Fig. 4.4 FTIR analysis of sponges obtained from electrolysis of Col-Chi-HAp solution

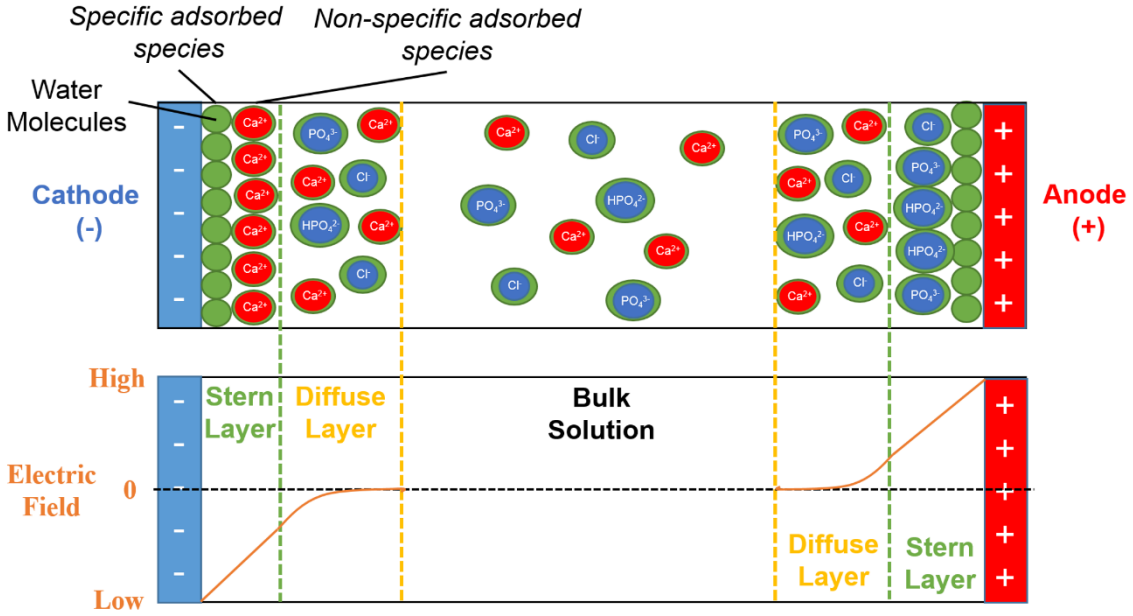

Fig. 4.5 Schematic drawing of initial ionic species distribution in electrolysis system of dissolved HAp/collagen. Water molecules non-specifically adsorbed on electrodes. Cationic and anionic ions screen the cathode and anode (stern layer), respectively, resulting in the decrease of electric field. Adjacent to stern layer is loose association of ionic species (diffuse layer) which further screen the electric field of electrodes, resulting in the nullified electric field in the bulk solution area.

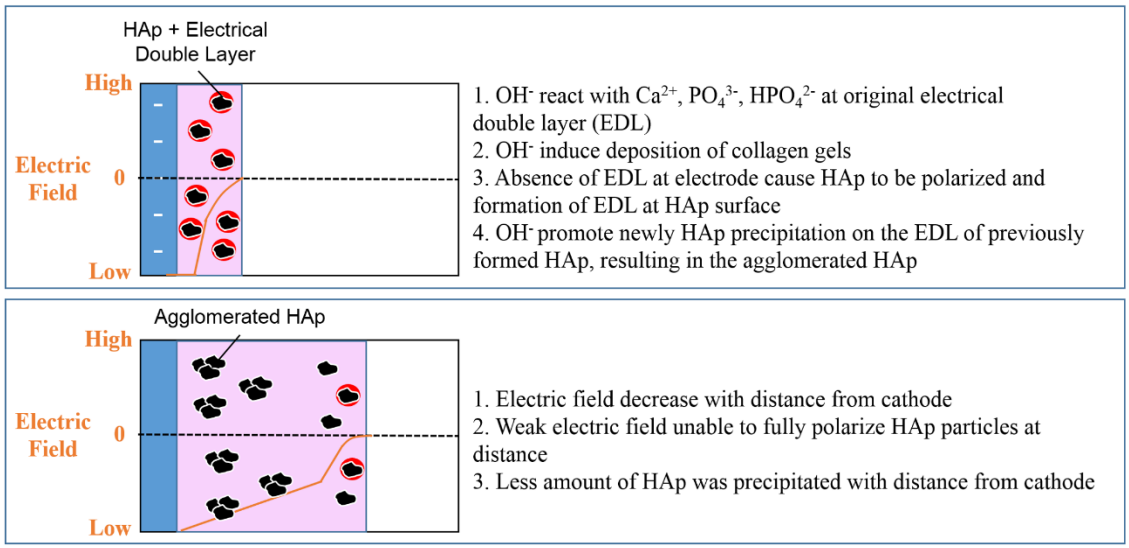

Fig. 4.6 Schematic drawing of HAp precipitation in the electrolysis system. (Top box) HAp precipitation at the initial time of electrolysis. (Bottom box) HAp precipitation at the latter time of electrolysis.

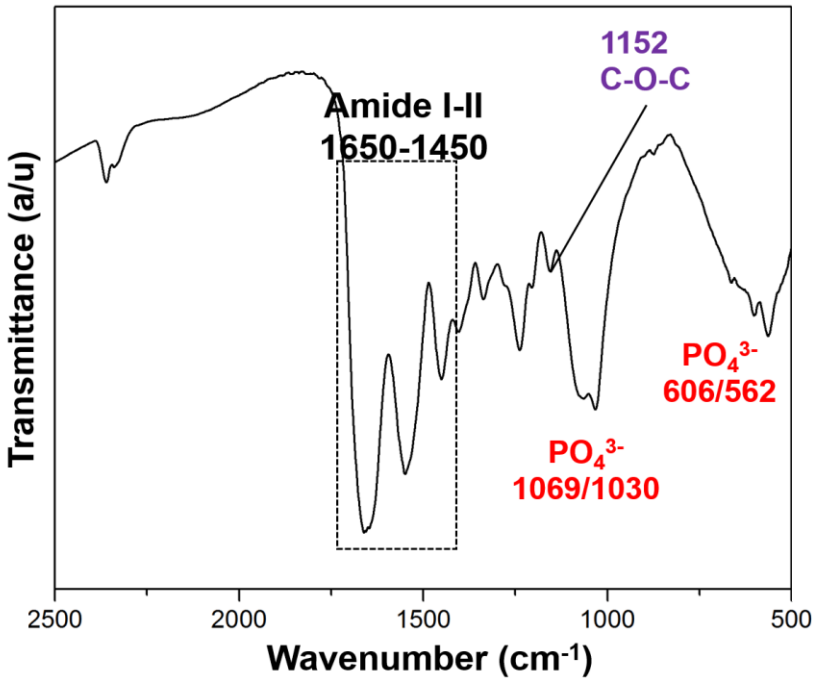

Fig. 4. 7 FTIR analysis of sponges obtained from electrolysis of Col-Chi-HAp solution

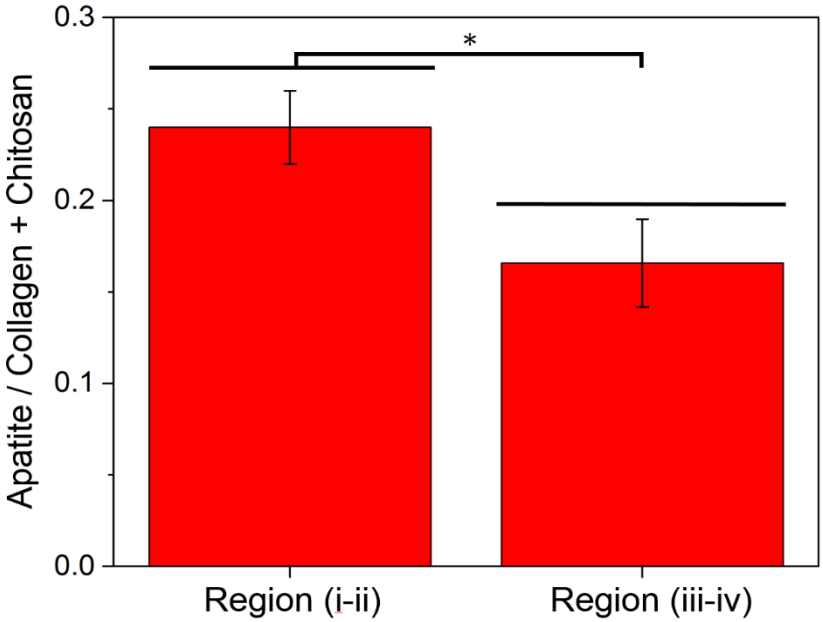

Fig. 4.8 Analysis of gradient composition for of sponges obtained from electrolysis of Col-Chi-HAp solution. *p<0.05 n= 3

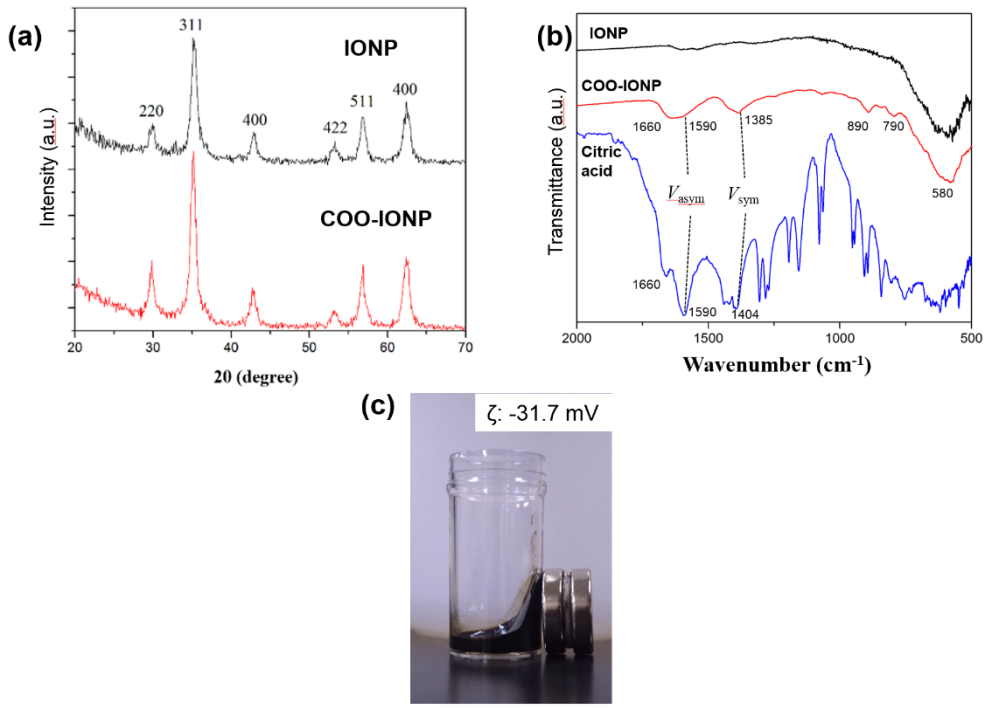

Fig. 4.9 (a) XRD pattern of IONP and COO-IONP, (b) FTIR spectra of IONP, COO-IONP and citric acid, (c) Appearance of COO-IONP (suspended in deionized water 5 mg/ml) and measured zeta potential.

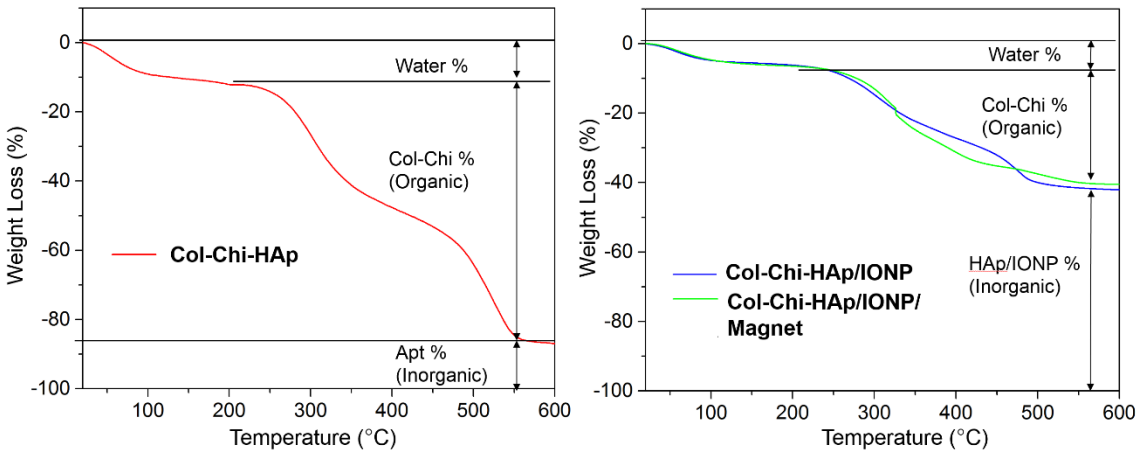

Fig. 4. 10 Thermal gravimmetry for all sponges. Legend indicate the line and type of sample

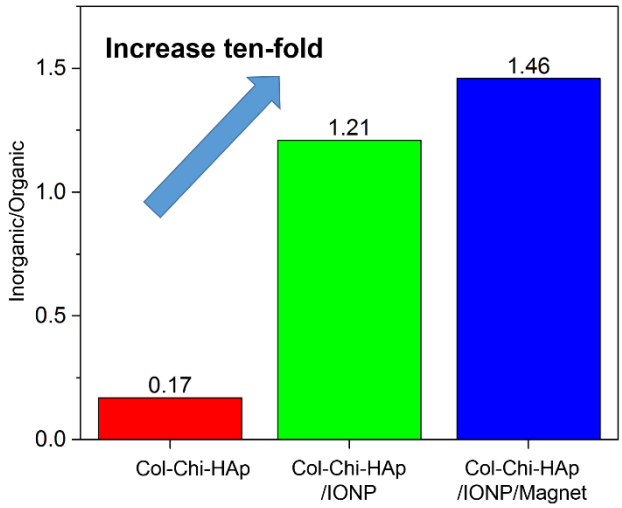

Fig. 4. 11 Summary of inorganic/organic ratio of sponges

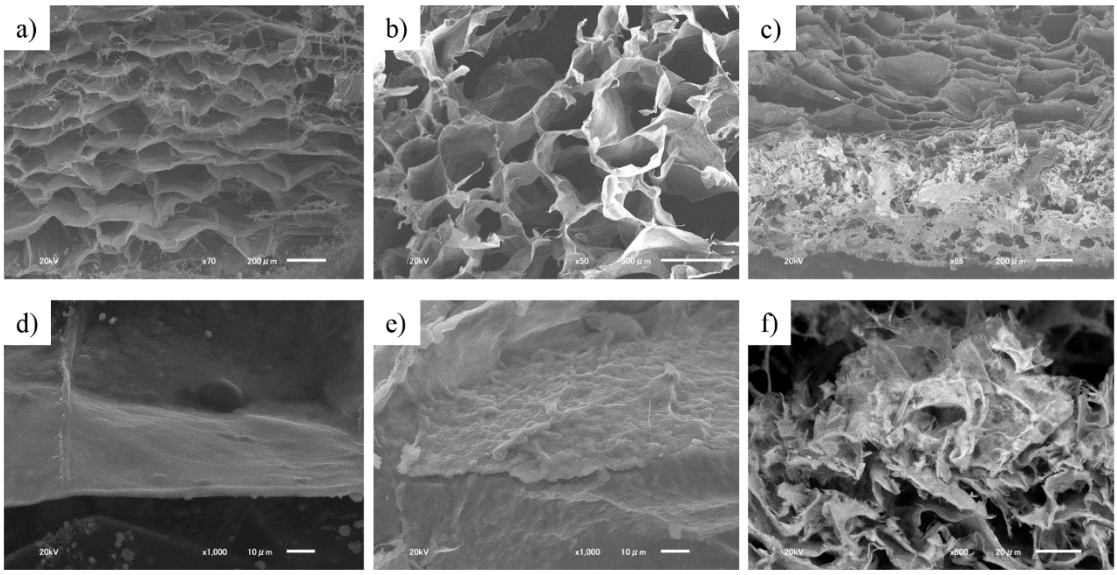

Fig. 4. 12 Backscattered electron images of (a) Col-Chi-Apt, (b) Col-Chi Apt/IONP, (c) Col-Chi-Apt/IONP/magnet. Higher magnification of pore walls obtained by secondary electron imaging of (d) Col-Chi-Apt, (e) Col-Chi-Apt/IONP, (f) Col-Chi-Apt/IONP/magnet.

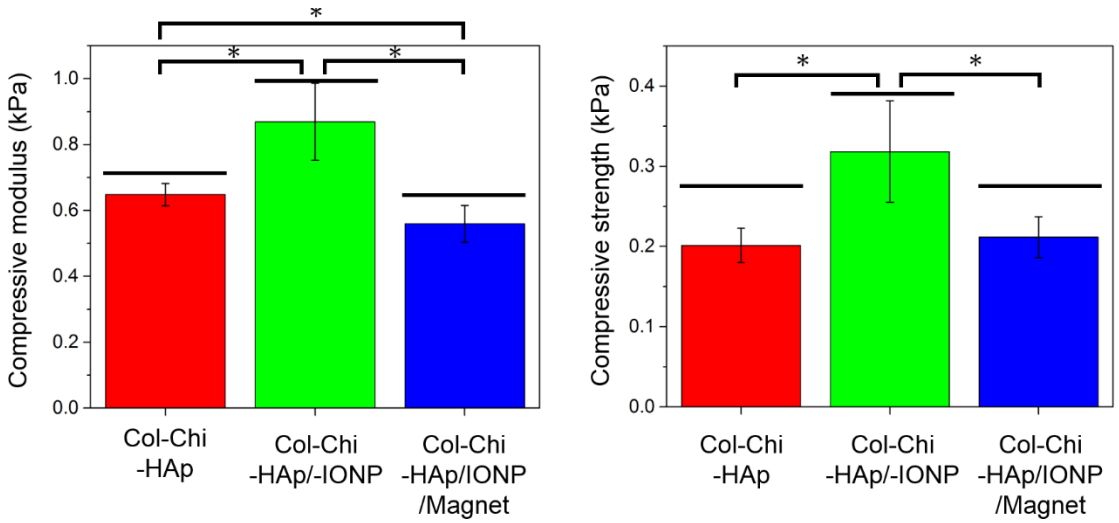

Fig. 4. 13 Compressive modulus and strength for electrolyzed sponges. *p<0.05 n= 3

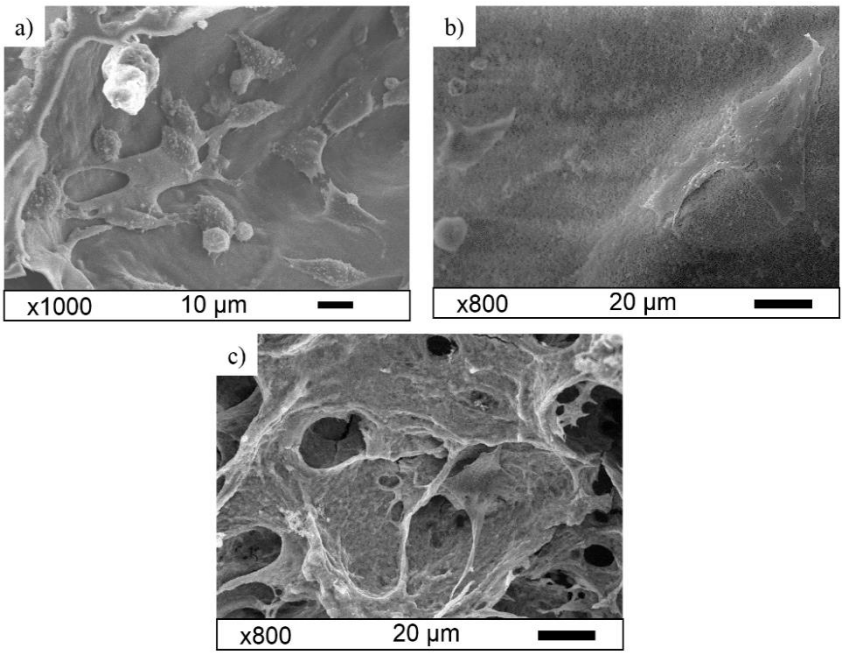

Fig. 4.14 Cell morphology of osteoblast attached on cathode side of (a) Col-Chi-Apt, (b) Col-Chi-Apt/IONP, (c) Col-Chi-Apt/IONP/magnet.

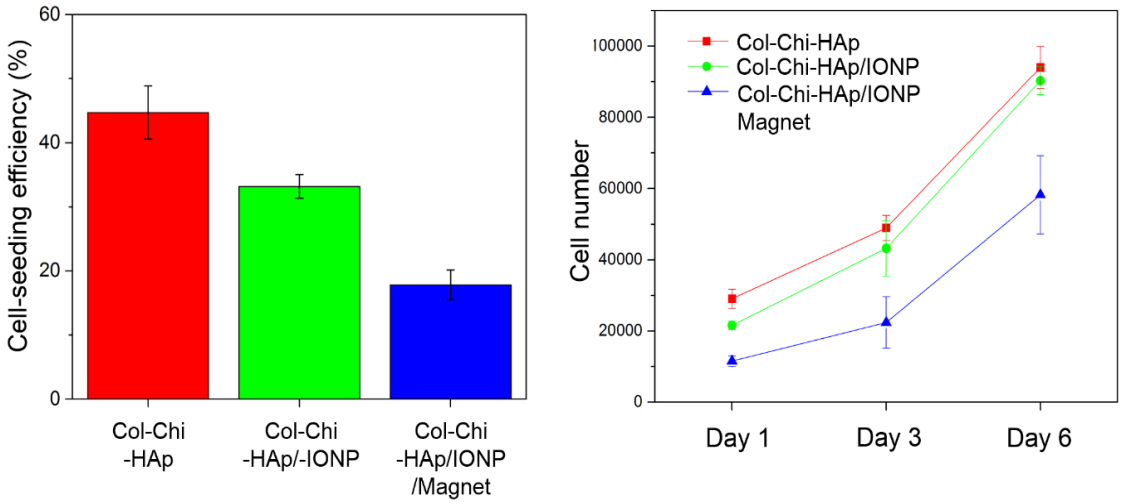

Fig. 4.15 Cell-seeding efficiency and cell numbers for Col-Chi-HAp, Col-Chi-HAp/IONP, Col-Chi-HAp/IONP/Magnet

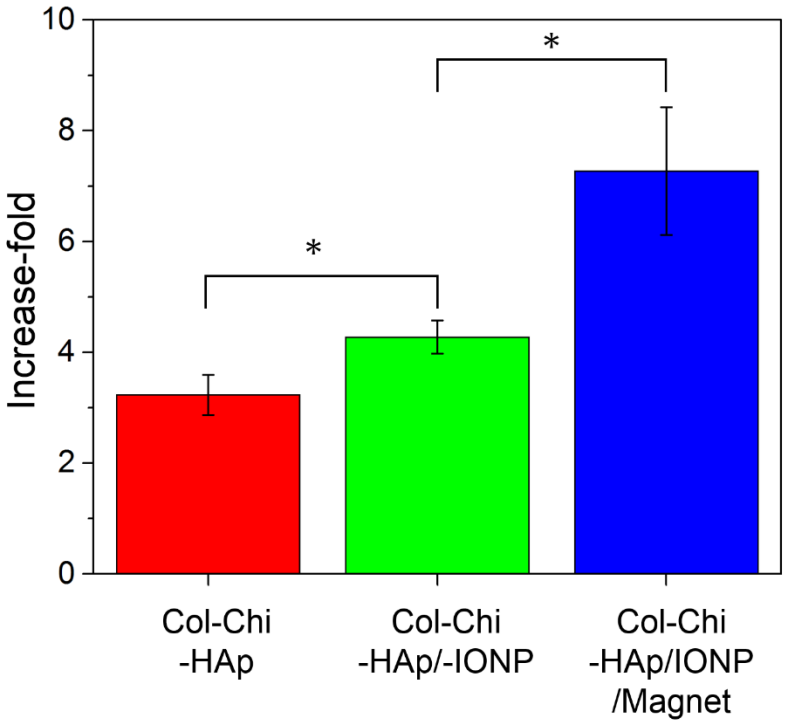

Fig. 4.16 Increase-fold of cell number cultured in various sponges. * $p<0.05$, n = 3

References

1 M. Kikuchi, T. Ikoma, S. Itoh, H. N. Matsumoto, Y. Koyama, K. Takakuda, K. Shinomiya and J. Tanaka, *Compos. Sci. Technol.*, 2004, **64**, 819-825.

2 I. Martin, S. Miot, A. Barbero, M. Jakob and D. Wendt, *J. Biomech.*, 2007, **40**, 750-765.

3 S. Miot, T. Woodfield, A. U. Daniels, R. Suetterlin, I. Peterschmitt, M. Heberer, C. A. Van Blitterswijk, J. Riesle and I. Martin, *Biomaterials*, 2005, **26**, 2479-2489.

4 N. Tran and T. J. Webster, *Acta Biomater.*, 2011, **7**, 1298-1306.

5 D. Septiadi, F. Crippa, T. L. Moore, B. Rothen-Rutishauser and A. Petri-Fink, *Adv. Mater.*, 2018, **30**, 1-30.

6 Q. Wang, B. Chen, F. Ma, S. Lin, M. Cao, Y. Li and N. Gu, *Nano Res.*, 2017, **10**, 626-642.

7 V. Irawan, T. Sugiyama and T. Ikoma, *Key Eng. Mater.*, 2016, **696**, 121-128.

8 S. Nigam, K. C. Barick and D. Bahadur, *J. Magn. Magn. Mater.*, 2011, **323**, 237-243.

9 T. Ikoma, H. Kobayashi, J. Tanaka, D. Walsh and S. Mann, *Int. J. Biol. Macromol.*, 2003, **32**, 199-204.

10 E. Szarawara, B. Trybalska, M. Cichocin, A. Stoch, W. Jastrze and A. Broz, *J. Mol. Struct.*, 1999, **512**, 287-294.

11 S. Koutsopoulos, *J. Biomed. Mater. Res.*, 2002, **62**, 600-612.

12 J. Wang, J. De Boer and K. De Groot, *J. Dent. Res.*, 2008, **87**, 650-654.

13 T. Hayakawa, C. Mochizuki, H. Hara, T. Fukushima, F. Yang, H. Shen, S. Wang and M. Sato, *J. Hard Tissue Biol.*, 2009, **18**, 7-12.

14 G. Mattei, C. Ferretti, A. Tirella, A. Ahluwalia and M. Mattioli-Belmonte, *Sci. Rep.*, 2015, **5**, 1-14.

15 V. Irawan, T.-C. Sung, A. Higuchi and T. Ikoma, *Tissue Eng. Regen. Med.*, 2018, **15**, 673-697.

16 Y. Ohyabu, T. Adegawa, T. Yoshioka, T. Ikoma, T. Uemura and J. Tanaka, *Mater. Sci. Eng. B Solid-State Mater. Adv. Technol.*, 2010, **173**, 204-207.

17 Y. Ohyabu, T. Adegawa, T. Yoshioka, T. Ikoma, K. Shinozaki, T. Uemura and J. Tanaka, *J. Biomater. Sci.*, 2009, **20**, 1861-1874.

18 L. Han, S. Galier and H. Roux-de Balmann, *Desalination*, 2015, **373**, 38-46.

19 Y. Wang, S. R. Narayanan and W. Wu, .

20 R. W. Impey, P. A. Madden and I. R. McDonald, *J. Phys. Chem.*, 1983, **87**, 5071-

5083.

21 V. Irawan, Y. Sasaki and T. Ikoma, *J. Mater. Chem. B*, , DOI:10.1039/C9TB00791A.

22 Y. S. Hwang, J. Liu, J. J. Lenhart and C. M. Hadad, *J. Colloid Interface Sci.*, 2007, **307**, 124-134.

23 M. Yamaura, R. L. Camilo, L. C. Sampaio, M. A. Macêdo, M. Nakamura and H. E. Toma, *J. Magn. Magn. Mater.*, 2004, **279**, 210-217.

24 G. Grundström, *Functional Studies of Collagen-Binding Integrins a2b1 and a11b1*, .

Chapter 5-Electrolysis Preparation of Bilayer Scaffolds of Hydroxyapatite Porous Body Coated with Magnetite and Hydroxyapatite-Collagen Sponge

Chapter 5 describes fabrication of a continuous bilayer structure consisting of fibrillar collagen/HAp sponge and HAp-sintered body and subsequent evaluation of magnetic properties and biocompatibility of bilayer structure after addition of iron-oxide nanoparticles. HAp-sintered body was fabricated as followed: green body of HAp was initially formed by gel-casting method. Next green body was sintered at 1200°C for 2 hours. The HAp-sintered body was placed in the cylindrical electrolysis mold; suspension of collagen/HAp was poured to fill the mold. After electrolysis, continuous bilayer structure of collagen/HAp gel and HAp-sintered body was obtained. The structure can be transformed into the porous structure by freeze-drying. Microstructure analysis revealed that collagen/HAp sponge penetrate the HAp-sintered body, suggesting formation of continuous interface. Mechanical test further showed that bilayer structure exhibited two-different elastic modulus, attributable to collagen sponge and HAp-sintered body, implying successful formation of continuous bilayer structure of collagen/HAp. Lastly, HAp-sintered body was successfully magnetized by immersion in the suspension of carboxylate-capped IONP of varying concentration (2 mg/ml, 10 mg/ml, 50mg/ml); in which, the magnetic pull-out force depended on the initial concentration of IONP solution. Cell culture experiment revealed that no negative effect was influenced by incorporation of IONP.

5.1 Introduction

In previous Chapters, electrolysis was demonstrated as a powerful tool to fabricate a continuous bilayer structure consisting of collagen sponge and gradient HAp content.

Despite the improvement of mechanical properties of bilayer structure (compressive modulus ~1 kPa) by addition of IONP, the compressive modulus is still far inferior to mechanical properties of bone tissue (compressive modulus: 100-200 MPa) [1]. HAp-sintered body exhibited compressive modulus: 6 MPa, which was deemed to be closer to the compressive modulus of bone. Thereby, a continuous bilayer structure consisting of fibrillar collagen and HAp-sintered body was considered as the promising alternative of a sponge-based bilayer structure previously given in the Chapter 4.

Implantation of scaffold into the osteochondral injury requires fixation by glue or knitting to firmly fix the scaffold at the defect area [2,3]. The procedure is time-consuming and technically demanding for surgeon. Other investigators had proposed alternative of these physical fixation method, that is by imparting magnetic properties into the scaffold and utilizing external magnet to firmly fix the scaffold location. It was hypothesized that magnetic properties can be imparted into bilayer structure of collagen sponge and HAp-sintered body by incorporation of IONP.

The main goal of the current chapter was to fabricate a continuous bilayer structure consisting of fibrillar collagen/HAp sponge and HAp-sintered body and subsequent evaluation of magnetic properties nad biocompatibility of bilayer structure after IONP incorporation.

5.2 Experimental and Methods

HAp powder was prepared by a wet chemical method[4] Briefly, 0.5 mol/L of $Ca(OH)_2$ suspension (2.0 L) was adjusted by the addition of ion exchanged water to CaO which was obtained by calcining $CaCO_3$ at 1050°C for 3 hours. 0.6 mol/L H_3PO_4 (1.0 L) was then slowly added into the suspension until the pH became 7.8. The suspension was spray-dried with a mini-spray drier (B-290, Büchi, Switzerland) under the inlet and outlet

temperatures of 180°C and 60°C.

5.2.1 *Fabrication of HAp-sintered body*

HAp porous body was prepared by gel-casting method [5]. 5.0 g of HAp powder was added to 15 ml of purified water and heated to 50°C. 1.25 g of gelatin powder was added to the HAp suspension. The mixture was homogenized with homogenizer 9000 rpm for 30 seconds and degassed with Awatori Neritaro (Shinky ARE-310). Homogenization and degassing were repeated several times until the mixture became uniform while keeping the solution temperature at 50° C. The suspension was subsequently poured into the silicon mold, frozen for 4°C for 2 hours. The obtained gelatin-HAp body was freeze-dried overnight at shelf-temperature 0°C. The obtained structure was named as HAp-green body. Lastly, the gelatin-HAp porous body was sintered at 1200°C for 2 hours (150℃ /hour).

5.2.2 *Fabrication of COO-capped IONP*

COO-capped IONP was fabricated in the similar method to previous Chapter (Chapter 4). IONPs were synthesized according to previous study [6,7]. 2.33 g of $FeCl_2 \cdot 4H_2O$ and 6.49 g of $FeCl_3 \cdot 6H_2O$ were added into 120 ml of nitrogen-purged ion exchanged water. The solution was rigorously stirred under N_2 gas, into which 120 ml of 0.8 mol/L of NaOH solution was added at a dropwise rate of 1.0 ml/min. The stirring was continued for 2 hours after complete addition of base and IONPs were washed with ion-exchanged water for three times. The washed IONPs agglomerate was prepared for citric acid.

Coating of IONPs with citric acid was conducted according to previous study [8]. 150 ml of citric acid solution (3.0 g) with pH adjusted to 4.6 was added into the IONPs

agglomerate. The mixture was heated at 60°C in water bath for 30 minutes and rigorously stirred for another 90 minutes. Citric acid-coated IONPs (COO-IONPs) were repeatedly washed for five times by water and acetone. Lastly, COO-IONPs were dried in a vacuum oven for 12 hours. The particles were suspended in ion-exchanged water in concentration (2, 10, 50 mg/ml).

5.2.3 *Fabrication of bilayer structure*

The spray dried HAp particles were suspended in 0.62 % wt collagen to obtain suspension of HAp (0.1wt%) / collagen. The electrolysis was conducted by using the custom-made polycarbonate mold (diameter: 23 mm, height : 40 mm). Three HAp-sintered bodies (d=10.0+-0.1 mm, t = 2.1+-0.1 mm) were placed inside the silicon mold; next, the HAp/collagen suspension was poured into the mold and the system was left to stand for 5 minutes. Electrolysis was applied by connecting bottom platina to negative potential and the upper platina covering silicon mold to positive potential. The used current density was i = 2.5 mA/cm^2 and the electrolysis time was 12 minutes. The obtained collagen gel was taken off by dismantling the custom-mold, and bilayer structure was obtained by punching the HAp-sintered body with biopsy cut (diameter: 10 mm). Bilayer structure was frozen on top of pre-cooled pan (-15°C) for 12 hours and freeze-dried overnight. To obtain IONP-impregnated bilayer structure, HAp-sintered body was initially immersed in COO-IONP solution with various concentrations (2, 10, 50 mg/ml). The excessive liquid was removed by placement in vacuum oven 60°C for 2 hours.

5.2.4 *Characterization of the samples*

5.2.4.1 *Measurement of porosity*

The physical dimension of for electrolyzed collagen and sintered HAp was measured with caliper; each layer in the multi-layer scaffold was measured in the same manner. The mass of electrolyzed collagen and sintered HAp was weighed with electronic balance. The total mass of bilayer structure was weighed; the mass of collagen layer was calculated by subtracting the total mass of multi-layer scaffold and the mass of sintered HAp. Density was calculated from the obtained mass and volume results. Porosity was defined as the percentage of void space in a 3D sponge and was calculated by the relative density:

$$\text{Porosity } (\%) = (1-\boldsymbol{\rho}_{porous}/\boldsymbol{\rho}_{solid}) \times 100$$

where $\boldsymbol{\rho}_{porous}$ is the density of collagen sponges/layer or HAp body/layer. $\boldsymbol{\rho}_{solid}$ is the density of corresponding sample (HAp: 4.3 g/cm^3 and collagen: 1.3 g/cm^3).

5.2.4.2 *Microstructure observation of samples*

The gross appearance of electrolyzed gel structure was recorded with photographic camera. The gel was subjected to freeze-drying and the obtained sponges was cut at the plane parallel to freezing direction. HAp-green body and sintered-body were cut in the similar manner. The sectioned area was thin-coated with platina before observation with scanning electron microscopy (SEM, JSM-6510, JEOL Co.). Pore size was measured with JSmile software. Pore size was obtained by measuring and averaging 40 instances of pores. The results are expressed in mean ± standard deviation.

5.2.4.3 *Compressive testing of the sample*

The mechanical properties of scaffold was characterized with compressive testing

(TA-XT2, Stable Micro Systems, UK) fitted with a 5-N load cell. Samples of 10 mm diameter and 5 mm height (n = 3 per group) were obtained for HAp porous body and multilayer scaffold; samples with similar dimension was obtained for collagen sponges by biopsy punching. Wet samples were pre-hydrated in PBS at 4°C for 24 h before testing. Amount of PBS was dropped onto samples during testing to keep the hydrated state of samples. Testing was conducted at a strain rate of 6 mm/min to achieve a strain. The compressive modulus for collagen/HAp sponge and HAp-sintered body was defined as the slope of a linear fit to the stress–strain curve over 0.05–0.10. For bilayer structure, a linear fit at 0.05–0.10 strain was defined for collagen layer; whereas, 0.10-0.15 was selected for HAp-sintered body

5.2.4.4 *Assessment of magnetic attraction*

Magnetic response of IONP-impregnated bilayer structure to magnetic attraction was characterized as followed: as-electrolyzed structures were placed on top of neodymium magnet, and structures were clamped with the TA-XT2 system (Fig. 5.1). As-electrolyzed structures were slowly pulled; and the force needed to pull the structures was recorded.

5.2.4.5 *Cell culture experiment*

NIH-3T3 (Wako Pure Chemicals Ltd., Japan) were expanded on 90 mm dishes using DMEM (DMEM; Wako Pure Chemicals Ltd., Japan) supplemented with 10% fetal bovine serum (FBS; CELLect, MP Biomedicals Inc., France) and 1% penicillin/ streptomycin (Wako Pure Chemicals Ltd., Japan). Cells were passaged at 80% confluence by using trypsin–ethylene diamine tetraacetic acid (Trpysin-EDTA; Wako Pure Chemicals Ltd., Japan) and cells below passage 20 were used for in vitro analysis (37°C, 5% CO2)

Bilayer structures were sterilized in 70% ethanol for 1 hour, 2 times. Structures were placed in the non-treated well plate; 100 μL of the cell suspension ($1.0x10^5$ cells) were dropped on top of the particular side of sponges (Col-HAp sponge: side facing the negatively charged cathode; Col-HAp/HAp sintered body: side of HAp sintered body). The well plate was returned to incubator and left for 3 hours to allow cell attachment. Following incubation, 400 μL of complete DMEM was added to each well and the plate was returned to the incubator.

The cell number was measured at day 1 after cell seeding by using Cell Counting Kit-8 (CCK-8: Dojindo Laboratories, Japan). Briefly, 50 μL of CCK-8 was added to each well and the plate was incubated at 37°C for another 2 h. An aliquot of 100 μL was taken from each well and transferred to fresh 96-well plate. The absorbance of these samples was measured at 450 nm with a spectrophotometric microplate reader (Bio-Rad 680, USA). The absorbance value was converted to cell numbers by using calibration curve of known NIH3T3 cell numbers vs absorbance of CCK-8. Cell attachment value was obtained by dividing cell number at day 1 to the initial cell number.

5.3 Results and Discussions

5.3.1 *Characterization of sintered HAp porous body*

FTIR analysis of HAp-green body (unsintered) and HAp-sintered body was given in Fig. 5.2. HAp-green body exhibited mixture of peaks of gelatin (amide I, II, and amide III) and HAp. The peaks corresponding to gelatin were clearly absent for HAp-sintered body; whereas peak attributable to HAp became clearer and more intense. HAp-green body (Fig. 5.3) exhibited large macropores with the size of 430 μm ± 38 μm, higher magnification revealed the gelatin network embroidded by HAp particles. HAp-sintered body exhibited shrinkage of macropores to 209 ± 38 μm. Higher magnification showed

the removal of gelatin network and the formation of dense structure, as evidenced from the compact packing of HAp particles. Moreover, micropores (~50 μm) was also present in the sintered body. HAp sintered body exhibited relatively larger value of porosity (86.0 ± 1.1%), compared to the previously reported porosity for HAp-sintered body [9]. In the current study, gelatin network, instead of isostatic pressure, was used to compact the HAp particles in the green bodies. As a result, coordination number of HAp particles was relatively lower for gelatin route, resulting in the more porous structure of sintered body. High porosity of HAp-sintered body was beneficial for tissue-engineering, as it allows cell penetration and distribution to the inner region of porous structure [10,11]. Moreover, high porosity was deemed to be necessary for the current study to allow complete filling with collagen/HAp suspension.

5.3.2 *Characterization of bilayer structure*

Gross appearance of HAp-sintered body, electrolyzed collagen/HAp gel and bilayer structure was shown in Fig. 5.4. In the bilayer structure, HAp-sintered body was encapsulated by electrolyzed gel, suggesting the formation of continuous structure. Microstructure of HAp-sintered body and freeze-dried collagen/HAp gel and bilayer structure was shown in Fig. 5.5. Both of HAp-sintered body and collagen/HAp sponge exhibited porous structure, with the pore size at 195 ± 7 μm and 258 ± 27 μm. Bilayer structure exhibited the continuously joined microstructures of collagen sponge and HAp-sintered body. Higher magnification of the joined interface suggested that collagen sponge interpenetrate HAp-sintered body region. The formation of continuous interface was explained as follow: before the electrolysis, HAp-sintered body (height: 20 mm) was initially immersed with the collagen/HAp suspension in the electrolysis mold. At this

stage, the suspension penetrates the pores of HAp-sintered body, thus forming the continuous system. During electrolysis, the formation of gel started initially from the suspension inside HAp-sintered body and gradually proceeded to the suspension outside HAp-sintered body. As a result, the HAp-sintered body was fully encapsulated in the gel structure, which in turn result in the continuous interface of collagen gel (sponge) and HAp-sintered body.

Stress strain curve of collagen sponge, HAp-sintered body, and bilayer structure was shown in Fig. 5.6. HAp exhibited linear stress line up to 0.1 strain before undergo failure; whereas, collagen sponge exhibited linear region of stress line (0.05-0.1 strain), followed by non-linear stress line (0.2-0.4 strain), and rapid increasing of stress line (0.4-0.6 strain). Linear region of collagen sponge corresponds to the elastic deformation of pore struts, non-linear region corresponds to the buckling of pore struts, rapid increasing of stress line corresponds to destruction of pore structures and densification of pore struts. Stress-strain curve of bilayer structure showed the presence of two linear regions, the first one (0.05-0.1 strain) was attributed to collagen sponge and the second one (0.1-0.15) was attributed to HAp-sintered body. The presence of two linear regions for bilayer structure suggested the successful formation of continuous interface between the two components (collagen/HAp sponge and HAp-sintered body). Elastic modulus was calculated from the gradient of linear region and the value for each sample and was given in the inset of Figure.

5.3.3 *Characterization of IONP-impregnated bilayer structure*

5.3.3.1 *Evaluation of magnetic properties*

The gross appearance of IONP-HAp was shown in Fig. 5.7 (a). IONP-HAp was colored in black, suggesting the successful impregnation with IONP. The black color of

HAp-sintered body became more intense with the increasing of IONP concentration, implying the larger amount of in-taken IONP. IONP-HAp was successfully fabricated into bilayer structure as given in Fig. 5,7 (b), with the IONP seemed to be unaltered by electrolysis process.

Minimum force to pull the bilayer structure from the magnetic attraction of neodymium magnet was given in Fig. 5.8. No force was obviously recorded for bilayer structure with pure HAp (0 g/L), implying absence of magnetic attraction. In contrast, the pulling force was recorded for bilayer structure with IONP-HAp (2 g/L) and the needed force became larger for structure immersed in the higher concentration of IONP (5 g/L, 10 g/L). These data suggested that the amount of IONP uptaken by HAp can be altered by varying the concentration of IONP. Furthermore, the magnetic response can be imparted to bilayer structure by impregnation of HAp-sintered body with IONP, consistent with previous studies [12].

5.3.3.2 *Evaluation of biocompatibility*

Fibroblast attachment on the control (tissue culture plate) and IONP-incorporated bilayer structure was given in Fig. 5.9. Control showed the highest cell attachment; in contrast the value significantly decreased for bilayer structure without IONP (0 g/L). Furthermore, no differences were observed between bilayer structure without and with IONP-incorporation, regardless of the concentration of IONP. In the current biocompatibility test, cell was seeded on the side of HAp-sintered body. It was shown that HAp lacked the active binding site for cells, resulting in the lower attachment value [13,14]. Moreover, incorporation of IONP did not significantly disrupt the attachment or viability of fibroblast [12,15].

5.4 Summary

HAp-sintered body with high porosity was fabricated through gelatin-mediated compaction and sintering. Furthermore, HAp-sintered body was simultaneously electrolyzed with collagen-HAp suspension to obtain bilayer structure with continuous interface. Magnetic properties can be imparted into bilayer structure by initially impregnating HAp-sintered body with COO-capped IONP. Magnetic strength can be adjusted by varying amount of in-take IONP, which in turn dependent on the initial concentration of COO-capped IONP. Lastly, the presence of IONP did not alter the biocompatibility of bilayer structure.

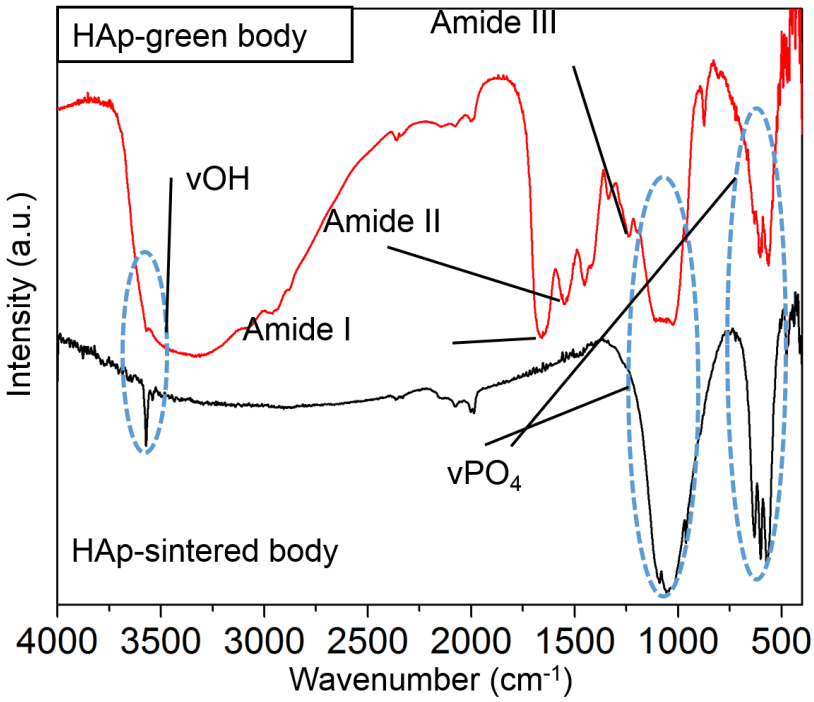

Fig. 5. 2 FTIR spectra of HAp-green body and HAp-sintered body

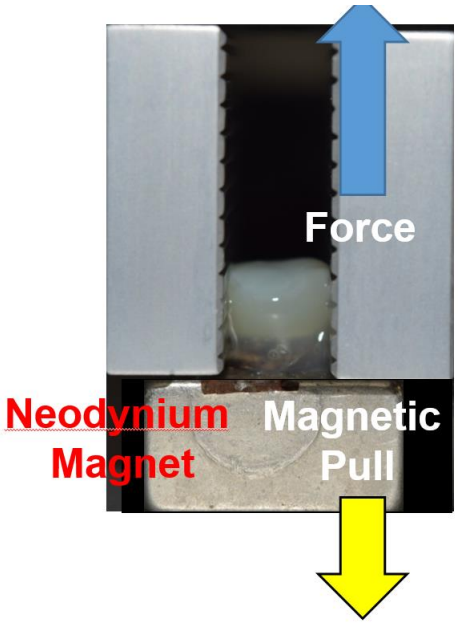

Fig. 5.1 Appearance of custom-designed test to evaluate magnetic properties of bilayer structure

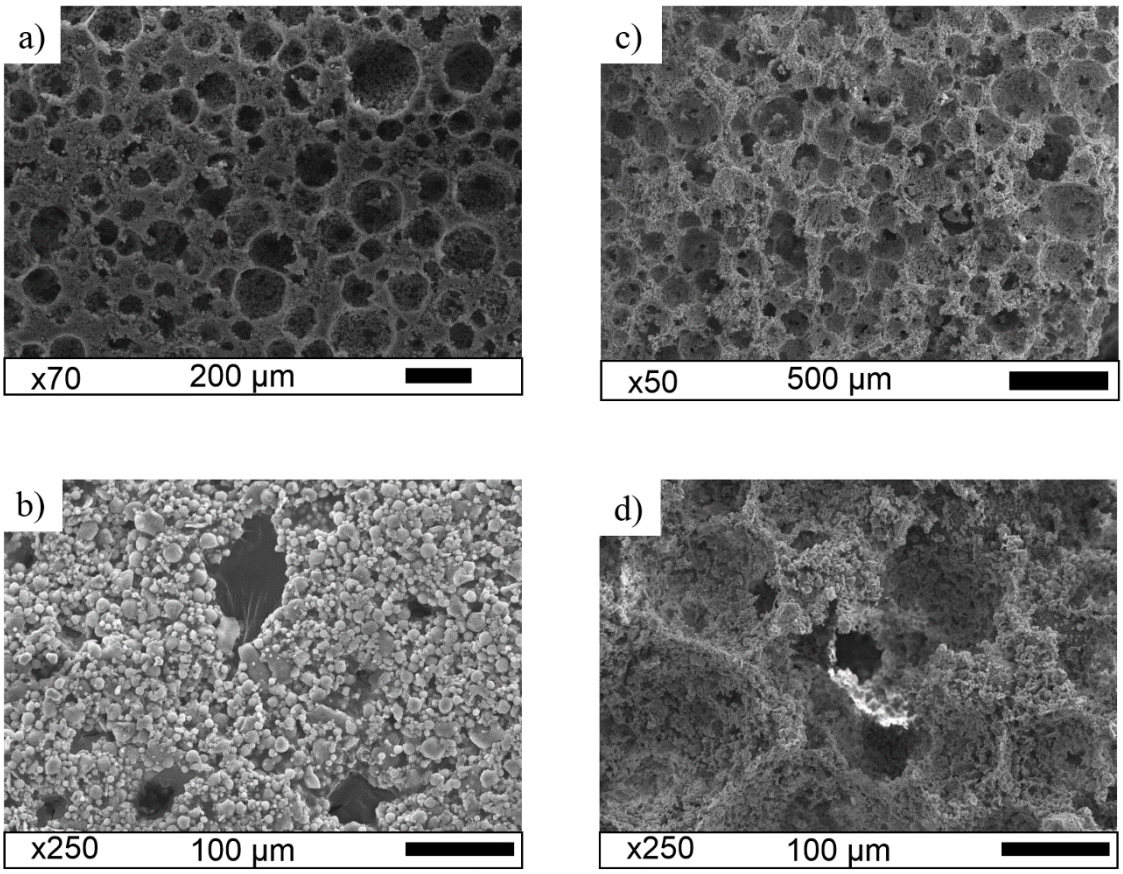

Fig. 5. 3 SEM images of (a, b) HAp-green body and (c,d) HAp-sintered body cross-sections

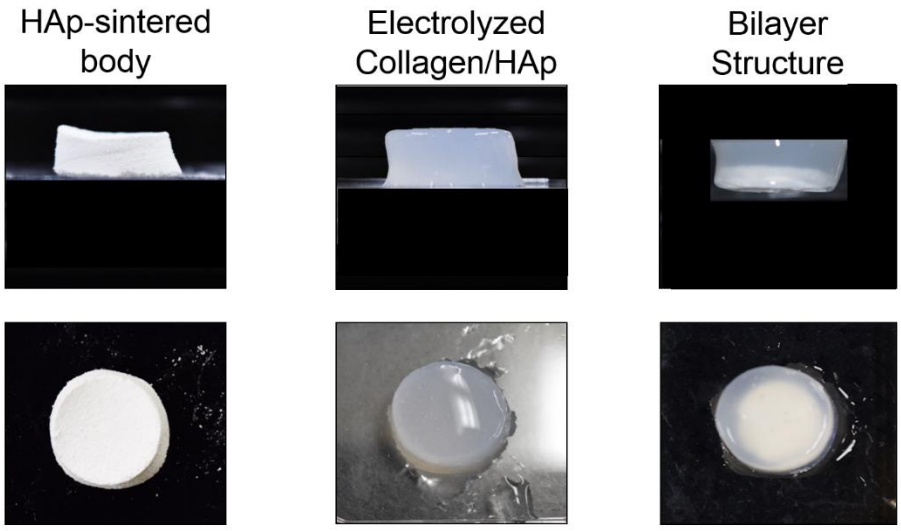

Fig. 5.4 Gross appearance of HAp-sintered body, electrolyzed collagen/HAp gel, bilayer structure

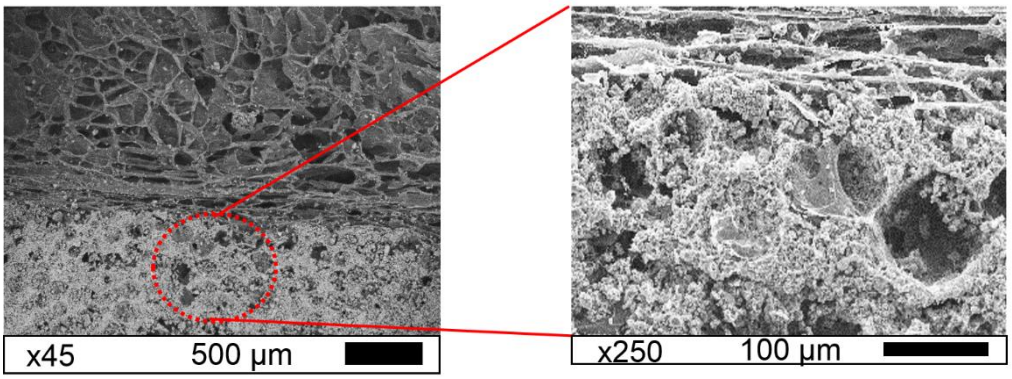

Fig. 5.5 SEM image of freeze-dried bilayer structure (left figure), higher magnification of interface region (right figure).

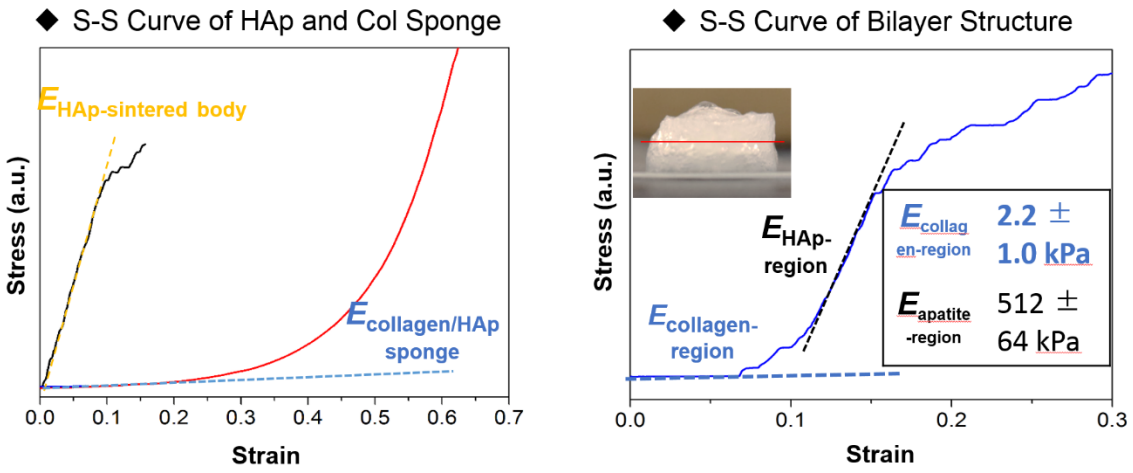

Fig. 5.6 Compressive stress strain curve of HAp-sintered body and collagen/HAp sponge (left figure), Bilayer structure (right figure). Dotted line indicate linear region of curve.

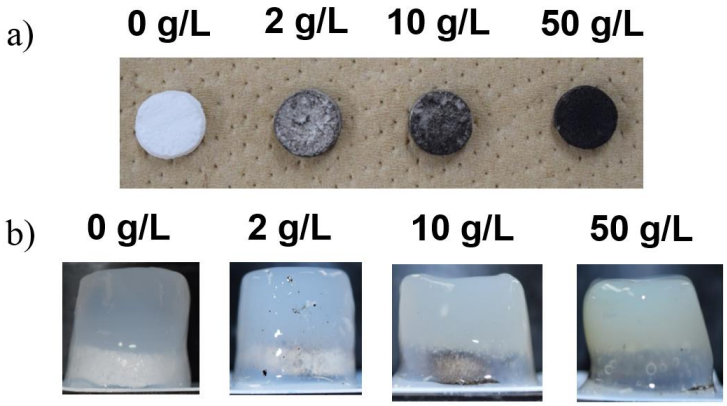

Fig. 5.7 (a) Gross appearance of IONP-impregnated HAp bodies, (b) as-electrolyzed bilayer structure containing HAp-sintered body previously impregnated by COO-IONP of various concentration.

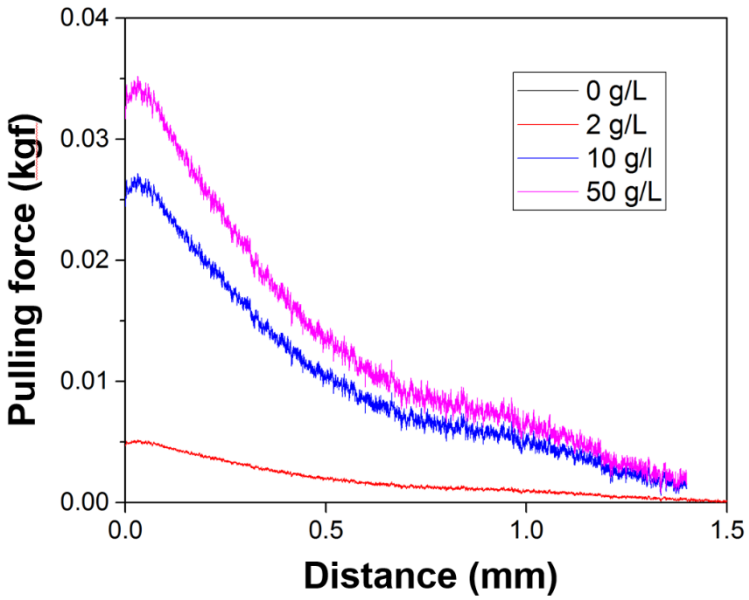

Fig. 5.8 Plot of pulling force per distance needed to pull IONP-impregnated bilayer structure from magnetic attraction of neodymium magnet

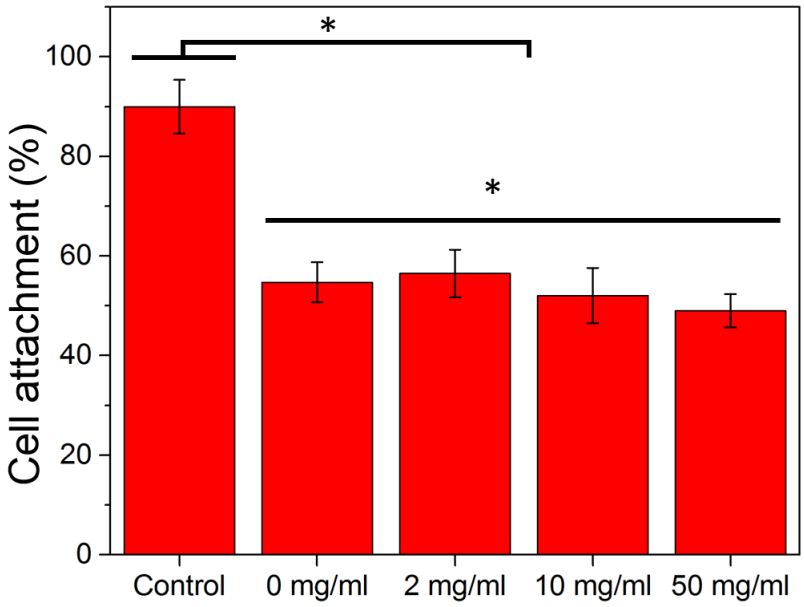

Fig. 5.9 Cell attachment of control (tissue culture plate) and IONP-impregnated bilayer structures. * p <0.05, n = 3.

References

1 P. Li, K. Nakanishi, T. Kokubo and K. de Groot, *Biomaterials*, 1993, **14**, 963-968.

2 G. Chen, T. Sato, J. Tanaka and T. Tateishi, *Mater. Sci. Eng. C*, 2006, **26**, 118-123.

3 S. Zhang, L. Chen, Y. Jiang, Y. Cai, G. Xu, T. Tong, W. Zhang, L. Wang, J. Ji, P. Shi and H. W. Ouyang, *Acta Biomater.*, 2013, **9**, 7236-7247.

4 T. Ikoma, A. Yamazaki, S. Nakamura and M. Akao, *J. Solid State Chem.*, 1999, **144**, 272-276.

5 W. Bian, D. Li, Q. Lian, X. Li, W. Zhang, K. Wang and Z. Jin, *Rapid Prototyp. J.*, 2012, **18**, 68-80.

6 V. Irawan, T. Sugiyama and T. Ikoma, *Key Eng. Mater.*, 2016, **696**, 121-128.

7 V. Irawan, M. Takeguchi and T. Ikoma, *J. Inorg. Organomet. Polym. Mater.*, 2019, 12-14.

8 S. Nigam, K. C. Barick and D. Bahadur, *J. Magn. Magn. Mater.*, 2011, **323**, 237-243.

9 E. Landi, G. Celotti, G. Logroscino and A. Tampieri, *J. Eur. Ceram. Soc.*, 2003, **23**, 2931-2937.

10 D. W. Hutmacher, *Biomaterials*, 2000, **21**, 2529-2543.

11 Q. Zhang, H. Lu, N. Kawazoe and G. Chen, *Acta Biomater.*, 2014, **10**, 2005-2013.

12 N. Bock, A. Riminucci, C. Dionigi, A. Russo, A. Tampieri, E. Landi, V. A. Goranov, M. Marcacci and V. Dediu, *Acta Biomater.*, 2010, **6**, 786-796.

13 W. Y., M. H., Y. X., P. J., G. Q., L. S. and W. A., *Biomed. Eng. Online*, 2014, **13**, 1-18.

14 M. C. Chang, T. Ikoma, M. Kikuchi and J. Tanaka, *J. Mater. Sci. Mater. Med.*, 2002, **13**, 993-997.

15 K. Lai, W. Jiang, J. Z. Tang, Y. Wu, B. He, G. Wang and Z. Gu, *RSC Adv.*, 2012, **2**, 13007-13017.

Chapter 6- Summary and Conclusion

6.1 Summary

Chapter 1: Introduction

Osteochondral injury affects both of cartilage and bone tissues, which requires simultaneous regeneration of the two tissues for effective treatment. Implantation of autologous osteochondral tissue is a gold standard for regeneration as it delivers new cells, matrix molecules, and bear load at injury site. As the alternative, investigators fabricate artificial tissue by initially growing stem cells inside the porous body (scaffold) and inducing cells to differentiate and secrete matrix components. Physical and chemical characteristics of scaffold have been known to influence the cells fate, thereby selecting scaffold material is crucial for success of tissue-engineering. To address the two-tissues at osteochondral region, two-layers of scaffold is joined in a single structure (bilayer scaffold). Collagen – a natural-based protein – and hydroxyapatite (HAp) – a calcium phosphate material – is used as cartilage and bone layer, respectively. Collagen in the monomeric or fibrillar form is fabricated as porous scaffold; however, a study comparing the capacity of monomeric / fibrillar collagen scaffold in supporting cell proliferation, differentiation, and matrix secretion capacity (cartilage tissue formation) has not yet been conducted. The current methods to fabricate bilayer scaffold is by knitting or gluing collagen sponge and HAp porous body, which pose risk of delamination after implantation. Therefore, a continuous bilayer scaffold: collagen sponge with gradient content of HAp is desired. Electrolysis was previously used to simultaneously deposit fibrillar collagen and HAp; in the current thesis, electrolysis was investigated to fabricate fibrillar collagen sponge with gradient HAp content. Furthermore, a number of studies had reported the combination of HAp with particular type of nanoparticles to promote bone cells proliferation, thereby the possibility to enhance bone layer by addition of iron-oxide nanoparticles (IONP) was also evaluated. This thesis initially aims to elucidate the advantage of fibrillar to monomeric collagen sponges as a cartilage tissue-engineering scaffold; thereafter, the thesis focuses to construct a continuous bilayer scaffold optimized for regenerating osteochondral injury.

Chapter 2: Influence of fibrillar/monomeric collagen on biological properties of Collagen /HAp sponges

The monomeric and fibrillar sponges were fabricated with similar initial conditions (chemical composition, crosslinking degree, HAp/collagen ratio). Fibrillar sponges exhibited slightly higher compressive modulus (~2.3 kPa) and strength (~0.79 kPa) to monomeric sponges (compressive modulus (~1.5 kPa) and strength (~0.4 kPa). Fibroblast attached on fibrillar sponge exhibited elongated (fillopodia) morphology, which in turn was associated with high cell proliferation capacity. In contrast, fibroblast attached on monomeric sponge exhibited flattened morphology, which is associated with low cell proliferation capacity. The results were explained based on the manner in which cell-binding sites were distributed for monomeric and fibrillar collagens. In conclusion, the fibrillar collagen was beneficial in supporting proliferation capacity of cells.

Chapter 3: Influence of monomeric/fibrillar collagen in Col/Chitosan/HAp sponges to the proliferation, chondrogenic differentiation and matrix secretion capacity of mesenchymal stem cells

Electrolysis was used to fabricate fibrillar collagen sponges. Chitosan addition was investigated to promote the formation of fibrillar collagen by electrolysis. Collagen/chitosan solution 87.5/12.5 (HAp 0.2wt%) was demonstrated as the optimal ratio to enhance fibril formation during electrolysis; the concentration was used for fabrication of monomeric and fibrillar collagen sponges. Fibrillar sponges supported rapid proliferation of MSC, reaching the maximum cell number at 14 days, at the cost of slightly inhibiting chondrogenic differentiation (gene expression analysis). Rapid proliferation of MSC in fibrillar sponges was beneficial for earlier and larger accumulation of matrix molecule (aggrecan - sulfated glycosaminoglycan (sGAG)) compared to monomeric sponges, which in turn contribute to more significant improvement of mechanical properties. In conclusion, fibrillar collagen/chitosan/HAp sponge was deemed suitable as a cartilage tissue-engineering scaffold in comparison to monomeric counterpart.

Chapter 4: Fabrication of a continuous bilayer scaffold of Col /Chitosan/IONP with gradient HAp content

Electrolysis was utilized to fabricate collagen-based sponge with the gradient HAp content; and the influence of IONP addition to the osteoblast-proliferation supporting capacity of fibrillar bilayer structure was conducted. Initial HAp concentration was beneficial to obtain the gradient HAp content in the collagen sponge. Addition of chitosan did not alter the HAp-gradient properties of collagen sponge. IONP (20 mg / ml) was further incorporated into electrolyzed sponge. The presence of IONP was beneficial for enhancing proliferation of osteoblast (bone cells). It was concluded that fibrillar collagen/chitosan/IONP with gradient HAp could act as a scaffold that simultaneously regenerate cartilage and bone tissue (bilayer scaffold).

Chapter 5: Fabrication of a continuous bilayer structure Col sponge and IONP-impregnated HAp sintered body

Simultaneous electrolysis of collagen/HAp solution and HAp-sintered body was used to fabricate a continuous bilayer structure consisting of collagen/HAp sponge and HAp-sintered body.The bilayer structure can be magnetized by incorporating IONP into the HAp-sintered body. It was concluded that electrolysis is a powerful tool to fabricate bilayer structure of collagen and HAp with continuous interface.

6.2 Applicability of The Current Finding to The Tissue-Engineering Industry

In the current thesis, it was shown that fibrillar state of collagen exert significant influence on the biological properties of collagen/HAp sponge. Fibrilar state of collagen was also demonstrated to strongly promote cell proliferation, while moderately inhibit cell differentiation compared to its monomeric counterpart. The success of tissue-engineering relies on three-key points: (1) sufficient cell number, (2) production of matrix molecules, (3) sufficient mechanical properties. Fibrillar collagen seemed to be discouraged the (2) point, suggesting the unsuitability for tissue-engineering application. However, the alternative point of view was offered.The clinically available scheme for tissue-engineering is as followed: hospital transfer cells of patient to the tissue-engineering company and request the company to devise the tissue-engineered construct

from the given cells. After finishing the tissue development, the company return back the scaffold to the hospital for implantation. Transporting the tissue-engineered construct introduce environmental stress to cells, which might induce dying of cells in the tissue-engineered construct. At this point, it is clear that scaffold promoting cell proliferation is a more practical option. Thereby, we concluded that fabricating fibrillar collagen as a tissue-engineering scaffold is a justifiable option.

6.3 General Conclusion

Fibrillar collagen sponge was shown to be suitable as tissue-engineering scaffold; electrolysis was demonstrated to be a powerful tool to fabricate a continuous bilayer sponge consisting of fibrillar collagen sponge and gradient HAp content. IONP was successfully incorporated into the sponge and the improvement of mechanical properties and osteoblast-proliferation supporting capacity were observed. On the other hand, an adjoined structure consisting of collagen/HAp sponge and HAp-sintered body was also obtained by electrolysis method. Each of two scaffold showed comparable biocompatibility; nonetheless, future study directly comparing the performance of bilayer sponge and bilayer structure as osteochondral tissue-engineering scaffold is necessary to elucidate the superior bilayer scaffold configuration.

Acknowledgement

Words fail to express debt and gratitude for my advisor Professor Toshiyuki Ikoma for the continuous and relentless support of my PhD study and for always teaching me how to write a numerous of research papers. His guidance helped me to finish the thesis and to prepare for my future. I could not have imagined having a better, kinder, patience and father-like figure advisor for my PhD study.

Besides my advisor, I would like to thank other people who helped me during the researches study: Prof. Akon Higuchi-Stem Cell Laboratory-National Central University, Taiwan for hosting and teaching me during my internship in Taiwan; Prof Guoping Chen-Biomaterial Laboratory-National Institute of Material Science (NIMS), for providing me the facility, knowledge, and equipment for stem cell researches; Mr. Sasaki Yusuke, for assisting me with the electrolysis researches; Mr Kyubae, NIMS, for assisting me with the technical knowledge regarding stem cell culture experiment.

My sincere thanks also goes to my laboratory member, since the first time I came to Ikoma Laboratory (Mr. Akiyama batch, Mr. Murai batch, Mr. Ishii batch, Mr. Suzuki batch, Mr. Torii batch, Mr. Shimada batch) for helping me with the researches discussion, equipment usage, and the most important for being a kind and supporting friends.

I would like to thank my family: Lay Ferry Irawan, Elizabeth Lina, Yolanda Irawan, and Gema Winarta for supporting me mentally and spiritually during my PhD study. Special gratitude for my aunt Yulia Lay and my passed away grandmother Moey Fun for supporting my financial condition during difficult bachelor study. Without all of them, I could not reach further to the final stage of my study

I would express my gratitude to my inner friends: Ms. Nadhilla Adelina, Ms. Clara Menna, Mr. Petrus Caesario and Mr. Kennardi Harriyanto for supporting me during the tough time of writing and making thesis presentation. Furthermore, I was lucky to meet such wonderful people who make my last year PhD more bearable: Ms. Chanissara Kajornchaikul, Mr. Chintammit, and Mr. Nicolas Debons.

Lastly, I would thank God and myself for not giving up until the very end.

Resume

Name	:	Vincent Irawan
D.o.B	:	Jakarta, 29 November 1992
Email Address	:	vince.irawan@yahoo.com

Education

August 2010	University of Indonesia	Bachelor of Engineering	Entry
March 2014	University of Indonesia	Bachelor of Engineering	Completion
October 2014	Tokyo Institute of Technology	Master of Engineering	Entry
September 2016	Tokyo Institute of Technology	Master of Engineering	Completion
October 2016	Tokyo Institute of Technology	Doctor of Engineering	Entry
September 2019	Tokyo Institute of Technology	Doctor of Engineering	Completion

Internship Experience

LABORATORY INTERN AT NATIONAL CENTRAL UNIVERSITY, TAIWAN, SEPTEMBER-OCTOBER 2017

Responsibility : Learn the extraction of mesenchymal stem cells from human tissue and basic of cell culture

CORROSION INTERN AT PT. ASMO INDONESIA, JUNE-JULY 2013.

Responsibility : Study the probablility of alternative means to prevent corrosion occurrence of fabricated product.

WELDING INTERN AT PT KOMATSU INDONESIA, AUGUST-SEPTEMBER 2013

Responsibility : Study the effect of high current welding for the operator and resulting product.

Doctoral Degree Information

Main Advisor	Toshiyuki Ikoma
Associated School and Department	School of Materials and Chemical Technology, Department of Materials Science and Engineering
Student Number	16D28059
Thesis Title	Study on hydroxyapatite and collagen-based bilayer scaffolds for osteochondral treatment

List of Publications

1. Irawan, Vincent and Toshiyuki Ikoma, “Apatite coating of iron oxide nanoparticles by alternate addition of calcium and phosphate solutions: a calcium and carboxylate (Ca-COO) complex-mediated apatite deposition.” *Journal of Inorganic and Organnometallic Polymers and Materials*, accepted (2019).
2. Irawan, Vincent, Yusuke Sasaki, and Toshiyuki Ikoma, "Fabrication of continuously apatite-graded collagen sponges with electrolysis method." *Journal of Materials Chemistry B*, **7** (2019): 4040-4048.
3. Irawan, Vincent, Akon Higuchi, and Toshiyuki Ikoma, "Physical cues of biomaterials guide stem cell fate of differentiation: The effect of elasticity of cell culture biomaterials." *Open Physics*, **16.1** (2018): 943-955.
4. Irawan, Vincent, et al. "Collagen scaffolds in cartilage tissue engineering and relevant approaches for future development." *Tissue engineering and regenerative medicine*, **15.6** (2018): 673-697.

5. Irawan, Vincent, Tomomei Sugiyama, and Toshiyuki Ikoma, "Magnetite/hydroxyapatite composite particles-assisted pore alignment of tilapia fish scale collagen-based scaffold." *Key Engineering Materials*. Vol. 696. Trans Tech Publications, 2016

Attended Conferences:

Presentation at International Conference

1. (Poster) Irawan Vincent, Ikoma Toshiyuki, "Pre-Magnetic Treatment and Electrolysis Methods as A Novel Strategy to Obtain Collagen and Apatite-based Tri-layer Scaffold", 5th Tissue Engineering and Regenerative Medicine International Society World Congress (5th TERMIS WC) (Kyoto, Japan), September 2018

2. (Oral) Irawan Vincent, Ikoma Toshiyuki, "Study of Electrolysis Method as a Novel Strategy for Obtaining Collagen Bilayer Scaffold", 4th International Symposium of Materials in Regenerative Medicine (ISOMRM 2017) (Taoyuan, Taiwan), August 2017

3. (Poster) Irawan Vincent, Sugiyama Tomomei, Ikoma Toshiyuki, "Magnetite/hydroxyapatite composite particles-assisted pore alignment of tilapia fish scale collagen-based scaffold", Bioceramics 27, (Bali, Indonesia), October 2015

4. (Oral) Irawan Vincent, Sugiyama Tomomei, Ikoma Toshiyuki, "Magnetite/hydroxyapatite composite particles-assisted pore alignment of tilapia fish scale collagen-based scaffold", The Asia-Oceania Top University League on Engineering Annual Meeting 2015 (AOTULE AM 2015), (Nanyang, Singapore), August 2015